Fall 12-21-2011

Enhancing Meniscus Repair through Biomaterial Design

Lara Ionescu Silverman
University of Pennsylvania, ionescu@seas.upenn.edu

Enhancing Meniscus Repair through Biomaterial Design

Abstract
The knee meniscus is prone to damage, which leads to pain and inhibits mobility in the joint long term. Due to the minimal vascularity, low cellularity and large mechanical forces imparted on the meniscus with normal use, endogenous repair is limited. Resection of the damaged region of the tissue (meniscectomy) remains the most common treatment for a torn meniscus, but this procedure results in cartilage degradation and other adverse changes in the knee joint. Given the prevalence of meniscus damage, there is thus a pressing need for novel approaches to meniscus repair. To address this issue, this thesis developed in vitro techniques to analyze the time-varying properties of the aging meniscus, and to address how the meniscus repair interface might be modulated through the use of growth factors. Further, electrospun scaffolds were designed to replicate key architectures of the native tissue while providing controlled release of biologic factors. Our findings demonstrated marked biological, biochemical, and structural changes in meniscus with age. These findings pointed to key factors that could play a role in meniscus integration (ie repair) capacity after meniscus injury; these factors were evaluated in the context of meniscus repair using a mechanical in vitro model. To address situations where substantial meniscus tissue would be removed, we tested the integration capacity of electrospun scaffolds with native tissue and maturation of these scaffolds in response to growth factor regimens, as well as how changes in scaffold characteristics (i.e. porosity and organization) and cell seeding techniques influence integration potential. Finally, we developed novel techniques to deliver bioactive growth factors and other molecules from components of electrospun scaffolds, including entrapped microspheres, with distinct release profiles. These novel, bioactive scaffolds were utilized to orchestrate complex regenerative signaling cascades from the scaffolds, with demonstration of efficacy via improved vascular density in an in vivo model. This work provides new approaches for the treatment of meniscus tears using novel electrospun materials, bringing us one step closer to new clinical options for meniscus repair.

Degree Type
Dissertation

Degree Name
Doctor of Philosophy (PhD)

Graduate Group
Bioengineering

First Advisor
Dr. Robert Mauck

Second Advisor
Dr. Jason Burdick

Third Advisor
Dr. Brian Sennett

Keywords
Scaffold, meniscus, tissue engineering, growth factor, microsphere, fiber

Subject Categories
Biological Engineering | Biomaterials | Molecular, Cellular, and Tissue Engineering

ENHANCING MENISCUS REPAIR

THROUGH

BIOMATERIAL DESIGN

Lara Ionescu Silverman

A DISSERTATION

in

Bioengineering

Presented to the Faculties of the University of Pennsylvania

in

Partial Fulfillment of the Requirements for the

Degree of Doctor of Philosophy

2011

Supervisor of Dissertation:

Signature _____
Dr. Robert Mauck, Associate Professor of Orthopaedic Surgery and Bioengineering

Graduate Group Chairperson:

Signature _____
Dr. Beth Winkelstein, Professor of Bioengineering

Dissertation Committee:

Dr. Jason Burdick	*Committee Chair,* Associate Professor of Bioengineering
Dr. Louis Soslowsky	Fairhill Professor of Orthopaedic Surgery and Bioengineering
Dr. Robert Mauck	Associate Professor of Orthopaedic Surgery and Bioengineering
Dr. Brian Sennett	Associate Professor of Orthopaedic Surgery
Dr. James Cook	Associate Professor of Orthopaedic Surgery and Small Animal Orthopaedics (*University of Missouri-Columbia*)

Dedication

This work is dedicated to my parents,

Dan and Wanda Ionescu,

who selflessly put my education above all else,
and taught me the importance of hard work and determination.
Their unending love and encouragement have inspired me to dig deeper and try harder,
and always seek out the next great adventure.

Acknowledgements

This thesis, and indeed this degree, could not have happened if it weren't for a number of extremely important individuals who helped me along the way. First of all, I would like to thank my adviser, Dr. Robert Mauck, for his tireless work ethic, persistent guidance and positive energy throughout my PhD. His ability to see the big picture, think forward to find the next exciting idea, and 'know everything about everything' has been a constant inspiration for me. He taught me how to ask the right questions and how to be a discerning scientist, and I will cherish and use these skills for the rest of my life. I would also like to especially thank Dr. Brian Sennett, who would often slip away from his duties as an Orthopedic Surgeon to provide clinical insight and a critical eye to my research. Further, I appreciate the support and input over the years from Dr. Jason Burdick, whose complimentary research provided unique perspectives on my work. Also, the wisdom and experience of Dr. Louis Soslowsky helped improve my research and goals for my thesis. Finally, I appreciate the input from Dr. Jimi Cook, who provided a unique perspective on translational tissue engineering.

During my graduate studies, I had the privilege of working in the McKay Orthopaedic Research Laboratory, a unique consortium of labs with many scientific resources that facilitated collaboration and expedited scientific discovery. McKay housed almost all of the resources, equipment and tools needed to complete this thesis. I would like to sincerely thank the support staff of McKay, including David Beason, Bob Caron, Ruth McCarrick-Walmsley, Barbara Gibson, and Arlene Adair. Also, I would like to thank the Mauck lab support staff over the years, including Tiffany Zachry, Elizabeth Henning, Suchin Heo and Minwook Kim. A large reason for my efficiency during graduate school

was these individuals, who managed and maintained the operational aspects of the lab so that I could focus on my research.

Next, I would like to thank the other students who helped me through the years, and also made the day-to-day process significantly more fun. I would especially like to thank Isaac Erickson, Matt Fisher and Jon Kluge for their contributions to my work, along with the rest of the Mauck lab, as well as Bioengineering students Jamie Ifkovitz, Julie Czupryna, Sudhir Khetan, Brendan Purcell, Elena Tous, Mike Dishowitz, Heather Ansorge, Jonathon Yoder, and Nathan Jacobs, and McKay members Kevin Egan, Josef Kaplan, and Salin Chakkalakal. Also, I am deeply grateful for the hard work and dedication of Greg Lee, who helped me significantly with lab work over the years, as well as Kevin Huang, Sylvia Qu, Grant Garcia, Jose Guevara and Kilief Zellars. I am particularly appreciative of having the opportunity to work with a number of Orthopedic Residents over the years, who taught me a lot about dissections, anatomy, and the 'real world' of orthopedic surgery, including Nicole Belkin, Mara Schenker, Roshan Shah, Ryan DeCoons and Albert Gee.

Finally, I would like to thank my close friends and family who supported me during graduate school, especially my siblings (of the Ionescu and of the Silverman variety) and all of my parents (Dan and Wanda Ionescu, Lorraine and Mark Ruhling). Most importantly, I would like to thank my husband, Dr. Brett Silverman, for being patient while I indulged in this degree, and for keeping me level-headed throughout this long (and sometimes stressful) process. I am grateful for his advice over the years (scientific and otherwise), and I am blessed to be able to share my life with him.

Abstract

ENHANCING MENISCUS REPAIR THROUGH BIOMATERIAL DESIGN

Lara Ionescu Silverman

Supervisor: Dr. Robert Mauck

The knee meniscus is prone to damage, which leads to pain and inhibits mobility in the joint long term. Due to the minimal vascularity, low cellularity and large mechanical forces imparted on the meniscus with normal use, endogenous repair is limited. Resection of the damaged region of the tissue (meniscectomy) remains the most common treatment for a torn meniscus, but this procedure results in cartilage degradation and other adverse changes in the knee joint. Given the prevalence of meniscus damage, there is thus a pressing need for novel approaches to meniscus repair. To address this issue, this thesis developed in vitro techniques to analyze the time-varying properties of the aging meniscus, and to address how the meniscus repair interface might be modulated through the use of growth factors. Further, electrospun scaffolds were designed to replicate key architectures of the native tissue while providing controlled release of biologic factors. Our findings demonstrated marked biological, biochemical, and structural changes in meniscus with age. These findings pointed to key factors that could play a role in meniscus integration (ie repair) capacity after meniscus injury; these factors were evaluated in the context of meniscus repair using a mechanical in vitro model. To address situations where substantial meniscus tissue would be removed, we tested the integration capacity of electrospun scaffolds with native tissue and maturation of these scaffolds in response to growth factor regimens, as well as how changes in scaffold characteristics (i.e. porosity and organization) and cell seeding techniques influence integration potential. Finally, we developed novel techniques to deliver bioactive growth factors and other molecules from components of electrospun scaffolds, including entrapped microspheres, with distinct release profiles. These novel, bioactive scaffolds were utilized to orchestrate complex regenerative signaling cascades from the scaffolds, with demonstration of efficacy via improved vascular density in an in vivo model. This work provides new approaches for the treatment of meniscus tears using novel electrospun materials, bringing us one step closer to new clinical options for meniscus repair.

Table of Contents

List of Figures

1: Introduction

1.1 Meniscus Structure and Function

The menisci are two semilunar cartilaginous structures in the knee that function to transmit and distribute load from the femur to the tibia [1, 2], maintain knee joint stability [3], and provide shock absorption [4]. The organization and composition of the meniscus allows it to withstand both tensile and compressive forces [5] in order to distribute load and protect the cartilage surfaces. The compressive equilibrium modulus ranges from 25-350 kPa [6, 7] and the tensile modulus ranges from 100-300 MPa [4, 8], depending on the species, sample location and testing parameters.

The tissue is composed primarily of water (72% of wet weight), as well as collagens (22% of wet weight), proteoglycans (0.8% of wet weight), and a number of other trace components that contribute to meniscus function [5, 9]. Meniscus is made up of sparsely populated fibrochondrocytes that vary in shape according to region [10]. Further, it withstands its complex loading environment with a carefully tuned architecture that features circumferentially oriented collagen bundles opposing tensile deformation [11] and glycosaminoglycans (GAG) concentrated in the inner region withstanding compressive deformation [12-14]. In the adult, the meniscus has a limited vascular supply, with vessel infiltrating only to the outer third [15].

1.2 Meniscus Injury and Repair

Tears or injury to the meniscus are very common, with 600,000 meniscus surgeries annually in the US [16] and meniscus surgery being the most prevalent of all orthopedic surgeries [17]. A typical procedure to address meniscus damage involves removal of the injured portion, since tears, particularly in the inner avascular region, rarely heal [18].

Unfortunately, resection changes load bearing and presages the long-term development of osteoarthritis [19, 20], prompting surgical methods towards maintaining as much of the original structure as possible [21]. Sutures [22], arrows or screws [23], and the use of the collagen implant [24] or a cadaveric allograft [25] in extreme cases, have all been explored with moderate clinical success.

Over and above stabilizing the damaged segment, many clinical solutions have been predicated on expanding the vascular supply to the damaged area to promote natural healing, since tears in the vascular region of the meniscus heal [18, 26-28]. Solutions such as rasping [29], vascular channels [26, 27], and the application of fibrin glue [30] all utilize this idea. The concept seems particularly promising as young patients with a more completely vascularized meniscus [15, 18, 26, 31, 32] rarely present with meniscal injuries [33].

Many interesting techniques have been recently explored that may some day be used in the clinic. Rather than connecting a meniscus tear with a fabricated material such as a suture, a biological 'glue' such as platelet rich plasm (PRP) [34] may support biomimetic integration. Further, rather than adding a material to promote repair, chemicals could be delivered locally that promote integration. For example, chemicals to suppress MMPs and cytokines could be used in order to bolster natural healing [35-39].

1.3 Tissue Engineering Strategies for Meniscus Repair to Date

In the instance where damage is too great, a meniscus replacement would be necessary to replace the resected tissue. This material could be permanent and impermeable to cells; however, such materials would likely face long-term issues such as dislodging, immune responses, wear, fatigue and failure. In contrast, a tissue engineering approach

could be utilized, where the combination of a temporary scaffold, chemical/mechanical cues and cells could be used to create meniscus tissue [40]. The integration of such a material into the existing tissue is of paramount importance in order to reestablish the mechanical and structural capabilities of the tissue. Other important factors are relevant mechanical properties as well as favorable conditions for the proliferation and matrix deposition by fibrochondrocytes or stem cells induced to become fibrochondrocyte-like cells. While many envision a temporary material to replace a region of meniscus, it may also be possible to design a full meniscus replacement that would feature bone insertions mimicking meniscal horns; however, such a material would provide significantly more design challenges.

Numerous materials have been tested for meniscus tissue engineering, including collagen [24], small intestinal submucosa (SIS) [41-43], dermis [44], estane [45], polyurethane [46], agarose gels [47] and alginate [48], to name a few [49]. While it is evident that many strategies have been explored, none except for the collagen meniscus implant has reached clinical availability, although its efficiency is not yet clearly demonstrated [24].

To expand the palette of materials for meniscus tissue engineering, we have developed a nanofibrous electrospun scaffold. This material mimics the mechanical properties of the tissue relatively well and emulates the collagen bundle architecture of native meniscus. The fabrication technique is relatively simple and robust, and it could be easily modified to incorporate other features, such a sacrificial fibers, microspheres, biological factors or cells. In these scaffolds, MFCs and mesenchymal stem cells infiltrate and deposit ordered matrix, generating an engineered tissue with physiologically relevant mechanical properties [50-53].

1.4 Thesis Overview and Specific Aims

In this thesis, we will explore the physiological properties of aging meniscus as well as potential biomaterials for its repair. Specifically, we will analyze changes in biochemical content and matrix formation capacity in the tissue with aging, and will test the repair potential mechanically using an *in vitro* integration model (**Chapter 2, 3**). These chapters address Aim 1: *Characterize fetal, juvenile and adult meniscus to define native tissue and cell properties, and potential limiters of adult healing*. We will also identify fundamental differences between immature and mature meniscus cells in both ovine and bovine tissue, and subsequently choose relevant growth factors that successfully bolster the repair of an avascular meniscus tear *in vitro* (**Chapter 3, 4**) according to Aim 3: *Promote meniscus integration in vitro through modulation of adult extracellular matrix (ECM) and soluble environment*. Next, we will apply the *in vitro* integration model to electrospun scaffolds, and analyze the role of growth factors in scaffold integration and maturation (**Chapter 4**). We will also modify the characteristics of the scaffold (porosity, alignment) and the cell seeding technique, and identify optimal conditions for repair (**Chapter 5**). Chapter 4 and 5 address Aim 4: *Investigate the integration and maturation of electrospun composites adjacent to native meniscus tissue in vitro*. In order to transition to the *in vivo* environment, we will review current techniques for delivering molecules from electrospun scaffolds, with a special focus on growth factors (**Chapter 6**). Next, we will present a novel fabrication technique to entrap drug-delivering microspheres between structural electrospun fibers (**Chapter 7**) that addresses Aim 2: *Create a microsphere/nanofiber composite scaffold with drug delivering capacity*. Finally, we will deliver growth factors from these microspheres, as well as from the fibers themselves, and stimulate both proliferation and angiogenesis *in vivo* (**Chapter 8**) as described in Aim 5: *Evaluate biomaterial-driven meniscus repair in an in vivo model*. This work represents significant steps forward in our understanding

of the knee meniscus and in the potential of using electrospun scaffold for meniscus tissue engineering.

2: The Differential Regenerative Potential of Fetal and Adult Meniscus Fibrochondrocytes

2.1 Abstract

The adult knee meniscus is prone to injury and has limited intrinsic healing potential, with few successful therapeutic options for repair. In order to direct the development of new approaches for meniscus repair, we investigated the properties of the fetal and adult meniscus tissue and isolated meniscus fibrochondrocytes (MFCs). While little data exists on meniscus repair potential as a function of age, other related fibrous and cartilaginous tissues have been shown to heal regeneratively in the fetal environment. Further, significantly fewer young patients present clinically with meniscus tears compared to adults. We hypothesized that fetal meniscus cells would be more active than their adult counterparts. Our results showed that while meniscus structure changed with development, cellular characteristics such as migration and proliferation were comparable. However, when cultured in three-dimensional pellets, adult cells responded less robustly than fetal cells to the addition of the chondrogenic growth factor TGF-β, with markedly lower improvements in weight, DNA, glycosaminoglycan (GAG), and collagen content after 42 days, supporting our hypothesis. Taken together, this work demonstrates that while the proliferative and migratory capacity of MFCs do not diminish with age in the ovine meniscus, the ability to deposit matrix in the presence of TGF-β decreases by adulthood. These findings may provide novel directions for adult meniscus repair strategies through the promotion of matrix deposition as well as guide the development of tissue engineered meniscus repair approaches.

2.2 Introduction

The menisci are two semilunar cartilaginous structures in the knee that function to transmit and distribute load from the femur to the tibia [1, 2], maintain knee joint stability [3], and provide shock absorption [4]. The organization and composition of the meniscus allows it to withstand both tensile and compressive forces [5] in order to distribute load and protect the cartilage surfaces. The tissue is composed primarily of water (72% of wet weight), as well as collagens (22% of wet weight), proteoglycans (0.8% of wet weight), and a number of other trace components that contribute to meniscus function [5, 9]. The meniscus withstands its complex loading environment with a carefully tuned architecture that features circumferentially oriented collagen bundles opposing tensile deformation [11] and glycosaminoglycans (GAG) concentrated in the inner region withstanding compressive deformation [12-14]. In the adult, the meniscus has a limited vascular supply, with vessel infiltration only to the outer third [15].

Tears or injury to the meniscus are very common and lead to degenerative changes in the knee such as osteoarthritis [19, 20]. A typical procedure to address meniscus damage involves removal of the injured portion, since tears, particularly in the inner avascular region, rarely heal [18]. However, resection changes load bearing and presages the long-term development of osteoarthritis, prompting surgical methods towards maintaining maintain as much of the original structure as possible [21]. Sutures [22], arrows or screws [23], and the use of a collagen implant [24] or allograft [25] in extreme cases, have all been explored with moderate clinical success.

Over and above stabilizing the damaged segment, many clinical solutions have been predicated on expanding the vascular supply to the damaged area to promote natural

healing. Solutions such as rasping [29], vascular channels [26, 27], and the application of fibrin glue [30] all utilize this concept. The concept seems particularly promising as young patients with a more completely vascularized meniscus [31] rarely present with meniscal injuries. In addition to vascular supply, other factors, such as cell density, extracellular matrix (ECM) properties and sensitivity to growth factors, may also distinguish healing in the young meniscus from the failure to heal in the adult meniscus. In fact, it has been observed that related fiber-reinforced fetal tissues with similarly limited vascular supply heal regeneratively, including articular cartilage [54] and tendon [55, 56]. Those findings suggest that meniscus may also heal regeneratively during fetal development based on factors not associated with is vascular network.

In this work, we explored how fetal and adult ovine menisci and meniscus fibrochondrocytes (MFCs) vary with development. Previous studies have shown that cells from related tissues, such as ACL fibroblasts [57], tendon fibroblasts [58], and chondrocytes [59, 60], lose the capacity to proliferate and/or migrate with age, while other tissues such as dermal fibroblasts do not [61]. Additional studies have demonstrated a marked decrease in matrix forming capacity with development [57-59, 61, 62]. Based on these findings, we hypothesized that the proliferation, migration and matrix forming capacity of meniscus fibrochondrocytes (MFCs) would decrease with age. To test this hypothesis, we extracted MFCs from fetal and adult ovine menisci and performed migration and proliferation studies. Further, we cultured pellets of MFCs in a chemically defined media with the addition of the chondrogenic growth factors TGF-β1 or -β3, known to be involved uniquely in the fetal environment and in adult healing [63, 64]. We found major changes in the ECM distribution and cell density between fetal and adult ovine menisci. However, fetal and adult MFCs proliferated and migrated at the same rate once extracted from the tissue. When grown in pellets, fetal MFCs responded

more robustly to TGF-β than adult cells by proliferating and depositing more ECM, particularly GAG. Our findings suggest that while adult MFCs do not lose the ability to migrate or proliferate to an injury site, a diminished capacity to deposit matrix may be a limiting factor in meniscus healing in adult tissue. Such findings may direct novel clinical solutions for meniscus injury repair in adults.

2.3 Materials and Methods

2.3.1 Tissue Source

Hinds limbs from mid gestation (~75 days) ovine fetuses and skeletally mature adults were isolated from waste tissue from an unrelated study. Approval from the Institutional Animal Care and Use Committee (IACUC) at the University of Pennsylvania was obtained for the transfer and use of all tissue.

2.3.2 Histological Analysis of Meniscus as a Function of Age

To establish baseline histological features of the meniscus as a function of age, hind limbs were isolated from ovine fetuses and disarticulated. The tibial plateau with adjoining menisci were fixed for 2-3 days in 4% paraformaldahyde and paraffin embedded. Similarly, maternal hind limbs were disarticulated and the medial menisci were carefully removed by cutting the horns and exterior rim of the synovium, fixed, and prepared for histology as above. Tissue was sectioned to 7 μm thickness in the axial and coronal directions and affixed to glass slides. Sections were stained with either Alcian Blue to identify proteoglycans (PG), Picrosirius Red to identify collagens, or hematoxylin and eosin (H&E) to identify cell nuclei and matrix structure.

2.3.3 Analysis of Migratory and Replicative Capacity of Fetal and Adult Meniscus Fibrochondrocytes

For cell culture studies, medial menisci from twin ~75 day old sheep fetuses and the corresponding maternal sheep were aseptically dissected. Care was taken to remove any remaining synovium from the outer rim of the menisci, and the entire meniscus tissue was plated due to the small size of the fetal tissue and resulting inability to separate inner and outer regions. The menisci were diced into 1 mm^3 pieces and plated onto tissue culture plates in a basal medium (BM) consisting of high glucose DMEM supplemented with 10% fetal bovine serum (FBS) and 1% penicillin/streptomyosin/fungizone (PSF). To determine the rate of emergence of MFCs from the tissue, ~20 mg of diced menisci was cultured for 7 days (ensuring sub-confluency) and the cells were trypsinized and counted. MFCs from each twin fetus and from the maternal source were maintained separately. Cell number was normalized by the initial tissue mass. For further studies, MFCs were expanded to passage 2 in BM.

To determine whether proliferation rate was age dependent, 20,000 passage 2 cells from each fetal and the maternal menisci were plated in BM in individual wells of a 6-well tissue-culture treated plate. Every day, in triplicate, MFCs were lysed with distilled water, dislodged with a cell scraper, and analyzed for DNA content using the PicoGreen dsDNA assay (Invitrogen, Carlsbad, CA). To assess migration capacity, confluent layers of cells on tissue-culture treated plastic were scratched using the tip of a 0.1-10 μl sterile plastic pipette. The wells were washed twice with PBS to remove cell debris and filled with BM. Light microscope images were captured at the onset and after 15 hours to observe cell migration into the gap. All studies were performed in triplicate, with one representative study shown.

2.3.4 Analysis of Matrix Accumulation in 3D Pellet Culture

After expansion through passage 2, 250,000 cells from each fetal meniscus and the maternal adult meniscus (fetus 1, fetus 2, adult) were formed into pellets in 96-well conical plates (Nunc, Thermo Scientific, Waltham MA). Pellet culture has been used previously as a three-dimensional chondrogenic environment that fosters meniscus-like tissue deposition [65]. Pellets were maintained in four media conditions: BM supplemented with 50 mg/ml ascorbate 2-phosphate; a chemically defined media (CDM-; high glucose DMEM with 1X PSF, 0.1 mM dexamethasone, 50 mg/ml ascorbate 2-phosphate, 40 mg/ml L-proline, 100 mg/ml sodium pyruvate, 6.25 mg/ml insulin, 6.25 mg/ml transferrin, 6.25 ng/ml selenous acid, 1.25 mg/ml bovine serum albumin, and 5.35 mg/ml linoleic acid); CDM supplemented with 10 ng/ml TGF-β1 (CDM+β1); CDM supplemented with TGF-β3 (CDM+β3).

At 2 week intervals, pellets were removed from culture, situated in agarose, paraffin embedded, sectioned and stained as described above. On additional sections, immunohistochemical analysis was carried out to visualize the location of Collagen I and Collagen II [66]. Briefly, samples underwent antigen retrieval with 300 mg/mL hyaluronidase (Type IV, Sigma, St. Louis, MO), 3% H_2O_2, and blocking reagent (DAB150 IHC Select, Millipore, Billerica, MA). Samples were then treated with antibodies (5 μg/mL) to Col I (MAB3391, Millipore) or Col II (11e-116B3, Developmental Studies Hybridoma Bank, Iowa City, IA) in 3% BSA (control sections treated with 3% BSA only). Finally, biotinylated goat anti-rabbit IgG secondary antibody conjugated with streptavidin horseradish peroxidase was localized to primary antibodies, and color developed with 3,30-diaminobenzidine (DAB) chromagen reagent (DAB150 IHC Select, Millipore).

Biochemical content of pellets from each condition was determined after papain digestion. The digestate was analyzed for DNA content (Picogreen Assay, Invitrogen, Carlsbad, CA), sulfated glycosaminoglycan (s-GAG) content (DMMB Assay [67]) and collagen content (OHP assay [68] using a conversion factor 7.14 to convert to collagen content. This work was performed in triplicate with n=3 (2 to 3 pellets per n), with the results of one representative study shown.

2.3.5 Statistical Analysis

Two-way analysis of variance (ANOVA) was carried out using SYSTAT software (Chicago, IL) with Bonferonni's *post-hoc* tests (n=3), with significance set at $p < 0.05$.

2.4 Results

2.4.1 Histological Analysis of Meniscus as a Function of Age

Histological analysis revealed considerable changes from the fetal meniscus to the mature, adult meniscus. Developmentally, the meniscus is distinct in composition from the underlying cartilaginous tibial plateau (**Fig 2-1A**). The fetal meniscus stained strongly for collagen (red) while the cartilage below stained strongly for proteoglycans (PG, blue). Further, only a faint quantity of PG was observed in the inner tip of the fetal meniscus (**Fig 2-1A**). Similarly, the adult meniscus stained strongly for collagen, but in contrast, PG was present throughout the meniscus, although less dense in the central region of the tissue (**Fig 2-1B**). Closer inspection revealed that the fetal meniscus was densely populated with cells located between thin and undulating collagen bundles (**Fig 2-1C**). In the adult meniscus, the cell density was considerably lower and the collagen bundles appeared linear and were larger and more robust (**Fig 2-1D**). Indeed, sectioning

for histology was more difficult when cutting perpendicular to the collagen bundles in the adult compared to the fetal meniscus.

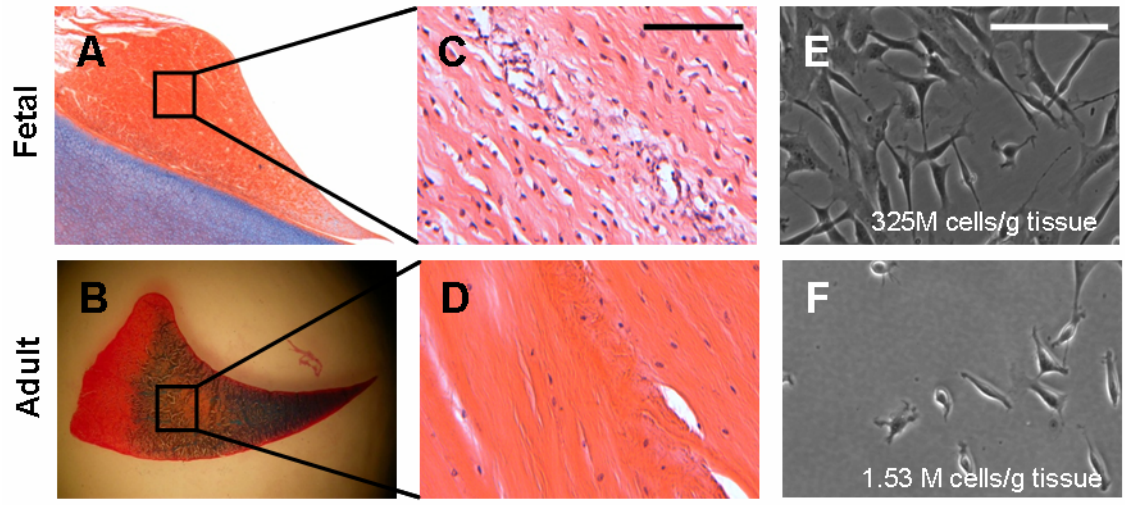

Figure 2-1 Histological sections of fetal (A) and adult (B) ovine meniscus, stained with Picrosirius Red for collagens and Alcian Blue for proteoglycans (PG). The meniscus increases in size as the animal matures and an increase in PG content and distribution is evident. (Adult: 13mm, Fetal: 1.5mm). Hematoxylin and eosin (H&E) staining of fetal (C) and mature adult (D) meniscus demonstrates a decrease in cell density and increase in collagen bundle thickness as the animal matures (Scale = 50 μm). After plating minced fetal (E) and adult (F) meniscus, light micrographs reveal significantly more cells emerging from the fetal tissue which were larger in size and more spindly. Quantification of the outgrowth indicated that over the first 7 days, 200 times the number of cells emerged from fetal compared to adult tissue, per gram of tissue. (Scale = 100 μm).

2.4.2 Migration and Proliferation Capacity of Adult and Fetal MFCs

When fetal and adult meniscus tissue was plated on tissue-culture treated plastic in basal media, MFCs emerged over the first few days of culture. Cells that emerged from the fetal meniscus were more spindle-like in appearance. When normalized to tissue weight, 200 times more MFCs emerged from the fetal tissue compared to the adult tissue (**Fig 2-1E, F**). Once removed from the tissue, however, proliferation rates of extracted fetal and adult MFCs did not differ over 12 days (**Fig 2-2A**). When a gap was introduced to a confluent monolayer, cells filled the new space completely within 24 hours (data not shown). Images acquired at 15 hours (prior to closure) showed equivalent migration by cells of both ages (**Fig 2-2B**).

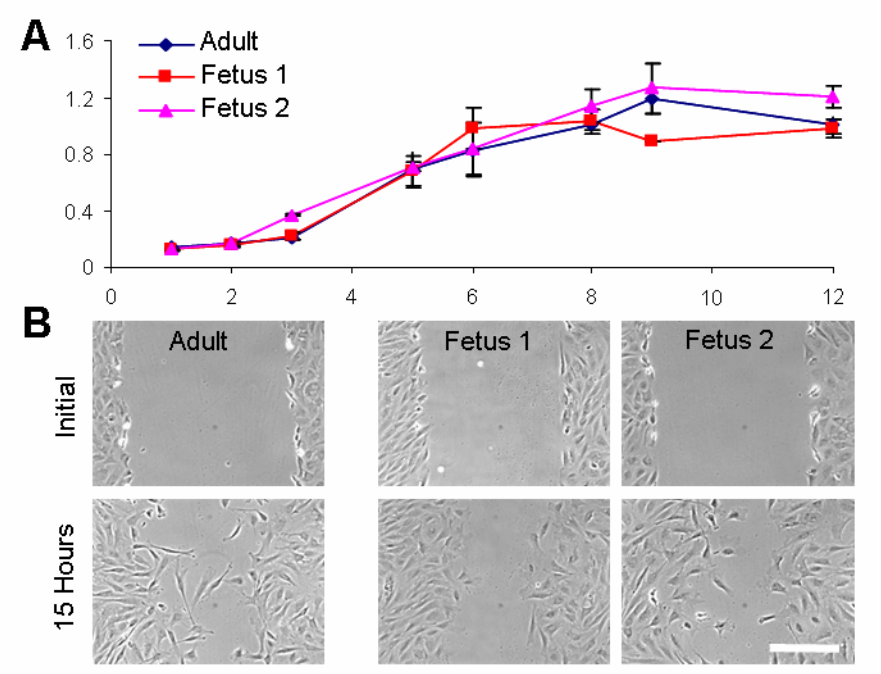

Figure 2-2: (A) Proliferation of fetal and adult MFCs in monolayer culture are comparable over 12 days (N=3, performed in triplicate). (B) Migration of fetal and adult MFCs into an artificial 'wound' occurred over a similar time course. (Scale = 200 μm).

2.4.3 Matrix Elaboration by Fetal and Adult MFCs in Pellet Culture

MFCs were formed into pellets and cultured in 4 different media types for 6 weeks. When cultured in basal media, fetal pellets did not remain viable, disintegrating by day 42. Adult pellets, on the other hand, remained viable though very little matrix deposition occurred (**Fig 2-4**). When cultured in the presence of CDM-, both fetal and adult cell pellets remained small, with comparable collagen (red) and PG (blue) deposition (**Fig 2-3, 2-4**).

Upon the addition of TGF-β, adult cell pellets increased in size by day 42 (**Fig 2-3**). Adult cells had a moderate response to TGF-β with 2 to 4-fold increases in pellet weight compared to CDM- conditions (**Fig 2-4A**). DNA content decreased, although not significantly, with the addition of TGF-β compared to CDM- conditions (**Fig 2-4B**). GAG and collagen content (normalized to DNA content) in adult pellets increased, although

not significantly, compared to CDM- condition (**Fig 2-4C, D**). TGF-β1 promoted the deposition of both collagen I and II, while TGF-β3 resulted in the deposition of collagen I with no deposition of collagen II (**Fig 2-3**). Overall, the addition of TGF-β bolstered deposition of a meniscus-like fibrocartilaginous extracellular matrix in adult MFC pellets.

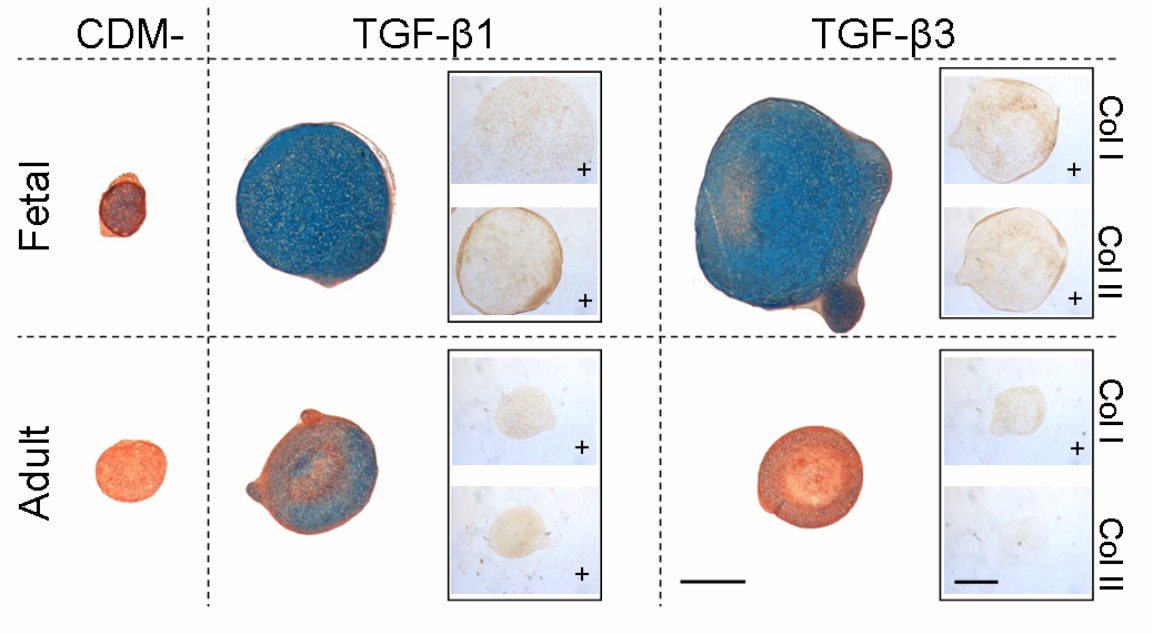

Figure 2-3: Histological sections of fetal and adult MFC cell pellets in CDM-, TGF-β1, and TGF-β3 media after 42 days in culture. Fetal MFCs produce larger pellets with more PG compared to adult MFCs (Scale = 500 μm). Inlays: Immunohistochemical staining for Collagen I and Collagen II. Collagen I and II are deposited in fetal tissue with exposure to both TGF-β isoforms, while adult MFCs produce only collagen I in with exposure to TGF-β1. Work was performed in triplicate, with one representative set shown. (Scale = 1000 μm)

Fetal pellets responded more robustly to the addition of TGF-β than adult pellets by day 42. Histological analysis showed a significant increase in deposition of PG and a 3 to 4-fold increase in pellet diameter with TGF-β compared to CDM- conditions (**Fig 2-3**). Pellet weights from Fetus 1 and 2 were 10- and 30-fold higher than CDM- conditions by day 42, respectively (**Fig 2-4A**). Further, the weight of fetal pellets was significantly higher than the adult pellets for both TGF-β isoforms. In contrast to adult MFC pellets, DNA content increased significantly in the presence of TGF-β1 and -β3 (**Fig 2-4B**). The

quantity of GAG and collagen produced per fetal cell was significantly higher in the presence of TGF-β compared to the CDM- condition. Further, this growth factor caused fetal MFCs to deposit significantly more matrix than adult MFCs (**Fig 2-4 C,D**), with the exception of fetus 2 pellets that had comparable collagen deposition. While the quantity of GAG deposited varied considerably between media conditions and tissue age, biochemical analysis and histological staining for picrosirius red alone (data not shown) showed that changes in collagen levels were less pronounced. Both collagen I and II were produced by fetal pellets in the presence of either TGF-β isoform (**Fig 2-3**). Overall, TGF-β had a stronger influence on fetal MFC pellets than adult MFC pellets, with significant increases in proliferation and meniscus-like fibrocartilaginous matrix deposition. However, even between twin fetuses, biological variability was observed in the magnitude of the response to these exogenous growth factors.

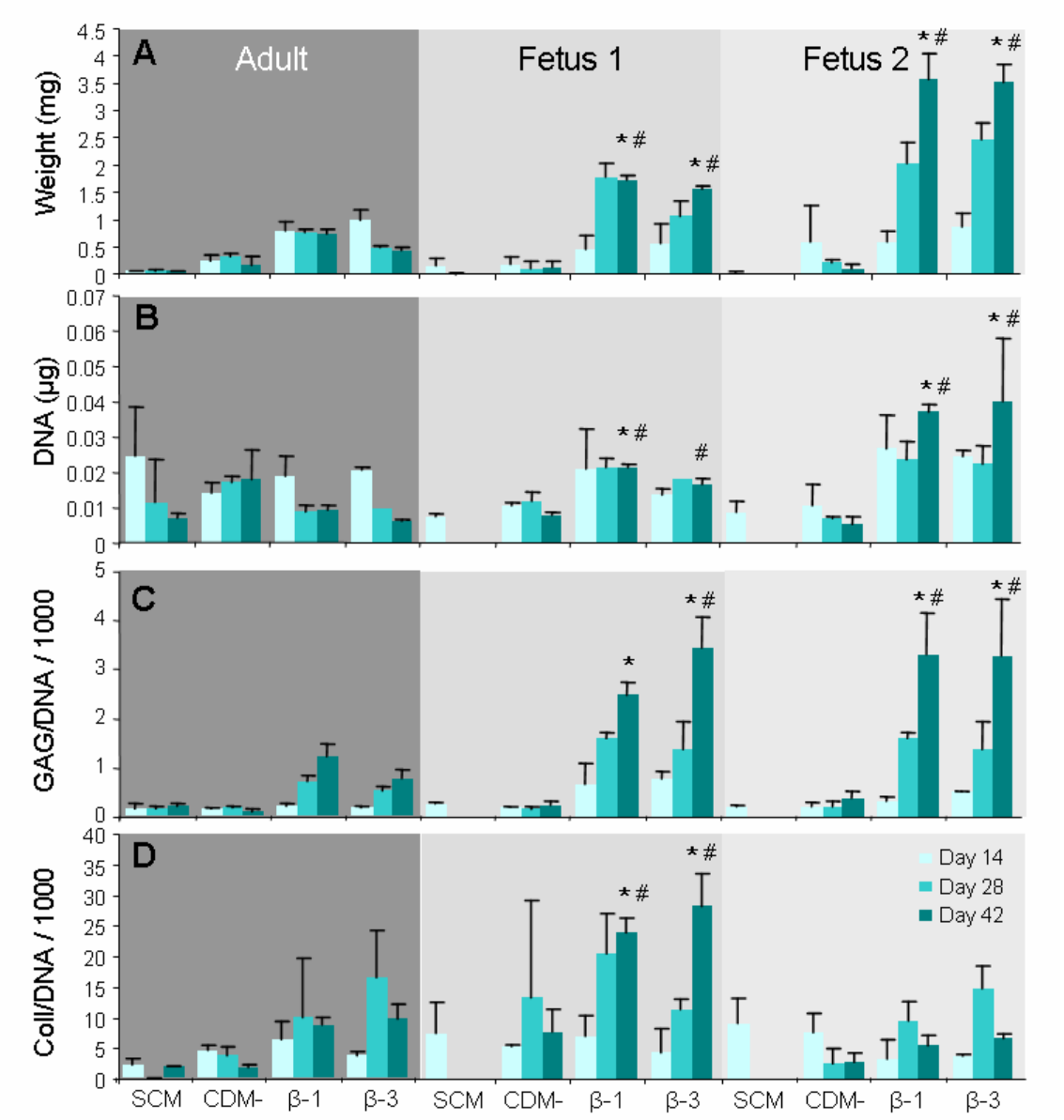

Figure 2-4 Biochemical analysis of fetal and adult MFC pellets. Serum-containing media did not support fetal pellet growth. With the addition of TGF-β, fetal pellets increased with size and matrix deposition compared to adult pellets. (A) Weight of all fetal pellets and TGF-β1-treated adult pellets increased compared to CDM-. (B) DNA content by day 42 increased with the addition of TGF-β for fetal cells compared to the CDM- condition and compared to adult MFCs. (C) GAG content (normalized to DNA) increased in all cases compared to CDM-, with fetal MFCs producing significantly more GAG/DNA compared to adult MFCs. (D) Collagen content (normalized to DNA) increased for fetus 1 MFCs and for adult MFCs. Fetus 1 also increased in collagen content with TGF-β compared to adult MFCs. * indicates significant difference via 2-way ANOVA compared to day 42 CDM- with $p < 0.05$. # indicates significant difference via 2-way ANOVA compared to adult with same TGF-β isoforms with $p < 0.05$.

2.5 Discussion

In this work, we explored tissue-, matrix- and cell-level differences between the fetal and adult ovine meniscus and the response of ovine MFCs to exogenous growth factors TGF-β1 and -β3 in three-dimensional culture. Because young patients rarely present with meniscus tears, understanding differences in cell behavior and ECM structure and production by age may better guide the development of meniscus healing algorithms through recapitulation of successful repair mechanisms in the younger meniscus. The work is further motivated by the observation that complete regenerative healing occurs for a number of tissues in the fetus including cartilage [54], tendon [55, 56], skin [69, 70] and bone [71]. Even in juvenile tissue, work has shown improved (although not scarless) healing compared to adult tissue in anterior cruciate ligaments [72]. While direct exploration of *in vivo* fetal meniscus healing has proved challenging, extraction of the meniscus to a controlled *in vitro* environment allows one to probe various aspects of cell and tissue behavior as a function of developmental stage.

Our results demonstrate that *in situ*, cell density and ECM distribution changed significantly with meniscus tissue maturation, from a cell-dense structure with thin collagen bundles and limited PG content (**Fig 2-1C**), to a cell-sparse structure filled with thick collagen bundles and significant PG distributed throughout the tissue (**Fig 2-1D**). Melrose and coworkers reported similar changes in PG deposition and collagen structure throughout development in sheep meniscus, although that work did not extend to the analysis of fetal meniscus specimens [73]. Clark and Ogden investigated human fetuses and young cadavers and described the progressive development of collagen bundles and decrease in cell density [31]. These findings are consistent with our observations and suggest that the sheep is a good model for the study of meniscus development.

When cells were extracted from the tissue, fetal and adult MFCs proliferated and migrated at the same rate (**Fig 2-2**). Previous work by Webber showed that juvenile and adult rabbit MFCs proliferate at the same rate [74], although they did not explore fetal cells. Interestingly, cells emerged from fetal tissue at a much faster rate compared to adult tissue. Because proliferation and migration did not vary between fetal and adult MFCs in monolayer, the high cellular density of the fetal tissue may explain the markedly higher cell emergence rate from fetal tissue. Further, limited GAG and smaller collagen bundles may create in a more porous ECM that is permissive for cell migration within and out of the tissue and onto the tissue culture plastic compared to dense adult tissue. Clinically, the apparent healing of meniscus in children may relate to the ability of cells to migrate, repopulate and ultimately heal injured regions in less dense immature meniscus. In contrast, cells in the adult meniscus tissue might be effectively trapped inside the dense matrix of their own creation. Work is ongoing to further explore this hypothesis, and preliminary findings suggest enhanced injury repair in immature bovine tissue using an *in vitro* meniscus defect model [75, 76].

When in pellet format, fetal and adult MFCs responded very differently to the chemical environment in which they were cultured. Barry and coworkers found that mesenchymal stem cells successfully differentiated in chondrocytes given the following three conditions: three-dimensional culture environment, serum-free medium, and exposure to a member of the TGF-β superfamily [77]. To maintain phenotype, meniscus fibrochondrocytes are often cultured under the same conditions [65]. In this work, when MFCs were cultured in a three-dimensional format in the presence of serum, fetal pellets were not viable. Histology of the fetal meniscus tissue revealed minimal PG deposition (**Fig 2-1A**), a hallmark of meniscus ECM, suggesting that fetal cells were not yet fully differentiated. Absent a committed fibrochondrogenic-like phenotype, the cells were

unable to withstand three-dimensional culture conditions without a chemically defined and pro-chondrogenic supplement such as TGF-β. In contrast, adult pellets remained viable but proliferated poorly and deposited little PG (Fig 4). Previous work by Mauck also demonstrated juvenile bovine meniscus fibrochondrocytes in pellet culture with serum were viable for 21 days, but exhibited little matrix accumulation [65]. Adult MFC pellets remained viable in serum-containing media, but serum alone could not support or maintain fetal MFCs in pellet form.

Pellets were also grown in a pro-chondrogenic chemically defined media without the addition of the essential growth factor TGF-β (CDM-). Both fetal and adult pellets showed little growth over time under these conditions. In fact, fetal pellets decreased in weight with culture time, perhaps showing a similar sensitivity to the lack of TGF-β as seen in the serum-containing media culture conditions. When TGF-β was added, growth and matrix production was significantly improved, particularly for fetal pellets (**Fig 2-3, 2-4**). Interestingly, Vavkin and coworkers found a decrease in TGF-β receptor density with increased donor age in ACL tissue, although fetal tissue was not assessed [78]. Numerous studies have demonstrated that the addition of TGF-β increases the quantity of DNA [79] and GAG [80-82] over time in meniscus cells. While distinctions between TGF-β isoforms 1 and 3 have been identified, no major differences in growth or matrix deposition were found in this cell type under the given conditions, with only a slight (but not significant) improvement with isoform 1 in adult pellets. TGF-β1 has been associated with an increase in matrix synthesis and a decrease in the production of matrix-degrading proteases in adults in fibroblasts [83, 84] as well as fibrotic scar healing of tendon [56, 85]. TGF-β3 has been shown to be more effective at inducing chondrogenesis than TGF-β1 in mesenchymal stem cells [86] and has been associated

with scarless fetal healing in skin [87]. Our work showed that MFCs responded similarly to both isoforms of TGF-β.

While this work presents compelling similarities and differences in meniscus tissue and cells through development, some limitations do exist. First, it is known that multiple cell types can be identified in the meniscus based on region [10, 79]. However, we did not account for these variations, and instead observed the cell populations in bulk. Further, we used cells at passage 2, where inherent differences may have already been erased due to dedifferentiation with culture expansion. Earlier passage cells may have revealed more about the *in situ* behavior of the cells. In this work, we did not analyze gene expression, which may provide mechanistic insight into the response of the MFCs by age and in response to TGF-β. Also, even when studying twins, the sensitivity to TGF-β was variable, suggesting that even wider variations would be observed between unrelated animals. Lastly, our work only studied the effects of TGF-β. A number of other growth factors might be relevant to explore and could provide additional insight into the differential response of fetal and adult MFCs. For example, Webber found that FGF [10], PDGF and IGF [88] all upregulate MFC proliferation. Despite these limitations, the present work advances our knowledge of meniscus architecture and sensitivity of meniscus cells to soluble factors through development.

2.6 Conclusions

Overall, this study highlights the changing regenerative potential of the meniscus and MFCs from fetal to adult stages. The tissue undergoes significant structural changes, with increases in collagen fiber thickness and decreases in cell density, along with changes in PG distribution. Further, the sensitivity to exogenous growth factors decreases significantly with maturity. Fetal MFC pellets were larger and contained

higher levels of GAG and collagen that increased progressively over 42 days. Taken together, this work suggests that TGF-β induced stimulation of MFC matrix production capacity decreases in adult tissue, and that clinical strategies to bolster matrix production may create a more regenerative state to promote adult meniscus healing.

2.7 Acknowledgements

This work was done in collaboration with Albert O. Gee, Brian J. Sennett, Kenneth W. Liechty and Robert L. Mauck, and was published in numerous abstracts. Funding was provided by the Penn Center for Musculoskeletal Disorders (NIH P30 AR 050950), the Veterans' Administration, an NIH pre-doctoral training grant (NIH T32 007132) and the National Institutes of Health (R01 AR056624)

3: Maturation State Dependent Alternations in Meniscus Integration: Implications for Scaffold Design and Tissue Engineering

3.1 Abstract

The knee meniscus is a crucial component of the knee that functions to stabilize the joint, distribute load, and maintain congruency. Meniscus tears and degeneration are common, and natural healing is limited. Notably, few children present with meniscus injuries, and other related fibrocartilaginous tissues heal regeneratively in immature animals and in the fetus. In this work, we evaluated fetal, juvenile, and adult bovine meniscus properties and repair capacity in vitro, and hypothesized that the properties and repair capacity would be modulated with age. While no changes in cell behavior (migration, proliferation) were noted with age, drastic alterations in the density and distribution of the major components of meniscus tissue (proteoglycan, collagen, and DNA) occurred with development. Coincident with these marked tissue changes, the in vitro healing capacity of the tissue decreased with age. Fetal and juvenile meniscus formed a robust repair over 8 weeks on both a histological and mechanical basis, despite a lack of vascular supply. In contrast, adult meniscus did not integrate over this period. However, integration was improved significantly with the addition of growth factor TGF-β3. Finally, to evaluate engineered scaffold integration in the context of aging, we monitored cellular infiltration from native tissue into engineered nanofibrous constructs. Our findings suggest that maturation processes that enable load bearing in the adult limit endogenous healing potential and identify new metrics for the development of tissue engineered meniscus implants.

3.2 Introduction

The meniscus is a fibrocartilage found in the knee whose primary function is mechanical, withstanding both compressive and tensile forces that arise with locomotion [5]. The extracellular matrix (ECM) is complex in architecture and composition, and is comprised of circumferentially-oriented collagen bundles interspersed with a dense proteoglycan (PG) network [4]. When acute injury or degenerative changes occur, meniscus load-bearing capacity is compromised [9]. Clinically, patients with meniscal tears are treated surgically, with the torn or frayed portion resected or, when possible, reattached [22, 23, 89]. When significant damage occurs, meniscus allografts can be utilized as a total replacement [90]. However, despite restoration of pain free motion with these interventions, the joint compartment remains predisposed to the development of osteoarthritis, as joint mechanics remain altered and non-ideal motion and mechanical forces are imparted to the surrounding tissues [19, 20, 91].

The adult meniscus has limited vascularity and healing capacity [18], and so simple repairs often fail over time. To better study meniscus healing, *in vitro* models have been developed. Early work by Webber and coworkers [92] demonstrated that meniscus sections remain viable in culture media supplemented with bovine serum or in a chemically defined media. Kobayashi and coworkers showed that outer meniscus defects heal better than inner meniscus, at least on a histological basis [93]. More recently, Hennerbichler and coworkers adopted a method commonly employed to assess cartilage-to-cartilage integration [94] to mechanically evaluate meniscus repair *in vitro*. This method involves the formulation of a cylindrical full thickness concentric defect within a meniscus explant [95]. Integration strength is determined by measuring the force required to extrude the inner core from the outer ring. Using this approach, no

measurable differences in mechanical integration were noted comparing the inner and outer regions. This technique has also been used to study the influence and interplay of inflammatory cytokines and matrix metalloproteinases in meniscus healing [35-39]. The organ culture model allows for the careful analysis of healing by region, the influence of soluble factors, and how repair changes over time—factors that are difficult to observe or control in the joint space.

While adult meniscus healing is limited, a number of observations in immature meniscus and related tissues suggest that young fibrocartilage may possess a greater healing potential. First, younger patients rarely present with acute meniscal tears [33]. The repair capacity may be due to the more complete vascular infiltration of immature meniscus compared to adult meniscus, which is only vascularized in the outer third of the tissue [31, 32]. Indeed, repairs to the more vascular outer region of the adult meniscus can have long-term success [26]. Further, *in vitro* studies have shown that juvenile cartilage heals better than adult cartilage even in the absence of a blood supply [96, 97]. Similarly, immature rat lateral collateral ligament heals better than mature ligament *in vivo* [98]. In the fetus, complete regenerative healing of tendon and cartilage has been observed [54-56]. Taken together, these findings motivated us to evaluate differences in healing potential between fetal, juvenile, and adult meniscus, as well as to characterize the properties of the meniscus and associated meniscus fibrochondrocytes (MFCs) as a function of age.

Beyond evaluation of natural tissue healing, this *in vitro* meniscus culture system can be used as a test bed for meniscus tissue engineering, similar to approaches used in cartilage tissue engineering [99-101]. Numerous materials have been tested for meniscus tissue engineering, including collagen [24], small intestinal submucosa (SIS) [42, 43],

estane [45], polyurethane [46], hyaluronic acid [102], agarose gels [47] and alginate [48]. However, due to the complex loading environment many of these approaches have shown limited success *in vivo*. The only material translated to the clinic in the U.S. is the Collagen Meniscus Implant (Menaflex), although its efficiency is not yet clearly demonstrated [24]. A polyurethane foam product (Orteq) is also available in Europe, although its use has not been approved by the US FDA. To expand the palette of materials for meniscus tissue engineering, we have developed a nanofibrous electrospun scaffold, with aligned fibers that mimic the native collagen architecture of meniscus. In these scaffolds, MFCs and mesenchymal stem cells infiltrate and deposit ordered matrix, generating an engineered tissue with physiologically relevant mechanical properties [50-53].

In this work, we evaluated cellular and architectural changes in the meniscus as a function of age. Further, we used an *in vitro* integration model to assess the healing capacity of fetal, juvenile and adult bovine meniscal defects. To expedite integration, we evaluated the effect of the exogenous addition of the chondrogenic growth factor TGF-β [35, 80-82] in explants of different ages. Finally, we established a test bed for the *in vitro* optimization of a tissue engineered meniscus construct by modifying the meniscus integration model to include an electrospun scaffold.

3.3 Materials and Methods

3.3.1 Age-Dependent Characteristics of Bovine Meniscus Fibrochondrocytes

Menisci from fetal (mid-gestation), juvenile (0-3 months) and adult (skeletally mature) cows were sterilely dissected with care taken to remove adherent synovium from the meniscal rim. A 5 mm radial slice was cut, minced into 3 mm^3 pieces and plated onto tissue culture plastic (Corning, Sigma-Aldrich, St. Louis MO) in basal media (DMEM

with 10% fetal bovine serum and 1% penicillin/streptomyosin/fungizone). MFCs emerged onto the plate and divided.

After one passage, cells from each age were used to assess proliferation and migration capacity [103]. Briefly, for proliferation, 20,000 cells were expanded in basal media in individual tissue-culture treated 6-well plates. Each day, in triplicate, the cells were dislodged using a cell scraper and DNA content analyzed using the PicoGreen assay (Invitrogen, Carlsbad, CA). The experiment was performed with three different donors, with one donor data set shown. To assess migration capacity, a defined 'wound' was created in a confluent monolayer with a 0.1-10 μl pipette. The wells were washed to remove cell debris and filled with basal media. Initial light microscope images were captured of the regions and the locations were marked on the plate. Over 15 hours, the same regions were photographed. Extent of infiltration was determined in duplicate using ImageJ (Wayne Rasband, NIH, USA) by measuring the change in area of the gap in a given sample over time.

3.3.2 Histological and Mechanical Alterations in Bovine Meniscus as a Function of Age

Axial and radial samples of meniscus (thickness = 5 mm) from each age were fixed in paraformaldahyde, embedded with paraffin and sectioned. Radial sections were stained with a mixture of Alcian Blue for proteoglycans (PG) and Picrosirius Red for collagens. Axial sections were stained with hematoxylin and eosin (H&E) to identify nuclei.

Unconfined compression testing was performed on native tissue as in [104]. A 4 mm circular explant was taken from the central region of the meniscus in the vertical axis using a dermal punch. The top and bottom of the explant was removed on a freezing

stage sledge microtome to produce cylindrical samples with parallel surfaces (3 mm height, n=6/age). Height was measured using a digital caliper before mechanical testing. Next, a creep test was performed in a PBS bath with a 0.05 N load applied for 5 minutes, with displacement noted at equilibrium. Finally, a stress relaxation test was performed by applying three step-wise compressive deformations of 3% of the post-creep thickness (at 0.05%/s) followed by 800 seconds of relaxation to equilibrium. The compressive equilibrium modulus was calculated from the equilibrium stress and strain values.

3.3.3 Biochemical Analysis of Bovine Meniscus as a Function of Age

To assess biochemical content of meniscus by age, radial sections from different menisci (n=6/age) were divided into three regions (inner, middle and outer) and weighed (**Fig 3**, top). After lyophilization, samples were reweighed to determine water content and digested in a buffer containing 2% papain at 60°C. The resulting digestate was used to assess DNA content (PicoGreen Assay, Invitrogen, Carlsbad, CA), glycosaminoglycan (GAG) content using the DMMB Assay [105] and collagen content using the OHP assay with a conversion factor of 7.14 [68]. Results are reported normalized to sample dry weight.

3.3.4 Integration Potential of Bovine Meniscus as a Function of Age

Fetal, juvenile and adult menisci were isolated as above. Using a sterile 8 mm diameter dermal punch, circular explants were excised from the tissue in the vertical axis. The top and bottom portions of the explant were removed with a scalpel to create parallel surfaces, creating a 3 mm tall cylinder. A 4 mm diameter dermal punch was used to create an inner core, with care taken to ensure that the cut was complete and that minimal rotation occurred (**Fig 3-4A**). Explants were cultured for 8 weeks in basal media supplemented with 50 μg/ml ascorbate-2-phosphate. At bi-weekly intervals, 2

constructs were processed for histology as above. Picrosirius Red stained sections were viewed under polarized light to assess collagen bundle organization at the injury site. At bi-weekly intervals, 7-12 samples were tested for mechanical integration using a custom testing device (Fig 4B) [75, 76, 106]. Briefly, an Instron 5848 was outfitted with a 3.5 mm diameter indenter in series with a 50 N load cell. This indenter was placed above a plate with a 5 mm diameter hole. The meniscus sample was placed onto the plate, and the indenter progressed through the defect site at a rate of 0.0833 mm/sec [95]. Integration strength was determined by normalizing the maximum force by the contact area between the core and annulus. This study was conducted in duplicate, with one representative data set presented.

3.3.5 Integration Potential in the Presence of TGF-β

To assess the influence of the proliferative and pro-chondrogenic growth factor TGF-β3 on the long-term culture and integration potential of meniscus, juvenile and adult meniscus explants were constructed as described above and cultured in either basal media supplemented with 50 μg/ml ascorbate-2-phosphate or basal media supplemented with 50 μg/ml ascorbate-2-phosphate and 10 ng/mL TGF-β3 for 8 weeks. Every 4 weeks, 2 samples were fixed for histology and 7-18 samples were tested for integration strength as above. After testing, both portions of the explant were digested for biochemical analysis. Likewise, histological analysis was conducted on fresh samples from each condition and time point.

3.3.6 Integration Potential of a Fibrous Scaffold

To assess the migratory potential of meniscus cells out of native tissue and through a 3-dimensional engineered structure, 8 mm diameter explants of juvenile and adult menisci were generated. As before, a 4 mm diameter internal core was created, but this time the

core was removed and replaced with an electrospun aligned poly(ε-caprolactone) multi-lamellar column (**Fig 3-8A**). The column was created by spot-welding multiple 4 mm discs of 1 mm thick scaffold at the center point and press-fitting the column into the meniscus annulus. At 4 and 8 weeks, samples were fixed in paraformaldehyde and frozen in OCT sectioning medium. Sections from the top, middle and bottom of each explant were stained with DAPI (Prolong Gold, Invitrogen, Carlsbad CA) to identify cell nuclei. A custom MATLAB program based on [107] was used to quantify cell infiltration by dividing the scaffold into 4 concentric zones with radii equating 25%, 50%, 75%, or 100% of the total scaffold radius. Images were converted to a binary image (**Fig 3-8B**), and for each zone, the cell density (cells/pixel) was normalized by the native tissue density in three 100x100 pixel squares of native tissue, and multiplied by the average native tissue cell count to allow for comparisons across sections and between juvenile and adult tissue.

3.3.7 Statistical Analysis

All statistical analysis was performed using SYSTAT (Chicago, IL) with Bonferonni's post-hoc tests and $p < 0.05$. One-way ANOVA was used to compare the compressive modulus of meniscus by age. For biochemical analysis, one-way ANOVA for age-related differences and two-way ANOVA for age and region differences were employed. Integration strength was compared with a two-way ANOVA with age and culture duration as independent variables. For the TGF-β integration studies, 3-way ANOVA was utilized. Finally, significant differences in cellular distribution in the scaffolds were evaluated via 2-way ANOVA.

3.4 Results

3.4.1 Age-Dependent Characteristics of Bovine Meniscus Fibrochondrocytes

The proliferation and migration capacity of MFCs isolated from fetal, juvenile and adult bovine menisci were compared. Across all ages, proliferation rates were consistent over 14 days (**Fig 3-1A**). Further, no difference in migration into an artificial 'wound' was observed (**Fig 3-1B, 3-1C**).

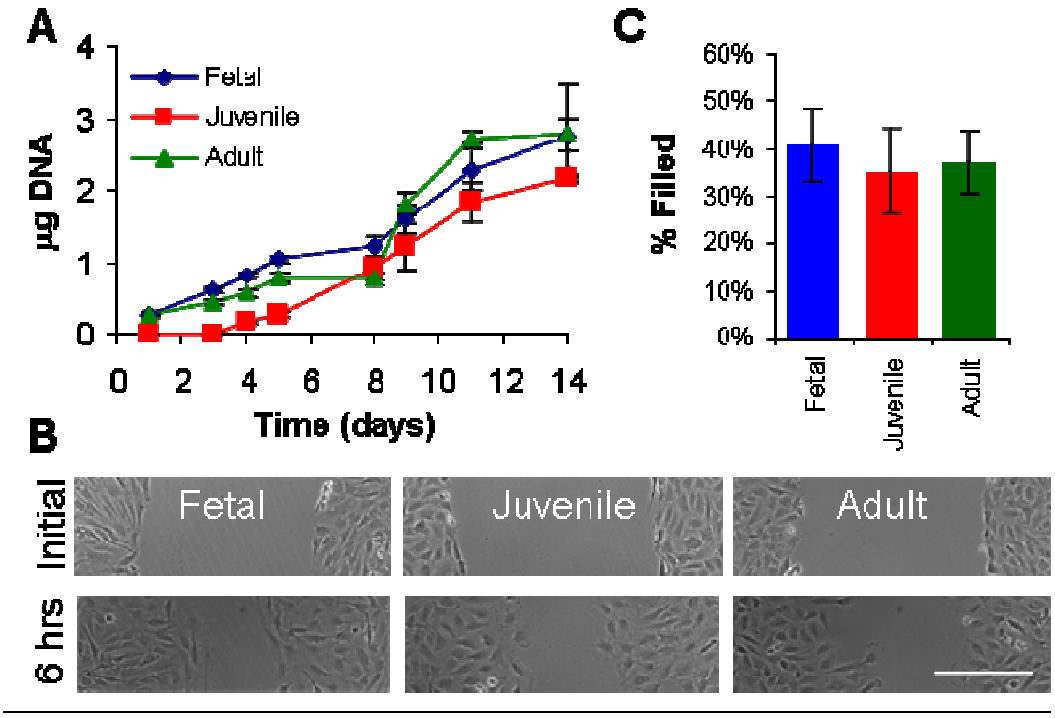

Figure 3-1: Proliferation and migration of fetal, juvenile and adult bovine MFCs are comparable. (A) MFCs proliferate over 14 days at similar rates (n=3/age). (B) Cell migration into a gap was tracked over 15 hours. Example images of the initial gap and appearance after 6 hours for MFCs from each age (Scale = 200 μm). (C) Image analysis of (B) demonstrates similar cell migration rates between MFC ages (n=3/age).

3.4.2 Histological and Mechanical Alterations in Bovine Meniscus as a Function of Age

Histological analysis revealed dramatic structural changes in meniscus through development. The meniscus increased in size with age, particularly in the medial-lateral direction (**Fig 3-2A**). In fetal and juvenile menisci, proteoglycan (PG) was concentrated

in the inner-most tip of the tissue (**Fig 3-2**, arrows) with little staining throughout the rest of the tissue. Adult menisci stained darkly for PG throughout the tissue. H&E staining showed a progressive decline of cell density with advancing age (**Fig 3-2B**). Morphologically, the thickness of collagen bundles increased through development (**Fig 3-2B**). The age-dependent changes observed histologically were concurrent with mechanical changes, with ~5-fold improvements in the equilibrium compressive modulus between each age tested.

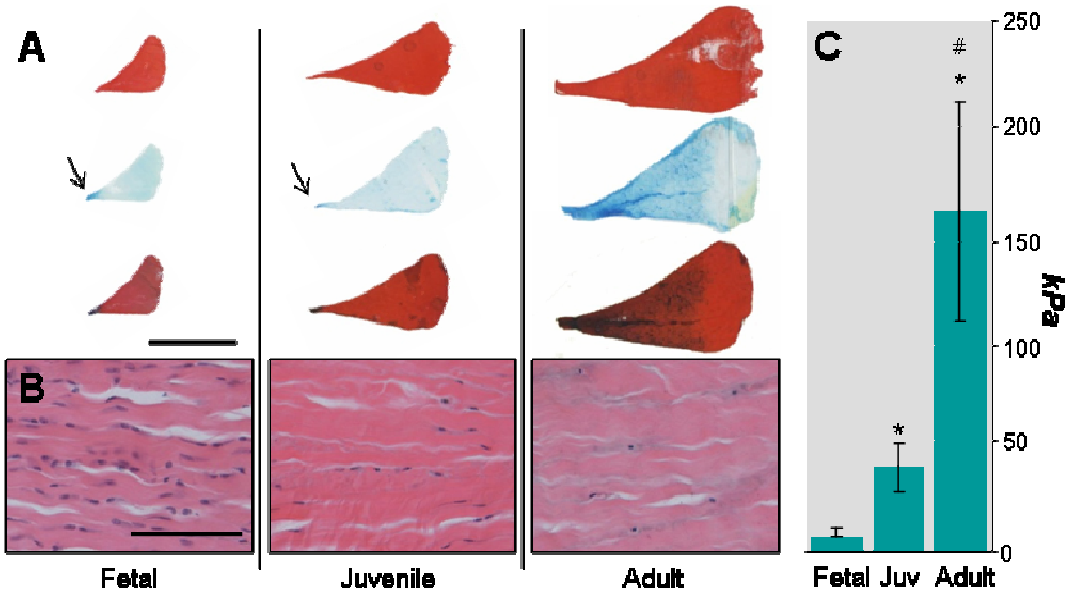

Figure 3-2 Histological and mechanical properties of bovine meniscus are modulated by age. (A) Radial sections from the central region of the meniscus stained with Picrosirius Red (top), Alcian Blue (middle), and a combination of the two (bottom) reveals changes in tissue size and PG distribution (blue) with age (Scale: 10 mm). Arrows indicate concentration of Alcian Blue staining at the inner tip. (B) Transverse sections of meniscus stained with H&E reveal decreasing cell density with age (Scale: 100 μm). (C) Compressive equilibrium modulus increases significantly with each increase in age (n=6). * indicates difference from fetal with $p<0.0001$. # indicates difference from juvenile with $p<0.0001$.

3.4.3 Biochemical Analysis of Bovine Meniscus as a Function of Age

Samples from the inner, middle and outer region of the meniscus were digested to elucidate biochemical changes with development. Overall, water content did not change with age (**Fig 3-3A**). In contrast, fetal and juvenile meniscus contained significantly

lower GAG content than adult meniscus (**Fig 3-3B**). Fetal meniscus had significantly more GAG in the inner region than the outer region, although by the juvenile stage, difference by region was less pronounced. Adult meniscus also had significantly more GAG in the inner region compared to outer region. Further, the relative proportion of GAG in the middle region of the meniscus increased in adult specimens. The overall collagen content increased significantly from fetal to juvenile meniscus, but remained the same between juvenile and adult meniscus (**Fig 3-3C**). The outer region of the fetal meniscus had significantly less collagen than the other regions, perhaps due a blending of the synovial rim with the tissue early in development. By juvenile and adult stages, there were no differences in collagen content between regions. Finally, adult meniscus had significantly less DNA content than fetal or juvenile meniscus (**Fig 3-3D**). Cell density in the fetal meniscus showed the largest distribution with location, with significantly more DNA found in the inner region compared to the outer region. With maturation, the distribution of DNA equilibrated.

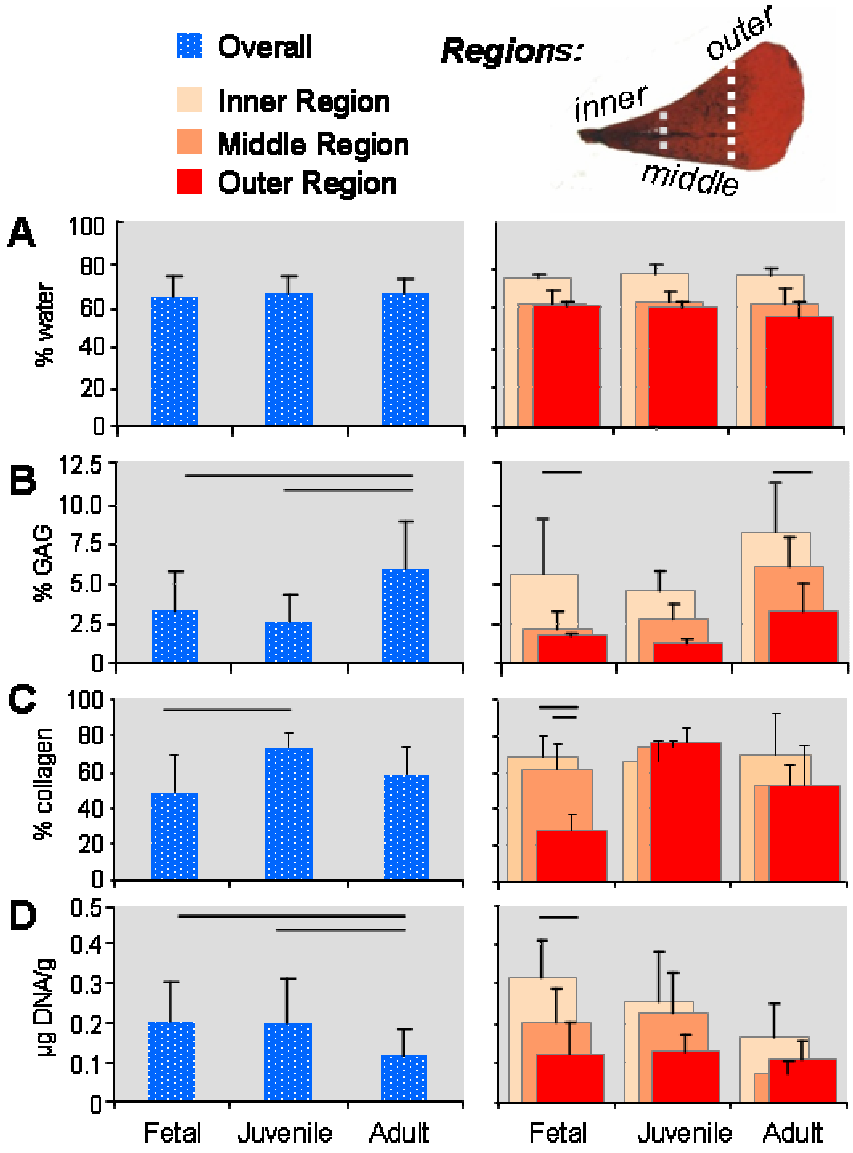

Figure 3-3 Biochemical content and distribution of the bovine meniscus is modulated by age. (A) Water content as a function of tissue wet weight. (B) GAG, (C) collagen content as a percent of dry weight. (D) DNA content per dry weight. N = 6/region/age. – indicates significant differences between groups with $p<0.05$.

3.4.4 Integration Potential of Bovine Meniscus as a Function of Age

For each age, circular meniscus explants with concentric full-thickness defects were formed and cultured for up to 8 weeks. Histology revealed continual improvements in matrix connectivity at the injury site in fetal and juvenile tissue. In contrast, no integration was seen in adult samples through 8 weeks (**Fig 3-5A**). Viewing the 'best'

integrated samples (juvenile, week 8) under polarized light microscopy showed that while new collagen was deposited at the injury site, this new matrix was not aligned or contiguous with the surrounding collagen bundles (**Fig 3-5A**, green arrows).

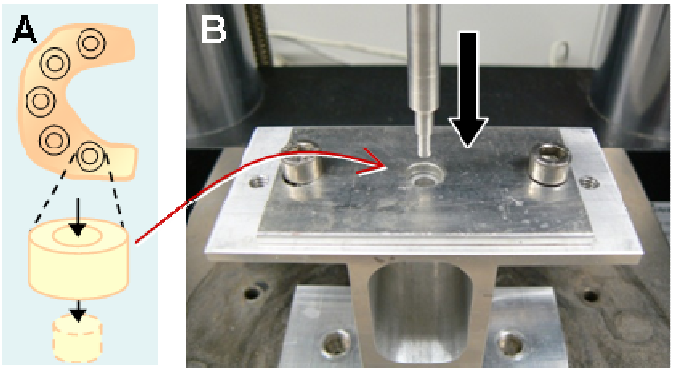

Figure 3-4 Experimental design for meniscus integration studies. (A) Cylindrical explants (8 mm) were removed sterilely from fetal, juvenile and adult meniscus. After flattening surfaces, central cores were punched with a 4mm dermal punch, removed, and replaced into the original position to simulate a full-thickness meniscus injury. (B) A custom mechanical testing device was used to measure the force required to extrude the inner core from the meniscus explant.

The mechanical testing results mirrored these histological observations. Fetal explants improved in integration strength over 8 weeks, with significant improvements at 6 and 8 weeks compared to week 0 ($p < 0.05$). Integration strength of juvenile defects increased at a slower pace, with significant improvements by week 8. The integration strength of adult samples did not change (**Fig 3-5B**).

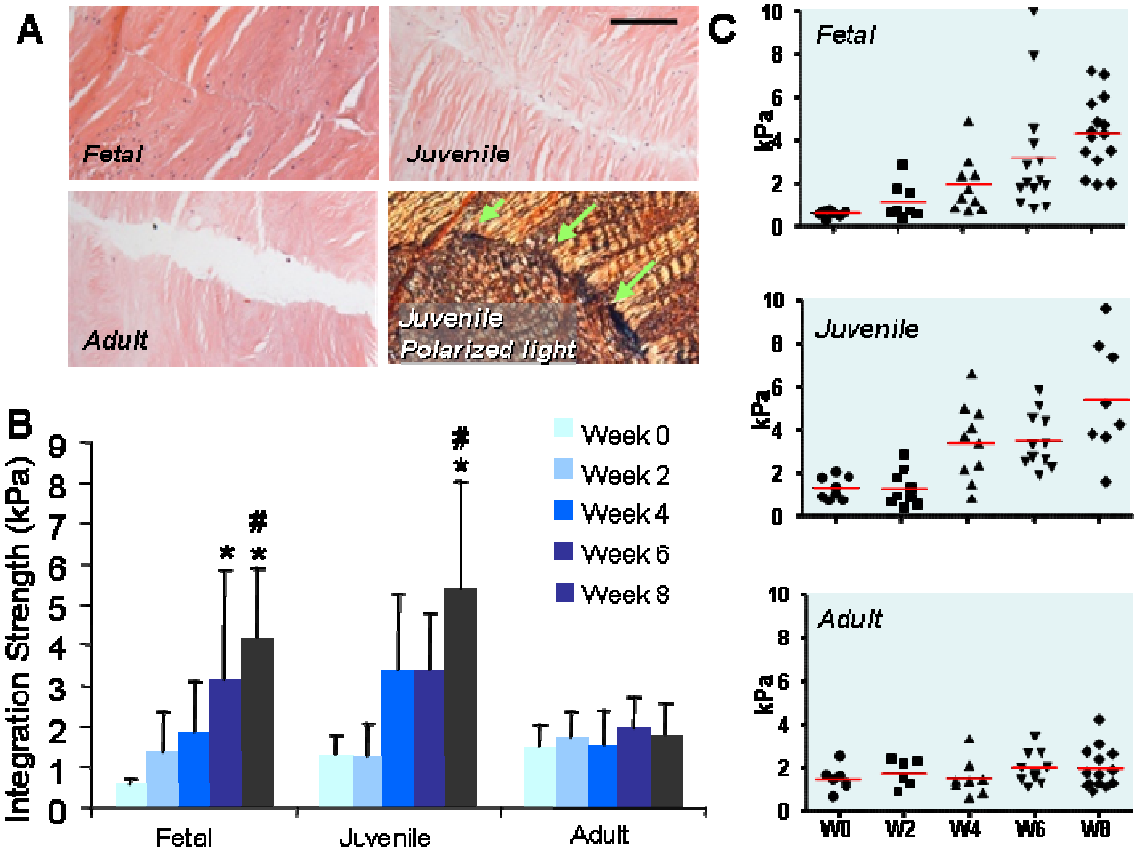

Figure 3-5 Age-dependent integration of bovine meniscus. (A) H&E staining of the injury site at week 8 shows signs of repair in fetal and juvenile tissue, but not in adult tissue (Scale = 200 μm). Lower right: Picrosirius Red staining of 8 week juvenile sample viewed under polarized light reveals lack of collagen continuity at the injury site. (B) Integration strength as a function of meniscus age with time in culture. Integration strength increases significantly for fetal and juvenile samples, but not for adult samples. (C) Mechanical testing results demonstrating variability in response between specimens. N = 7-12. * indicates significant difference ($p < 0.05$) from week 0. # indicates significant difference ($p < 0.05$) compared to adult week 8.

3.4.5 Integration Potential in the Presence of TGF-β

To further improve repair, juvenile and adult meniscus explants were cultured with and without 10 ng/mL TGF-β3, a concentration previously shown to promote matrix deposition in meniscus fibrochondrocytes [50, 51, 65]. Addition of TGF-β3 increased matrix deposition at the injury site in both juvenile and adult samples (**Fig 3-6A, B**). Picrosirius Red staining revealed no major changes in collagen levels (**Fig 3-6C, D**). However, Alcian Blue staining of PG was significantly greater in explants cultured in the

presence of TGF-β (**Fig 3-6C, D**). Even in the presence of TGF-β, some sections of the injuries appeared to be disconnected. It is unclear if this is an artifact from histology, or if these regions contribute to the variability seen in the mechanical testing results.

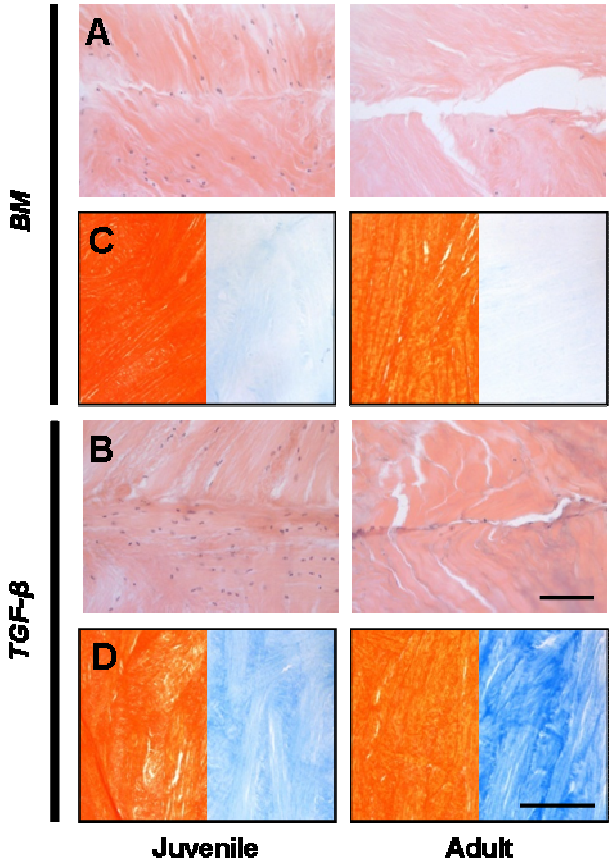

Figure 3-6 Histological analysis of integration in the presence or absence of TGF-β after 8 weeks of in vitro culture. (A) H&E staining reveals that while the juvenile sample appears to have healed across the injury site, no obvious integration is visible in the adult sample. (B) The addition of TGF-β improved cell and matrix formation at the injury site for both juvenile and adult samples. Scale = 100 μm. (C and D) Picrosirius Red staining (left) is consistent across samples at 8 weeks. However, Alcian Blue staining (right) of PG reveals significant depletion in the presence BM compared to TGF-β in both juvenile and adult specimens. Scale = 500 μm.

The integration strength of both juvenile and adult meniscus explants improved 7-fold by 8 weeks with the addition of TGF-β, reaching 97 kPa and 57 kPa, respectively (**Fig 3-7A**). Continued exposure to TGF-β for 8 weeks resulted in significant improvements from week 4 and compared to basal media alone. Further, juvenile meniscus integration

strength was significantly higher than adult meniscus integration strength by 8 weeks. Biochemical analysis of the tissue after mechanical testing showed that GAG content decreased over time when cultured in basal media; GAG content was far below native tissue, particularly for adult tissue (**Fig 3-7B**, dotted line). Conversely, addition of TGF-β maintained native levels of GAG in the explants. Due to the lower initial concentration of GAG in juvenile tissue, the quantity of GAG in the explants cultured in TGF-β did not increase significantly. However, adult explants had almost 2-fold more GAG by 8 weeks than explants cultured in basal media alone. Further, adult explants contained significantly more GAG than juvenile explants cultured in the same conditions, similar to the trend in native tissue. These quantitative measures of GAG content correlate well with histological staining (**Fig 3-6C and 3-6D**). Even in the presence of TGF-β, DNA content in explants fell below native levels (**Fig 3-7C**). Similar to native tissue, adult explants had significantly less DNA than juvenile explants. As shown via histology (**Fig 3-6C, 3-6D**) and by quantification (**Fig 3-7D**), collagen content did not change between groups or over time.

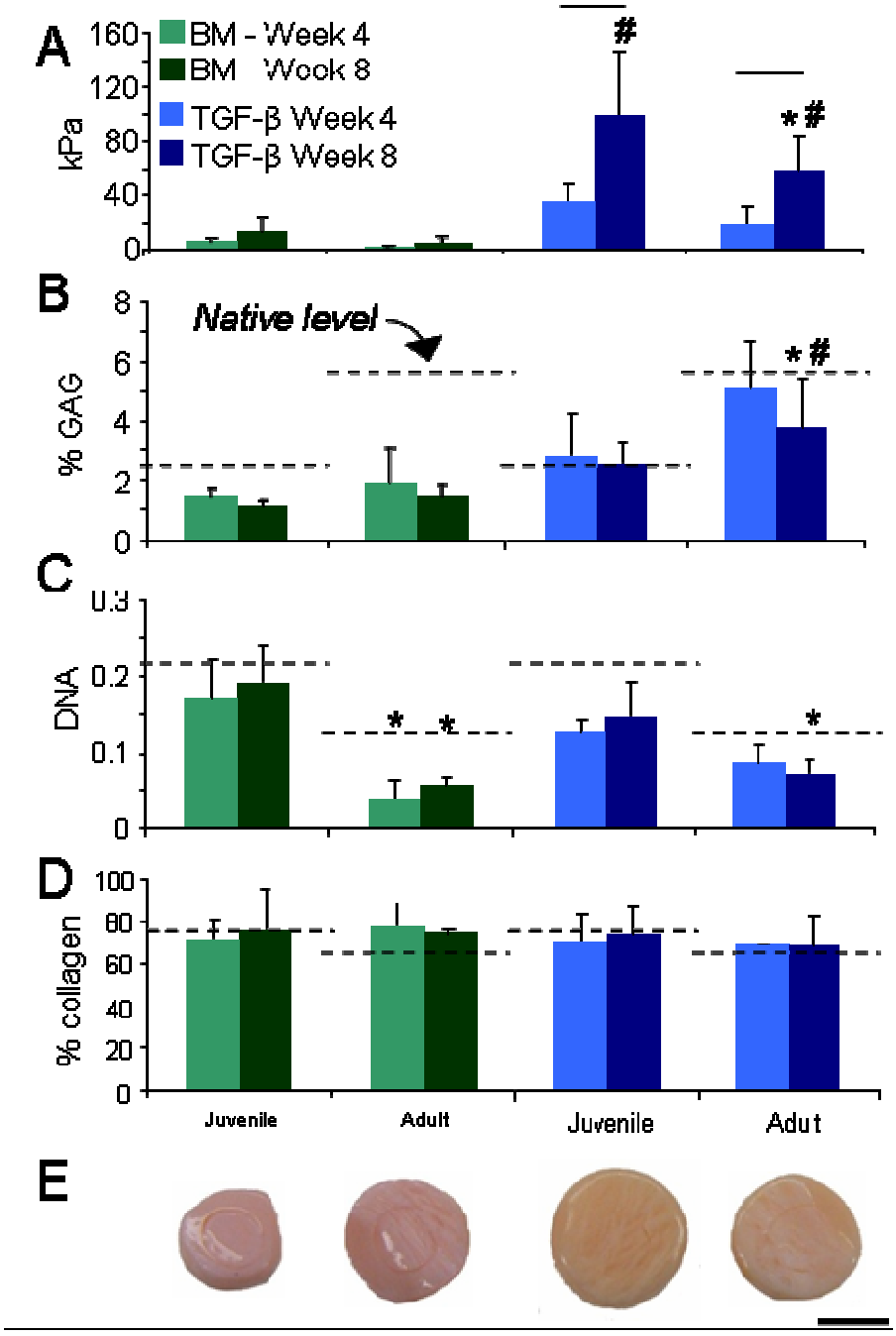

Figure 3-7 TGF-β improves integration strength and preserves explant GAG content after 8 weeks of in vitro culture. (A) Integration strength of juvenile and adult defects improved in the presence of TGF-β (n = 7-18) compared to basal media (BM). (B) GAG content was depleted in the absence and maintained in the presence of TGF-β (n = 6) compared to native tissue (dashed line). (C) DNA content decreased in all conditions. (D) Collagen content remained consistent across all conditions. (E) Appearance of explants after 8 weeks in culture. Scale = 5 mm. * indicates significant difference ($p < 0.05$) between ages within a given media condition and time point. # indicates significant difference ($p < 0.05$) between media conditions at a given time point. – indicates significant difference ($p < 0.05$) between time points within a given media condition and age.

3.4.6 Integration Potential of a Fibrous Scaffold

To evaluate integration between engineered materials and native meniscus, PCL was electrospun in 1mm thick aligned sheets and cut into 4mm diameter discs. These discs were subsequently spot-welded to one another to form columns (**Fig 3-8A**) that were situated inside juvenile and adult meniscus explants and cultured for 1, 3 and 6 weeks. Despite the significantly higher native tissue density of juvenile tissue, similar numbers of cells populated the scaffolds by 6 weeks (**Fig 3-8D**). The infiltration was progressive and occurred more quickly for juvenile compared to adult explants, with significantly fewer cells in the adult scaffold than in the juvenile scaffold at 3 weeks. No differences were detected in cell density between the bottom, middle and top of the column, suggesting uniform infiltration from the exterior circular wall of the native tissue. In terms of location (**Fig 3-8E**), most cells were located in the outer-most zone (1) adjacent to the native tissue and the fewest cells reached the center region (4). Although juvenile tissue had almost 5-fold higher average cell density, the zonal cell density was similar between juvenile and adult tissue.

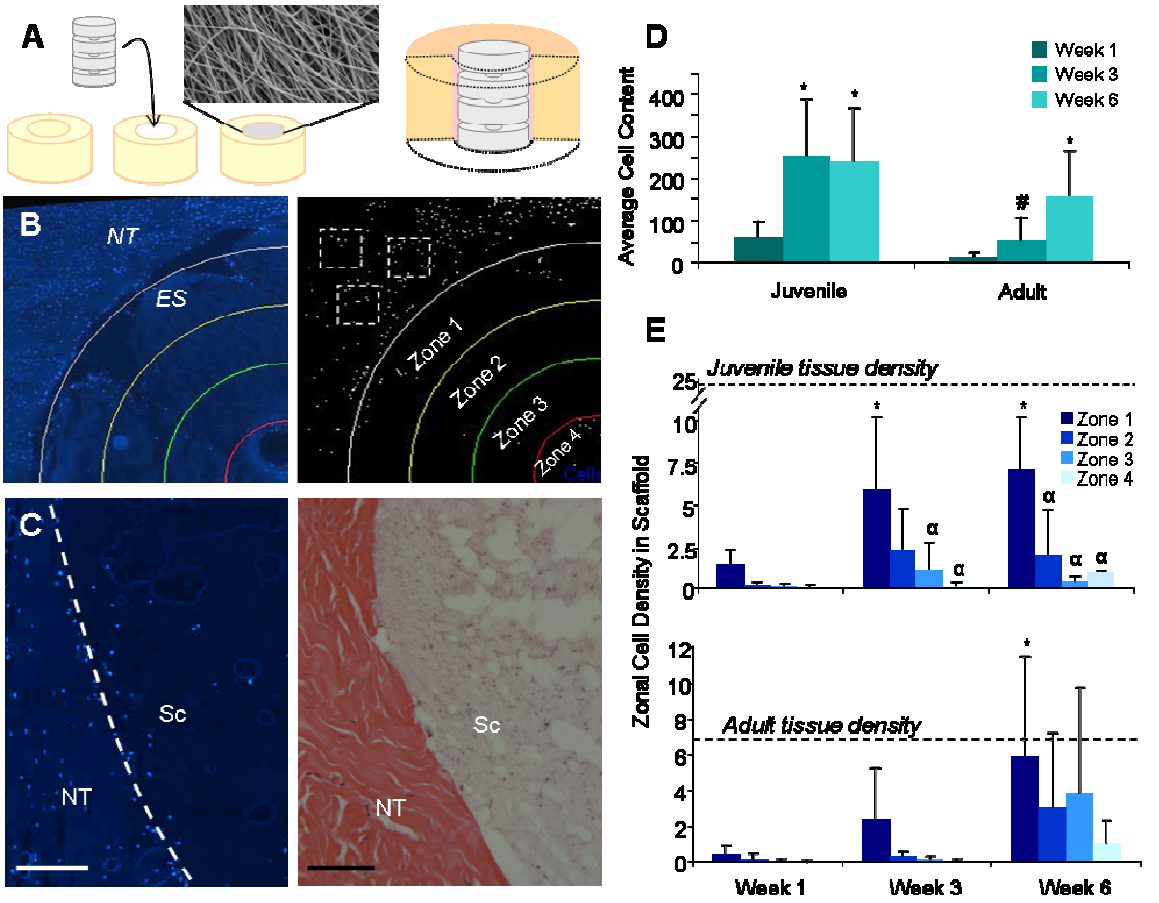

Figure 3-8 Comparable cellular infiltration in juvenile and adult meniscus defects repaired with nanofibrous scaffolds. (A) Cylindrical meniscus explants were formed, and a central core was removed and replaced with a column of electrospun poly(ε-caprolactone) nanofibrous scaffold disks welded together at the central point. (B) Cell infiltration into the cylindrical constructs was quantified using a custom MATLAB program. Left: Excerpt of image of the DAPI-stained composite with the electrospun scaffold (ES) region divided to quantify cell infiltration from the surrounding native tissue (NT). Right: Cells were counted in binary images by zone. Native tissue density was determined using 3 regions from each image (boxes) and averaged across all samples. (C) Left: DAPI staining of integration zone between native tissue (NT) and scaffold (Sc). Scale bar = 100 μm. Right: H&E staining of integration zone. Scale bar = 500 μm. (D) Significant cell infiltration was seen after 3 and 6 weeks for juvenile and adult meniscus defects, respectively. By week 6, scaffold infiltration was comparable between ages (n=9/age/timepoint). (E) Juvenile cells populated the scaffold more rapidly than adult scaffolds, although the overall densities were comparable despite a significantly higher starting density in juvenile native tissue. * indicates significant difference ($p < 0.05$) from week 1. # indicates significant difference ($p < 0.05$) between ages. α indicates significant difference ($p < 0.05$) from zone 1.

3.5 Discussion

While injury to the meniscus is the leading cause for orthopedic surgery [17], therapeutic options are limited and still often lead to the development of osteoarthritis [19, 20, 108, 109]. In this work, we characterized cell behavior, tissue architecture, and integration potential of the meniscus as a function of age given prior evidence of healing in immature meniscus [33] and in related juvenile [72, 96, 98] and fetal [54-56] fibrocartilaginous tissues. Further, we established a test bed for the optimization of a tissue engineered scaffold.

When bovine MFCs were extracted from fetal, juvenile and adult menisci, age did not alter their behavior in monolayer culture. Consistent with these findings, we have previously shown that in the ovine model, fetal and adult MFCs proliferate and migrate at the same rate [103]. In contrast, related cell types, such as ACL fibroblasts and dermal fibroblasts, lose proliferation and migration capacity with age [57, 58].

At the tissue level, meniscus size and architecture changed with development. In fetal and juvenile meniscus, cell density was higher, collagen bundles were smaller, and PG was concentrated in the inner tip of the tissue. In adult tissue, PG filled the majority of the tissue, DNA content decreased and became more uniform, and collagen fiber bundles increased in thickness. The majority of these changes occurred upon skeletal maturity (i.e. from juvenile to adult), rather than progressively through early development. Our findings are corroborated by other work in the field; similar changes in PG deposition and collagen development were noted by Melrose and coworkers in an ovine model [73]. Chen and coworkers found that PG content increased with age, DNA content decreased, and collagen content increased in the inner region of the meniscus from the fetus to

adult in bovine meniscus tissue [110]. Further, Clark and Ogden observed progressive changes in collagen bundle thickness and cell density in human fetal and juvenile meniscus [31].

These architectural changes corresponded to functional improvements in the compressive moduli concomitant with the increasing weight-bearing demands in the joint. The equilibrium compressive modulus (163 kPa) for adult bovine tissue was higher than that found in human tissue (25-37 kPa) [6] and is similar to that reported for porcine meniscus (170-350 kPa) [7]. Chen and coworkers found similar compressive properties for fetal tissue, but a significantly lower compressive modulus (30 kPa) in the adult [110]. The differences in adult compressive modulus may be attributed the location from which the samples were obtained; Chen and coworkers tested explants from the inner region perpendicular to the femoral surface of the meniscus, while we tested explants taken from the middle region of the meniscus perpendicular to the tibial surface.

The similarities between fetal and juvenile meniscus were also apparent in the explant integration studies (**Fig 3-5**). Both fetal and juvenile defects increased in integration strength by 8 weeks, although fetal explants improved at a faster rate. In contrast, and as is seen clinically in the avascular region, adult meniscus showed very little healing [26]. Interestingly, DiMicco and coworkers demonstrated that fetal cartilage does not heal as well as juvenile cartilage *in vitro* [96], suggesting that although the meniscus and cartilage are related, the healing mechanisms at young ages may be different between these tissues.

TGF-β is known to promote the deposition of a fibrocartilaginous matrix and the maintenance of phenotype in MFCs [65, 79, 80, 82]. Exposure of meniscus explants to 10 ng/mL of TGF-β3 for 8 weeks improved integration strength significantly, to 7 times the level of basal media alone (~100 kPa) (**Fig 3-7A**). Adult meniscus healed significantly better with the addition of TGF-β, though juvenile meniscus improved more than adult meniscus. Previously, McNulty and coworkers utilized a similar *in vitro* model to evaluate the dose responsivity (0.1-10 ng/mL) to TGF-β1 and found a small but significant improvement at the 1 ng/mL dose (12 kPa) after 14 days. TGF-β played a number of roles that may contribute to the observed improvement in healing. First, it maintained the PG content of explants over 8 weeks (**Fig 3-6D**) compared to basal media alone. Imler and coworkers previously showed that the addition of TGF-β to meniscus explants increases sulfate incorporation [111]. Interestingly, GAG content in the explants cultured in basal media were comparable between ages at 8 weeks, despite significantly higher initial GAG content in adult explants. Further, the loss was progressive, with adult meniscus segments failing to maintain native levels of GAG at 8 weeks, even in the presence of TGF-β. While leaching or degradation of PG may an artifact of *in vitro* culture, the power of TGF-β to promote PG deposition to native levels may contribute to the regeneration of meniscus-like ECM at the site of injury. In keeping with these findings, Wilson and coworkers recently showed that PG levels in meniscus explants decreased over time in culture, and that the addition of TGF-β increased PG levels in the tissue [112]. Further, exposure to a broad-spectrum metalloproteinase inhibitor significantly reduced PG loss over time [113].

While no quantitative improvements in collagen content were found, histology of the injury site suggested that more collagen was deposited with exposure to TGF-β3. Further, we have previously found that immature ovine MFCs deposit more collagen

than adult MFCs in the presence of TGF-β when cultured in pellets [103]. DNA levels decreased in all explants to 50-75% of native levels. Cell death may occur early in culture due to the lack of physiologically relevant stimuli, impaired nutrition, or from the process of defect formation itself. These observations are another artifact of *in vitro* culture, but must be considered when endeavoring to develop *in vitro* protocols for meniscus repair.

Translating this work to tissue engineering approaches, we incorporated electrospun scaffolds into this *in vitro* defect model. These scaffolds support MFC proliferation and matrix deposition over time, and increase in mechanical properties *in vitro* using both bovine and human cells [50, 51]. Despite marked differences in tissue structure and composition, implanting these scaffolds into juvenile and adult meniscus defects yielded surprisingly similar results. While the infiltration of the scaffold was somewhat faster in younger tissue, after 8 weeks the average cell number within was comparable, despite significantly more cells adjacent to the scaffold in the juvenile tissue (**Fig 3-8C**). Similar to the behavior in monolayer culture (**Fig 3-1**), migration into and subsequent proliferation in the scaffold were comparable by age, although perhaps slightly better distributed in the scaffold containing adult MFCs. The finding suggests that while heightened cell density at the injury site may promote integration, it may not improve colonization and maturation of a tissue engineered scaffold.

Identifying distinguishing features of immature, healing meniscus may provide new directions for advancing repair in the adult and tailoring engineered scaffolds to advance regeneration. Specifically, we noted a simultaneous loss of healing capacity with increased GAG concentration, decreased DNA content, and thickening of collagen bundles. Modifying the structure of mature meniscus to more closely resemble immature

meniscus might promote healing. While depletion of GAG appears to be an interesting therapeutic option, GAG levels depleted quickly and significantly during *in vitro* culture (**Fig 3-7B**). The addition of TGF-β maintained near-native levels of GAG content and improved integration, suggesting that GAG depletion may in fact hinder meniscus repair rather than promote it. Similarly, the quantity of DNA dropped in all meniscus samples with *in vitro* culture. While the addition of TGF-β did not change the overall DNA content of the explants, it is possible that small local increases in cell density occurred at the injury sites and bolstered healing. Drug delivery of TGF-β directly to the site of injury at high doses through a system such as the one described in [114] may support local proliferation at the injury site. While bulk collagen content did not change progressively with tissue maturation, the bundle size increased. No major changes in collagen content were observed during *in vitro* culture, even in the presence of TGF-β. However, it is possible that small increases in collagen content occurred at the injury site. It may be speculated, but remains to be seen, that decreasing collagen bundle size through partial degradation might enhance tissue healing.

Although this work contributes to our knowledge of the meniscus and develops an *in vitro* test bed for the integration of tissue engineered materials with native tissue, some limitations do exist. First, we only analyzed overall collagen and GAG content, rather than considering individual components that may vary with development. While culturing explants for 8 weeks allowed us to evaluate the reparative capacity of the tissue, this *in vitro* environment is artificial, with no mechanical loading and loss of PG and cellularity. Also, we have only explored one concentration of TGF-β, whereas other concentrations may have yielded different or improved integration levels. Given that matrix formation, integration, and healing will depend on both anabolism and catabolism, it will be important to explore expression and activity of matrix

metalloproteinases (MMPs) and other matrix modulating enzymes in future studies. Further, although cells infiltrated the electrospun scaffold, minimal matrix was deposited (data not shown) due to a lack of additional matrix stimulating factors in the media that might also influence migration, proliferation, and tissue formation. Finally, while this *in vitro* test bed provides a facile system for understanding meniscus healing and optimizing scaffold design, it may not translate directly to the *in vivo* articular environment. Future work will include extending these experiments to clinically relevant large animal models, as well as models involving human meniscus tissue to ensure that our *in vitro* findings translate to clinical applicability.

3.6 Conclusions

Overall, this study explored developmental changes in bovine meniscus in terms of tissue architecture, extracellular matrix distribution and content, and cell behavior. These changes corresponded to differential integration capacity of the meniscus with aging. Integration was significantly enhanced by the addition of the exogenous growth factor TGF-β, which also served to better maintain overall explant properties. Moreover, we showed that *in vitro* models such as this can be test beds for optimizing engineered meniscus scaffolds before *in vivo* implantation. To glean instructive information regarding healing with age, we noted that while cell behavior did not change with age, the overall balance between cells, GAG and collagen content in the meniscus changed markedly. While loss of GAG content to immature meniscus levels (a natural consequence of the *in vitro* culture system) did not promote adult meniscus healing, increasing local DNA content or decreasing collagen fiber diameter remain viable targets for enhancing repair. As such, this work identifies new targets for meniscus tissue engineering as well as a method for testing and optimizing potential clinical solutions for meniscus repair.

3.7 Acknowledgements

This work was done in collaboration with Gregory C. Lee, Grant H. Garcia, Tiffany L. Zachry, Roshan P. Shah, Brian J. Sennett, and Robert L. Mauck, and was published Tissue Engineering Part A (2011 Jan;17(1-2):193-204). Funding was provided in part by the National Institutes of Health (R01 AR056624 and T32 AR007132) and the Penn Center for Musculoskeletal Disorders.

4: Growth Factor Supplementation Improves Native and Engineered Meniscus Repair *in Vitro*

4.1 Abstract

Few therapeutic options exist for meniscus repair after injury. Local delivery of growth factors may stimulate repair and create a favorable environment for engineered replacement materials. In this study, we hypothesized that basic fibroblast growth factor (bFGF) (a pro-mitotic agent) and transforming growth factor beta 3 (TGF-β3) (a pro-matrix formation agent) would modulate meniscus repair and the integration/ maturation of electrospun poly(ε-caprolactone) (PCL) scaffolds for meniscus tissue engineering. Circular meniscus defects were formed and refilled with either native tissue or scaffolds. Constructs were cultured in serum-containing media for 4 and 8 weeks with various growth factor formulations, and assessed for mechanical strength, biochemical content and histological appearance. Our results showed that either short-term delivery of bFGF or sustained delivery of TGF-β3 increased integration strength for both juvenile and adult bovine tissue, with similar findings for engineered materials. While TGF-β3 increased proteoglycan content in the explants, bFGF did not increase DNA content after 8 weeks. This work suggests that *in vivo* delivery of bFGF or TGF-β3 may stimulate meniscus repair, but that the timecourse of delivery will strongly influence success. Further, electrospun scaffolds are a promising material for meniscus tissue engineering with comparable or superior integration properties compared to native tissue.

4.2 Introduction

The meniscus is a C-shaped fibrocartilage in the knee that distributes load from the femur to the tibia [1, 2]. Its unique architecture, composed of aligned collagen bundles and centrally-located proteoglycan, allow it to withstand both tensile and compressive forces in order to maintain joint stability during movement [3]. Due to the strong forces imparted on the tissue [5], both acute and degenerative tears are common, and natural repair capacity is limited, especially in the inner avascular regions [15]. Of the 850,000 meniscus surgeries performed annually in the US [115], resection is the most common technique to alleviate symptoms associated with meniscal tears. However, the procedure can result in joint incongruency and significantly increased loads on the surrounding cartilage, which can lead to osteoarthritis [19, 20]. Few procedures exist to repair the meniscus and none have gained widespread acceptance. Thus, there is a need for novel repair strategies for meniscus repair.

Delivery of biological factors may stimulate tissue repair either alone or in combination with mechanical stabilization. Early work delivered vascular endothelial growth factor (VEGF) from sutures to stimulate blood vessel formation in the damaged region [116]. However, delivery of VEGF from sutures failed to improve healing *in vivo* in a number of studies, perhaps due to suboptimal timecourse of delivery [117, 118]. Rather than modulating the vascular supply, another approach is to alter the biochemical properties of the tissue using different growth factors. During repair, new matrix must be formed by nearby cells to bridge the wound edges, creating a mechanically stable interface across the damaged region. Increasing the amount of matrix deposited by each cell or increasing the overall number of cells (or a combination of the two) would improve repair. One of the most potent stimulators of matrix deposition by meniscal cells is

transforming growth factor beta 3 (TGF-β3) [65, 77, 80, 104, 111], although other growth factors such as bFGF, PDGF-AB, IGF-1 and EGF all increase matrix production to a lesser extent [119]. Basic fibroblast growth factor (bFGF) strongly stimulates proliferation of meniscus cells in monolayer culture as well as in tissue engineered constructs [10, 119-121]. Both TGF-β3 and bFGF were identified as potential repair factors for meniscus by Kasemkijwattana *et al* [122], and Imler *et al* showed that TGF-β3 stimulated protein and proteoglycan deposition more than bFGF in meniscus explants [111]. Due to the ability of these growth factors to stimulate matrix deposition and improve cell density, they are promising candidates for repairing avascular meniscus tears as well as promoting the maturation and integration of engineered materials *in vivo*.

Another important parameter is the timecourse for delivery of these factors. Many growth factors function during a very specific window and at precise doses, and may work in concert with other cues [123]. Clinically, growth factors could be delivered with a bolus injection or via sustained release from a biomaterial over a given period of time; continual delivery of growth factors over a long period of time is not a clinically relevant dosing regimen. Fortunately, recent work suggests that short-term exposure to growth factors may actually have superior efficacy compared to continual delivery, perhaps due to reduced receptor desensitization [124]. For example, agarose hydrogels containing bovine chondrocytes were exposed to 2 weeks of TGF-β3, and had more matrix deposition than continual delivery of TGF-β3 for 2 months [125]. Similar results were found when dynamic loading was applied [126] and with mesenchymal stem cells [127].

Chemical cues alone may not be sufficient to restore meniscus function in situations where repair is not possible. To address this issue, tissue engineering generates

structures that, with time *in situ*, recapitulate native tissue architecture and behavior [14]. Recently, biodegradable scaffolds composed of porous collagen (Menaflex) or porous polyurethane (ActiFit) were developed to replace regions of resected meniscus, but their use is limited due to questions surrounding their efficacy. Another promising approach to meniscus repair utilizes electrospun scaffolds, which are fabricated by collecting nano-sized synthetic and biological polymeric fibers on electrically charged surfaces [53]. These scaffolds are amenable to cell attachment, proliferation and infiltration [107, 128, 129]. Further, they can be functionalized to release chemicals such growth factors [130-132]. More work is needed to understand how electrospun scaffolds become colonized by native cells, what is the strength of the scaffold/meniscus interface, and what are the key modulators in this integration process.

Because large animal studies of meniscus repair are quite costly, smaller *in vitro* experiments are beneficial for assessing the potential of novel therapies [94]. Early work demonstrated that meniscus tissue remains viable when cultured in proper media conditions [92]. Later, concentric explants were used to test the influence of inflammatory cytokines and matrix metalloproteinases on meniscus integration [35]. More recently, we have used this model to demonstrate that, in accordance to observations made clinically [33], immature meniscus heals better than mature meniscus *in vitro* [128] and that TGF-β3 bolsters that integration [35, 128]. Also, we filled meniscus rings with electrospun scaffolds and demonstrated increased colonization of scaffolds with time in culture [128]. While juvenile tissue is significantly more cellular than adult tissue, both were colonized at the same rate, suggesting at innate speed for colonization despite starting cell density [128]. In order to further functionalize these scaffolds, we also developed a technique to deliver drugs from PLGA microspheres entrapped between electrospun fibers using a sacrificial fiber population, with limited

impact on mechanical properties and independent release profiles [114]. These microspheres could eventually release growth factors to promote repair in meniscus.

To further these lines of inquiry, we treated juvenile and adult bovine meniscus defects with TGF-β3 and bFGF for both short-term (1 week) and sustained (8 weeks) timecourses, alone and in combination, and assessed the mechanical integration strength of the repair as well as the biochemical content of the repair material. Further, we 'repaired' meniscus defects with electrospun scaffold and tested the mechanical integration of the two materials under various growth factor delivery schemes and timecourses. If successful, growth factors found to improve repair could be released from fibers or entrapped microspheres *in vivo*. We hypothesized that bFGF would improve integration properties by increasing the cell density in the tissue, and that short-term delivery of the growth factors would result in comparable integration to continual delivery. Further, mechanical integration of electrospun scaffolds would be comparable to tissue integration.

4.3 Materials and Methods

4.3.1 Evaluation of Meniscus-to-Meniscus Repair with Growth Factor Addition

Menisci were dissected from the knee joints of juvenile (0-3 months old) and adult (skeletally mature) bovine limbs in a sterile manner. Cylinders (8 mm diameter x 3 mm thick) were excised centrally in the axial direction using a dermal punch (Miltex, Plainsboro, NJ), as shown in **Figure 4-1A**. To simulate a meniscus tear, a full-thickness inner columnar defect (4 mm diameter) was made and the core reinserted with care to maintain fiber alignment, as shown in **Figure 4-1B-C**.

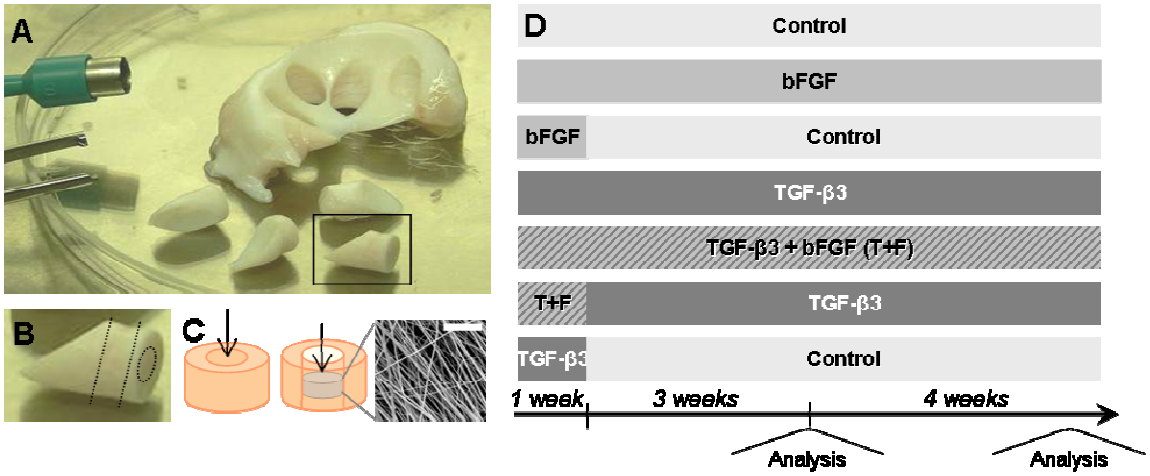

Figure 4-1 Experimental set-up and design. (A) 8 mm cylinders were excised from bovine meniscus. (B) The cylinders were flattened and a smaller biopsy punch was used to remove a 4 mm core. (C) The core was either reinserted back into the tissue (left), or replaced with a 1 mm thick disc of electrospun PCL (right, inlay scale = 20 μm). (D) Temporal schematic of media formulations over 8 weeks and testing timepoints.

Meniscus repair constructs were cultured in control media (Dulbecco's modified Eagle's medium (DMEM) with 10% fetal bovine serum (FBS), 1% penicillin/streptomysin/ fungizone (PSF), 50 μg/mL ascorbate-2-phosphate) supplemented with 5 different growth factor regimens: continual 50 ng/mL bFGF, 1 week of bFGF, continual 10 ng/mL TGF-β3, combined continual bFGF and TGF-β3, combined 1 week bFGF and continual TGF-β3, or 1 week of TGF-β3 (**Figure 4-1D**). After 4 and 8 weeks of culture, the mechanical integration strength was evaluated using a custom testing device [128]. Briefly, an Instron 5848 was outfitted with a 3.5 mm diameter indenter in series with a 50 N load cell. This indenter was placed above a plate with a 5 mm diameter through-hole. The meniscus sample was placed onto the plate, and the indenter progressed through the defect site at a rate of 0.0833 mm/sec. Integration strength was calculated as:

$$Integration\ Strength = \frac{Maximum\ \ force\ (N) \cdot 1000}{2\pi r \cdot h}$$

where r was the core radius (2 mm). Height (h) of the interface was determined by averaging four caliper measurements of the construct prior to testing (n=5-8/condition, work performed in triplicate for control, TGF-β3 and bFGF conditions, duplicate for all other conditions, all data shown).

4.3.2 Biochemical and Histological Analysis of Meniscus-to-Meniscus Repair

After testing, the meniscus-to-meniscus construct was reassembled and prepared for biochemical analysis by lyophilizing and digesting the tissue in a buffer containing 2% papain at 60°C. The resulting digestate was used to assess DNA content (PicoGreen Assay, Invitrogen, Carlsbad, CA), glycosaminoglycan (GAG) content (DMMB Assay [67]) and collagen content (OHP assay with a conversion factor of 7.14 [68]). Results were normalized to sample dry weight. Histological analysis was conducted on fresh, untested samples at each condition and time point. Constructs were fixed in phosphate-buffered 4% paraformaldahyde (PFA), embedded in paraffin and cut into 8 μm sections that were placed onto glass slides. Samples were stained with Alcian blue for proteoglycans (PG), Picrosirius red for collagen, and DAPI (Prolong Gold, Invitrogen, Carlsbad, CA) or a mixture of hematoxylin and eosin (H&E) to identify cell nuclei. Immunohistochemical staining for anti-phospho-histone H3 (Sigma-Aldrich, Saint Louis, MO), a proliferation marker, was performed after antigen retrieval (2% hyaluronidase), followed by exposure to hydrogen peroxide and background blocking (Background Buster, American Master Tech, Lodi, CA) for 10 minutes each, using 8 μm sections of rat spleen as a positive control (*data not shown*). The primary antibody was incubated for 90 minutes at room temperature, with subsequent secondary antibody incubation and color development using the SuperPicture DAB kit (Invitrogen, Carlsbad, CA). Images were acquired at 20X using a Nikon Eclipse 50i microscope with NIS Elements F3.0 software

4.3.3 Formation of Electrospun Scaffolds

To generate electrospun scaffolds for meniscus repair, 14.3% w/v poly(ε-caprolactone) (PCL, 80 kDa, Sigma-Aldrich, St. Louis MO) in a 1:1 mixture of tetrahydrofuran (THF, Fisher Chemical, Fairlawn NJ) and N,N-dimethylformamide (DMF, Fisher Chemical) was mixed overnight. A 20 mL syringe was filled with PCL electrospinning solution and fitted with a stainless steel 18G blunt-ended needle that served as a charged spinneret. A flow rate of 2.5 mL/h was maintained with a syringe pump (KDS100, KD Scientific, Holliston, MA). A power supply (ES30N-5W, Gamma High Voltage Research, Inc., Ormond Beach, FL) applied a +13 kV potential difference between the spinneret and the grounded mandrel located at a distance of 12 cm from the spinneret. Additionally, two aluminum shields charged to +10 kV were placed perpendicular to and on either side of the mandrel to better direct the fibers towards the grounded mandrel. The mandrel was rotated via a belt mechanism conjoined to an AC motor (Pacesetter 34R, Bodine Electric, Chicago, IL) at a speed of 10 m/sec to form 800 μm thick mats.

4.3.4 Evaluation of Meniscus-to-Scaffold Repair

After scaffold fabrication, 4 mm scaffold discs were excised using a dermal punch and sterilized under UV light for 10 minutes. Meniscus constructs were created as previously described, but instead of reinserting the central core of the construct, a disc of scaffold was press fit into the defect **(Figure 4-1C)**. The scaffold repair constructs were cultured in 5 different growth factor regimens: control, continual 50 ng/mL bFGF, 1 week of bFGF, continual 10 ng/mL TGF-β3, or combined 1 week bFGF and continual TGF-β3 (n=8-10/condition, performed in duplicate for control and TGF-β3 conditions). After 4 weeks, mechanical integration was assessed as described above, with h of the scaffold disc measured using an OptoNCDT laser measuring device (Micro-Epsilon, Raleigh, NC) after testing. Scaffolds were digested and analyzed for biochemical content as previously

described. Similarly, histology was performed by fixing samples in 4% PFA, embedding in Cryo-OCT Compound (Tissue Tek, Fisher, Fairlawn, NJ) with an axial orientation, sectioning and staining as previously described.

4.3.5 Statistical Analysis

For this work, 2-way ANOVAs were performed using SYSTAT software (Chicago, IL) to compare timepoints and conditions using Tukey's post-hoc test. In some conditions, non-TGF-β3 groups were considered separately from TGF-β3 groups, as indicated. Significance was set at $p \leq 0.05$.

4.4 Results

4.4.1 Evaluation of Meniscus-to-Meniscus Repair with Growth Factor Addition

Meniscus-to-meniscus repair constructs were formed and cultured *in vitro*. Overall, and similar to previous findings [128], juvenile tissue integrated to a greater extent than adult tissue, with 2- to 4-fold differences in integration strength after 8 weeks **(Figure 4-2A,B)**. After 8 weeks, short-term (1 week) delivery of 50 ng/mL bFGF resulted in better integration compared to control conditions or continual addition of bFGF for both juvenile and adult tissue. Exposure to TGF-β3 resulted in more extensive improvements in integration strength compared to all non-TGF-β3 groups after 4 weeks in juvenile and after 8 weeks in adult meniscus-to-meniscus samples. In this context, transient bFGF did not further improve repair. Interestingly, continual delivery of bFGF in the context of continual TGF-β3 resulted in integration properties comparable to those found in the absence of TGF-β3. Transient delivery of TGF-β3 resulted in comparable integration strength to continual TGF-β3 exposure after 4 weeks but not after 8 weeks.

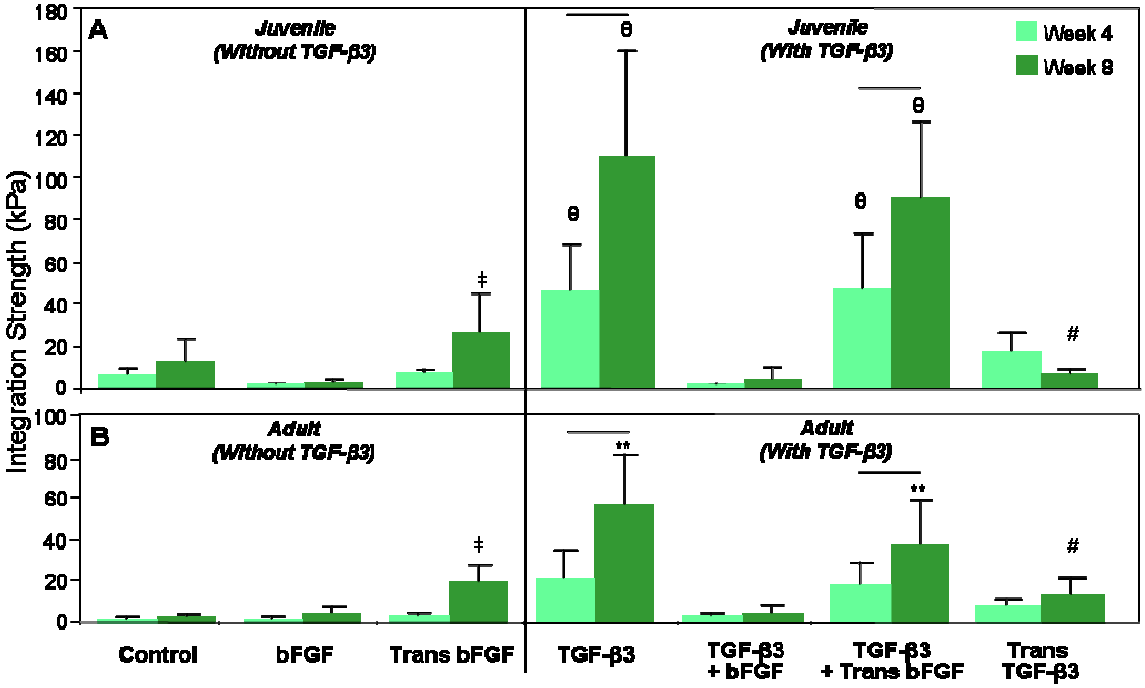

Figure 4-2 Integration properties of meniscus-to-meniscus repair constructs. (A) Juvenile integration strength. (B) Adult integration strength. Growth factors and timecourse of delivery strongly influenced integration properties, with TGF-b3 increasing integration strength the most, followed by transient bFGF. Continual bFGF or a mixture of bFGF and TGF-β3 did not improve integration. ‡ indicates difference from control and continual bFGF, comparisons made only between non-TGF-β3 groups. θ indicates difference from all non-TGF-β3 groups and bFGF+TGF-β3. Line indicates difference between timepoints. # indicates difference from TGF-β3 and transient bFGF+TGF-β3. For all comparisons, $p < 0.05$; n = 10-24/condition.

Biochemical analysis revealed minor fluctuations in DNA content across all groups, with increases after 4 weeks in the continual presence of bFGF and in conditions of transient bFGF. However, these effects were no longer apparent at 8 weeks **(Figure 4-3B)**. GAG content was higher and closer to native levels in all samples exposed to TGF-β3, with some variations in the group containing TGF-β3 and bFGF **(Figure 4-3C)**. Juvenile and adult tissue responded in similar patterns to the different media formulations in terms of biochemical content.

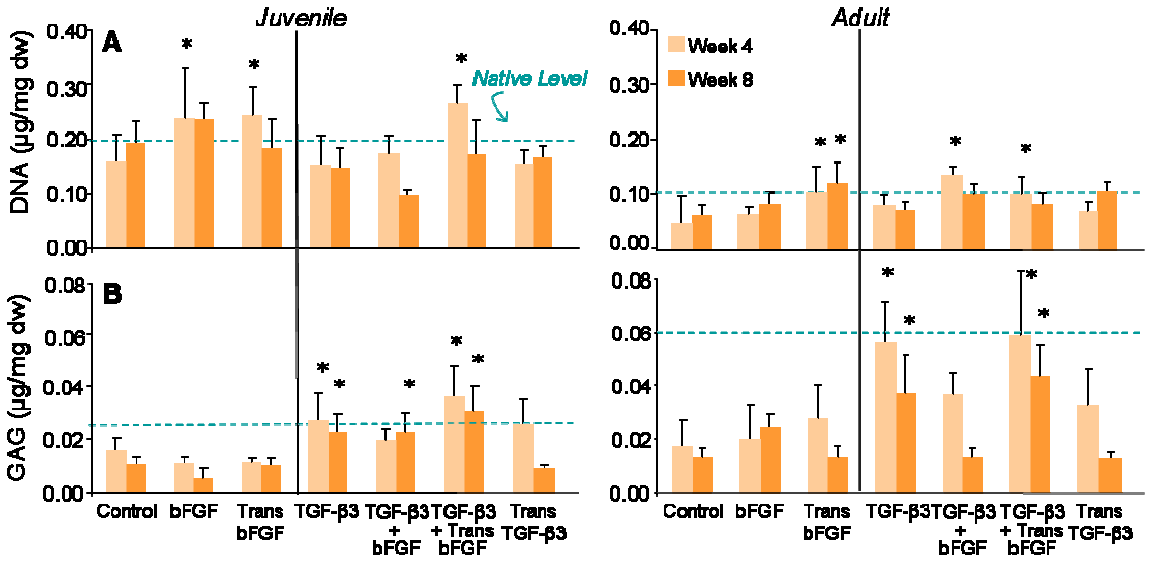

Figure 4-3 Biochemical content of meniscus-to-meniscus repair constructs. (A) Short term and continual bFGF increased DNA content at 4 weeks, but the effect mostly subsided by 8 weeks. (B) Continual delivery of TGF-β3 stimulated GAG deposition in the constructs. Data normalized to dry weight. * indicates difference from control. For all comparisons, $p < 0.05$.

Histologically, cells populated the injury rim in all conditions, with more tissue bridging the injury region in constructs cultured with continual TGF-β3 alone. No connections formed when TGF-β3 and bFGF where delivered simultaneously **(Figure 4-4Ai)**. The injury region did not stain strongly for proliferating cells, despite the presence of bFGF **(Figure 4-4Aii)**. While few significant differences were noted between groups at the injury region, there were major differences at the exterior edge of the tissue, where a thick cell sheath formed in the presence of TGF-β3 **(Figure 4-4Bi)** that stained strongly for proliferating cells only when bFGF was added **(Figure 4-4Bii)**. Because continual combined delivery TGF-β3 and bFGF also resulted in sheath development and exhibited low integration strength, the sheath alone does not account for the large forces required to separate the tissue explants. In contrast, only a very thin layer of cells stained positively for proliferation in the presence of bFGF alone. Overall, the groups exposed to TGF-β3 had the greatest PG staining in the bulk of the tissue **(Figure 4-4Biii)** compared to non-TGF-β3 groups.

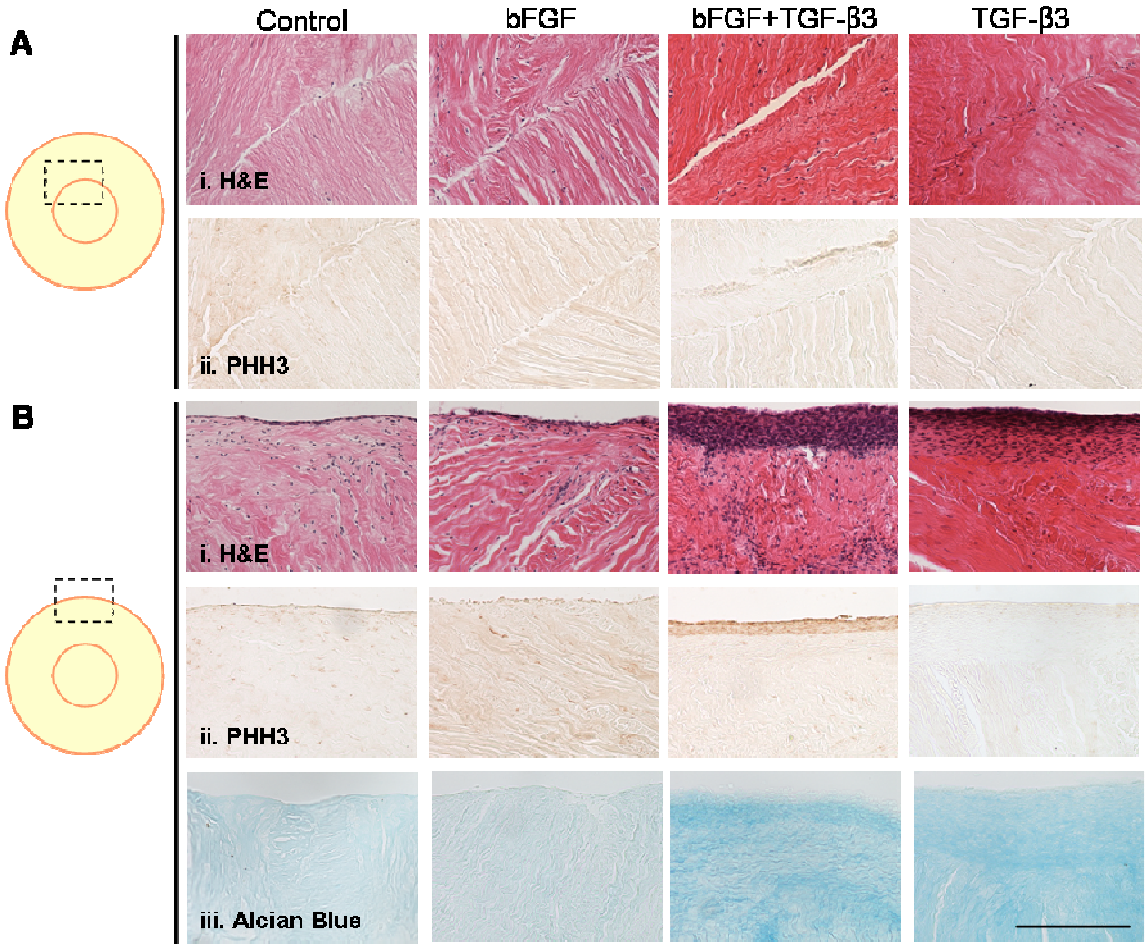

Figure 4-4 Histology of meniscus-to-meniscus repair constructs. (A) The injury region and (B) the outer edge after 8 weeks in either control media or media supplemented with bFGF, both bFGF and TGF-β3, or TGF-β3. H&E (i) identifies cell nuclei, PHH3 (ii) identifies cells in mitosis, and Alcian Blue (iii) stains for glycosaminoglycans. Scale = 200 μm.

4.4.2 Evaluation of Meniscus-to-Scaffold Repair with Growth Factor Addition

Aligned PCL electrospun scaffolds **(Figure 4-5A)** were used to fill meniscus defects in order to form meniscus-to-scaffold repair constructs. Generally, the integration properties of meniscus-to-scaffold constructs in various media conditions followed the same pattern as meniscus-to-meniscus repair constructs **(Figure 4-5A)**. In control conditions, meniscus-to-scaffold integration strength was 2- to 3-fold greater than meniscus-to-meniscus integration. Unlike meniscus-to-meniscus repair constructs, transient application of bFGF did not further improve integration strength. Similar to

meniscus-to-meniscus repair, the continual addition of bFGF significantly decreased integration strength. The addition of TGF-β3 resulted in 2-fold improvements in integration strength that were comparable to meniscus-meniscus construct integration. Similar to previous findings, transient bFGF did not improve integration in the presence of TGF-β3. Unlike the native tissue, biochemical content of the scaffolds did not vary significantly, with inclusion of bFGF only slightly improving cellularity and TGF-β3 producing small increases in GAG and collagen content compared to controls **(Figure 4-5B)**.

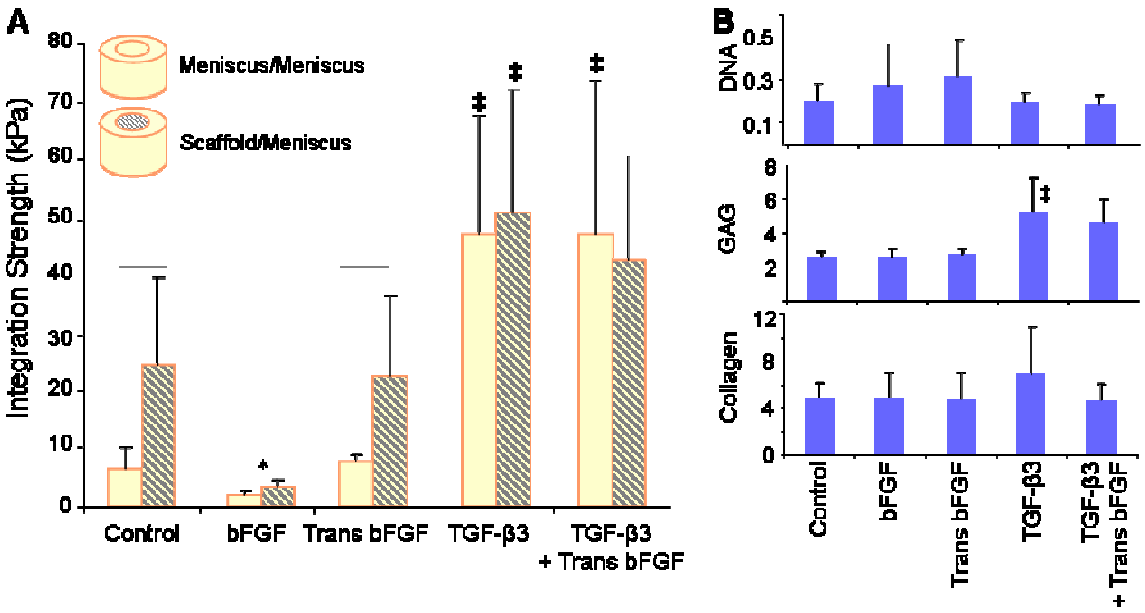

Figure 4-5 Integration properties of meniscus-to-scaffold repair constructs. (A) Scaffold-to-meniscus integration is better than meniscus-to-meniscus integration in the absence of TGF-β3 after 4 weeks. Integration strengths are comparable in the presence of TGF-β3. (B) Cell density and collagen content does not change in different media conditions; TGF-β3 increases GAG content slightly. Line indicates difference between groups and * indicates difference from control and transient bFGF, considering only non-TGF-β3 groups. ‡ indicates difference from non-TGF-β3 groups. For all comparisons, $p < 0.05$; n = 8-20/condition.

Histologically, we observed that meniscus cells from the tissue colonized the scaffold, populating the outer regions most densely after 4 weeks **(Figure 4-6C)**. Both collagen (red) and proteoglycan (blue) were found throughout the scaffold **(Figure 4-6D)**, particularly when constructs were cultured in the presence of TGF-β3 **(Figure 4-6E)**. In the absence of TGF-β3, little tissue was found bridging the scaffold and the native tissue compared to constructs exposed to TGF-β3 **(Figure 4-6F)**.

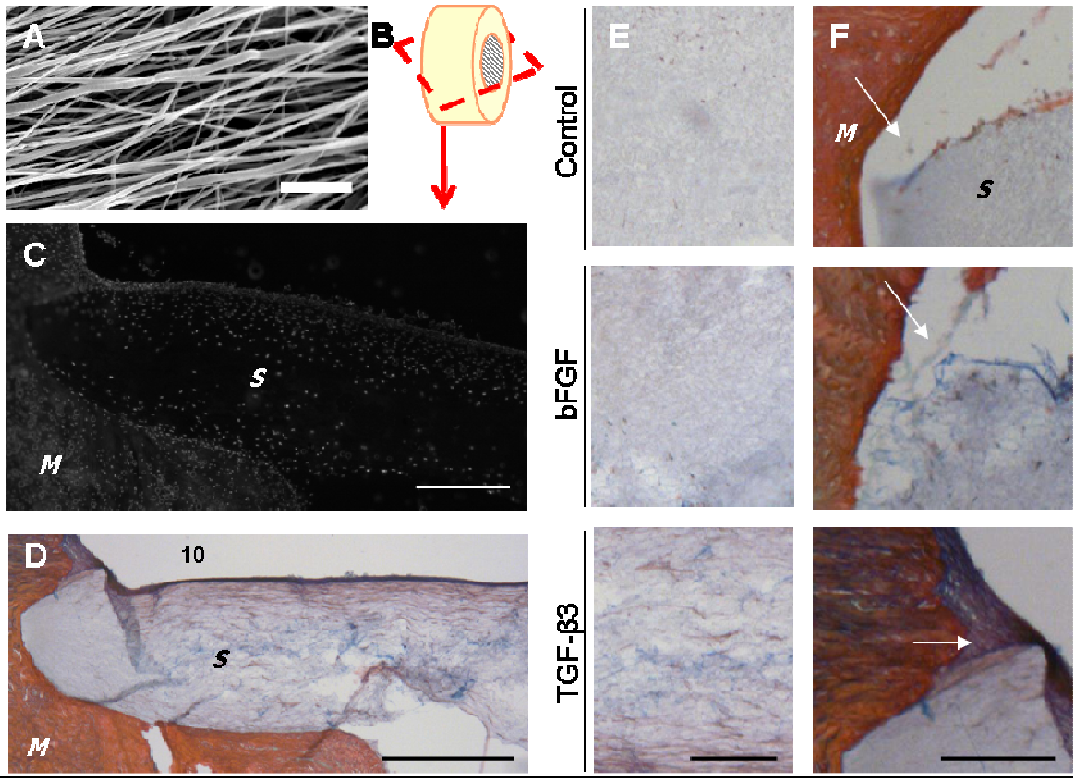

Figure 4-6 Histology of meniscus-to-scaffold repair constructs. (A) SEM of electrospun scaffolds (scale = 10 μm). (B) Schematic of sectioning plane for histology. (C) DAPI staining reveals cells in the scaffold ('S ') and in the meniscus ('M ') after 4 weeks (scale = 500 μm, TGF-β3 treated). (D) Collagen (red) and GAGs (blue) are found in the scaffold, although are not as dense as the native meniscus tissue (M) (scale = 500 μm, TGF-β3 treated). (E) Matrix deposition in the scaffold in various media conditions (scale = 200 μm). (F) Neo-tissue (white arrows) bridges the scaffold and meniscus in TGF-β3 conditions, but not in control or bFGF conditions (scale = 200 μm).

4.5 Discussion

Clinical techniques to repair or replace the knee meniscus remain limited. Here, we explored how delivery of various growth factors, their combination and the duration of delivery might modulate the repair response. First, we studied growth factors in the context of acute, avascular meniscal tears, which represents 2/3 of the tissue [26]. Hypercellular juvenile and hypocellular adult meniscus tissue were studied, and patterns of repair were similar across both groups, with juvenile tissue healing twice as strongly as adult tissue [128]. These findings suggest that there are no innate differences to growth factor response by age. Growth factors were provided to the tissue through the aqueous environment; however, *in vivo* delivery will require a finite delivery time course, and so short-term, 1-week delivery schemes were also explored. Short-term delivery of bFGF was superior to continual bFGF and control conditions, although neither bFGF conditions resulted in a sustained increase in cell density beyond 4 weeks, contrary to our hypothesis. This finding suggests that cells in meniscus explants are not as sensitive to the mitogenic effects of bFGF as cell in monolayer [10, 119-121]. Perhaps the differences in response can be associated with modification of cell phenotype when in monolayer expansion; Kato *et al* found that chondrocytes, a related cell population, only had elevated matrix synthesis with exposure to bFGF during the logarithmic cell expansion phase and not after becoming confluent [133]. Supporting this theory, cells in bFGF-containing media did not stain more for the proliferation marker PHH3 within the bulk of the tissue or at the injury site, but only at the very exterior of the tissue.

In contrast to the 2- to 4-fold increases in integration strength resulting from short-term bFGF exposure, the addition of TGF-β3 resulted in greater than 10-fold improvements in integration strength in meniscus-to-meniscus repair constructs. Unfortunately, combining these two successful regimens did not result in further, synergistic

improvements. While long-term delivery of TGF-β3 improves integration the most, short-term delivery of bFGF offers some important benefits over that delivery scheme. bFGF is significantly less expensive than TGF-β3 and requires a shorter time of exposure, resulting in less volume of growth factor overall. Further, while the primary effect of bFGF may be mitosis, it also stimulates matrix deposition, although not as robustly as TGF-β3 [111, 121, 134]. Interestingly, combined continual delivery of TGF-β3 and bFGF decreased the integration properties compared to continual TGF-β3 alone, demonstrating that together, the growth factors would not support repair *in vivo*. Also, short-term TGF-β3 did not improve integration strength past 4 weeks, contrary to our hypothesis. Previous work that examined fibrochondrocytes in agarose gels from the temporomandibular joint, a related structure, found continuous TGF-β3 exposure improved properties better than intermittent exposure in agarose gels [135], consistent with the findings of the present study. Taken together, these findings illustrate the importance of delivery duration and growth factor combination when repairing meniscus tears.

In addition to meniscus-to-meniscus integration, we evaluated the integration and maturation of electrospun PCL scaffolds as a meniscus repair material. Such a therapy is useful for instances where meniscus damage is too severe for repair to be attempted. In these cases, it would be beneficial for the damaged portion to be replaced with a synthetic material capable of mimicking the ECM of native tissue and sustaining cell viability. Further, this electrospun scaffold could be used to deliver growth factors to the repair site through the use of heparin binding, emulsion electrospinning, coaxial electrospinning or other novel techniques [130-132]. Cells from the native tissue densely colonized the exterior of the scaffold and then uniformly infiltrated the scaffold, without favoring the region closest to the tissue itself **(Figure 4-6C)**. However, a practical

limitation of implanting an acellular scaffold is that patient mobility would be limited to minimize scaffold compression prior to cell infiltration and matrix deposition. Scaffold preseeding techniques are currently being explored.

The meniscus-to-scaffold repair constructs integrated equivalently or better than the meniscus-to-meniscus repair constructs, as hypothesized. Similar to native tissue, integration strength increased with short-term exposure to bFGF, and increased further with continual TGF-β3 delivery, where new tissue bridged the scaffold with the native meniscus **(Figure 4-6F, arrows)**. While growth factors influenced the integration properties of meniscus-to-scaffold repair constructs, they did not result in significant changes in the bulk characteristics of the scaffold after 4 weeks. In contrast, Pangborn *et al* demonstrated that exposure to TGF-β1, an isoform of TGF-β3, stimulated significantly more collagen and proteoglycan deposition than exposure to bFGF in scaffold-based approaches to meniscus engineering [136]. Also, bFGF was found to increase cell density in PLLA scaffolds compared to control conditions [134]. However, these studies and other work from our group that demonstrated more significant matrix deposition [50] utilized serum-free media, suggesting that serum may have mitigated the effect of growth factors in our experiment.

Although this work represents novel approaches to identifying targets for meniscus repair and replacement, some drawbacks can be identified. The work was performed on bovine rather than human tissue, so some differences may develop when this work is translated to humans. Further, the synovial environment of the knee was not captured in the culture system. Finally, while growth factors are extremely potent, their half-life tends to be short, so they will need to be stabilized in some way. Previous work tried to overcome the problem through gene therapy approaches [122].

4.6 Conclusions

Identifying novel approaches to meniscus repair and replacement require the screening of many candidate molecules and materials. This work clearly shows that growth factor regimen and timecourse of delivery play a key role in repair success. Future work will translate this research into large animal studies, as we continue to develop our understanding for how to bolster repair mechanisms in tissue and promote successful formation and maturation of synthetic meniscus. With this work, we hope to develop novel approaches to meniscus repair and replacement.

4.7 Acknowledgements

This work was done in collaboration with Gregory C. Lee, Kevin L. Huang, and Robert L. Mauck, and will be submitted for publication at Acta. Biomaterialia. We would like to thank Mr. Kilief Zellars for his assistance with the OHP assay, and Dr. Salin Chakkalakal and Mr. Kevin Egan for their advice on IHC staining. Funding was provided in part by the NIH (RO1 AR056624 and T32 AR007132), the Department of Veteran's Affairs, and the Penn Center for Musculoskeletal Disorders.

5: Porosity and Preseeding Influence *in vitro* Electrospun Scaffold Maturation and Integration Capacity

5.1 Abstract

Electrospinning generates fibrous scaffolds ideal for engineering soft orthopedic tissues, such as the knee meniscus. By modifying the electrospinning apparatus, scaffolds with many different structures can be created. For example, fibers can be aligned in one direction, or the porosity of the scaffold can be modified through the use of multi-jet electrospinning and the removal of sacrificial fibers. In this work, we investigated the role of fiber alignment and scaffold porosity on construct maturation and integration within *in vitro* meniscus defects. Further, we explored the effect of preseeding expanded meniscus fibrochondrocytes (MFCs) onto the scaffold at a high density prior to *in vitro* repair. Our results showed that high porosity electropun scaffolds integrated better to native tissue and matured to a greater extent than low porosity scaffolds, while scaffold alignment did not influence integration or maturation. Further, the addition of expanded MFCs to scaffolds prior to *in vitro* repair improved integration with native tissue, but did not influence maturation. In contrast, preculture of these same scaffolds for 1 month prior to repair decreased integration with native tissue, but resulted in a more mature scaffold compared to cellular scaffolds or acellular scaffolds. This work informs scaffold selection in future *in vivo* studies, bringing us closer to identifying an ideal scaffold for meniscus tissue engineering.

5.2 Introduction

Interest in electrospun scaffolds for fibrous tissue engineering has grown dramatically in recent years. In this technique, electrostatic forces are used to generate nano- to micron-sized fibers that resemble the collagen fibers found in orthopedic soft tissues, including the knee meniscus. Electrospun scaffolds can mimic both the anisotropy of fibrous tissues as well as withstand the high loads that are imposed on the tissues during physiologic deformation [52]. Depending on the choice of material, cells will attach, proliferate and deposit matrix in these structures, improving the mechanical properties of the scaffolds over time [53]. Further, electrospun scaffolds have been used in a wide range of applications, including cardiovascular, orthopedic, skin and neurological tissue engineering [137-140]. The ability to electrospun a wide range of materials, including synthetic and natural polymers, the potential to include drug delivery components, and the ease of tuning fiber properties provide a wide array of scaffolds to explore [53].

Previously, we assessed the role of fiber alignment on electrospun scaffold maturation *in vitro*. By collecting fibers onto a rotating mandrel rather than on a flat surface, one can form aligned architectures that resemble native tissue structures. When cells were seeded onto these scaffolds and cultured for 10 weeks *in vitro*, total matrix production was comparable between disorganized and aligned scaffolds, increasing with time in both conditions. However, the tensile modulus in the fiber direction of aligned scaffolds was 7-fold higher than disorganized scaffolds, approaching that of native meniscus [50]. These findings indicate that scaffold architecture can dictate long term maturation properties. Beyond internal organization, sheets of electrospun fibers can be organized into tissue-like structures. For example, bilayers of electrospun scaffold were assembled into rings and filled with a hydrogel to form an engineered intervertebral disc, a fibrous tissue related to the meniscus, with histological and mechanical properties similar to the

native tissue [129]. Also, sheets of electropun scaffold can be folded into a wedge-shaped structure resembling native meniscus [141].

For meniscus tissue engineering, different cell types can be isolated, expanded and manually seeded onto the surface of electrospun scaffolds prior to implantation in order to expedite the regenerative process. Over time, these cells (along with host cells) will migrate into the scaffold, depositing both proteoglycan and collagen [50]. There are a number of potential cell sources for meniscus tissue engineering. One option is to use autologous meniscus fibrohcnodrocytes (MFCs). This would require a surgery prior to implantation to isolate the cells, followed by a period of expansion prior to seeding, maturing and implanting the scaffold. While MFCs are already conditioned for the specific mechanical environment and nutrient levels in the knee, and will produce appropriate extracellular matrix, this approach has a number of drawbacks, including the costs associated with a second knee surgery and cell handling, and potential MFC dedifferentiation during expansion. Another cell source is mesenchymal stem cells (MSCs). These cells can be differentiated into numerous musculoskeletal phenotypes [142]. When bovine MSCs were seeded onto electrospun scaffolds in a pro-chondrogenic media, higher amounts of matrix were deposited compared to expanded MFCs [50]. Notably, the behavior of MSCs on electrospun scaffolds appears to differ by species; while bovine MSCs performed better than their associated MFCs, human MSCs performed significantly worse than their associated MFCs, with limited cell infiltration and matrix deposition over 9 weeks [143]. Finally, cells from related tissues, such as synovial cells, chondrocytes or fibroblasts, could also be a viable cell source with potentially beneficial properties [144, 145].

Regardless of the starting cell source, one drawback of electrospun materials is that the structure is quite dense, which can limit cell infiltration into the center of the scaffold. Uneven distribution of cells prevents the development of a homogeneous matrix, and so limits the improvement of tensile strength over time. To promote cell infiltration and matrix production, we have explored a number of different techniques. One approach is to modify the culture conditions; culturing these materials on a rocking bioreactor after seeding resulted in better cell infiltration, although the technique limited matrix accumulation over time [146]. Alternatively, multi-jet electrospinning can be used to create scaffolds with distinct fibers populations that degrade at different rates. Slow-degrading poly(ε-caprolactone) (PCL) fibers can be intermixed with water-soluble poly(ethylene oxide) (PEO) fibers. Upon hydration, these 'sacrificial' PEO fibers dissolve, leaving a more porous architecture of PCL fibers. Scaffolds of varying porosities can be fabricated by changing the relative percentage of sacrificial PEO fibers. Previously, we found that increased porosity resulted in better cell infiltration and matrix distribution, although there was an associated decrease in mechanical strength and architectural stability at very high sacrificial levels [107]. This finding might be remedied with the inclusion of a third fiber population (e.g. PLGA) that has an intermediate degradation rate, helping to maintain higher mechanical properties within a dynamic scaffold that changes in porosity over a longer period of time [147].

While cell-seeded electropun scaffolds will mature *in vitro*, another equally important consideration is how such materials integrate with native meniscus tissue. If electrospun scaffolds are to replace regions of resected tissue (as is commonly done during meniscectomy, the most prevalent orthopedic surgery in the US [115]), their initial and long term integration with native structures is of paramount importance. Previously, we utilized an explant defect model to assess the integration potential of native tissue as a

function of age [128]. In this system, the force required to separate apposing pieces of tissue formed into concentric circles (i.e. the integration strength) was determined. This approach has been used in both meniscus and cartilage tissue engineering to assess tissue-tissue and tissue-biomaterial integration [35-37, 94]. In our prior study, we also replaced the inner core of the meniscus defect with a disc of electrospun scaffold, and found that native meniscus cells infiltrated the material well after 6 weeks of *in vitro* culture. In this work, we expanded upon this model to test the mechanical integration strength between electrospun scaffold and native tissue. We hypothesized that increasing scaffold porosity would improve both the maturation and integration strength of the scaffolds *in vitro*.

Clinically, the implantation of an acellular material into a meniscal defect would be the simplest and most cost effective approach for repair. As previously noted, prior studies have demonstrated that nanofibrous materials are readily populated by native meniscus cells *in vitro*. Indeed, other acellular scaffolds, such as the collagen meniscus implant (CMI) [24], have been implanted adjacent to the meniscus and became colonized by endogenous cells. However, acellular electrospun scaffolds are delicate materials, and are particularly susceptible to compaction upon exposure to compressive forces. Thus, post-operative rehabilitation will require a significant period of non-weight bearing, similar to the post-operative procedure for the CMI. As the scaffold becomes colonized by local cells and matrix is deposited, the new extracellular matrix will reinforce the nanofibrous architecture. As previously discussed, one approach to reduce the non-weight bearing period would be to implant mature scaffolds that are already colonized with cells. Pre-seeded or pre-matured scaffolds might also integrate more rapidly with native tissue given the increase in early cell number at the construct border. To address this issue, we evaluated the effect of the direct addition of expanded MFCs to the scaffold

immediately prior to *in vitro* defect repair, as well as placement after a 1-month preculture period. With this work, we hope to better understand the optimal properties for electrospun scaffolds with respect to both maturation and integration with native tissue. These findings will guide our selection for material implantation in future large animal studies.

5.3 Materials and Methods

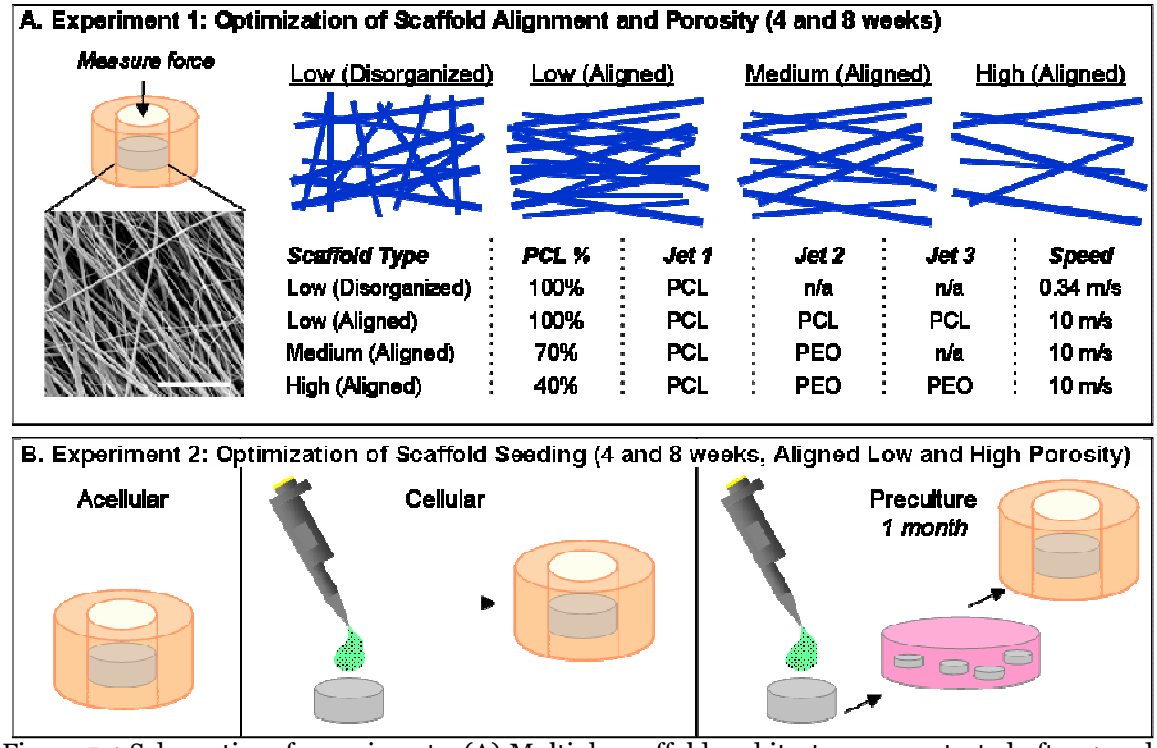

Figure 5-1 Schematics of experiments. (A) Multiple scaffold architectures were tested after 4 and 8 weeks of in vitro culture in the presence of FBS and TGF-β3 to determine the scaffold with the best maturation and integration properties (scale = 20 μm). (B) Different seeding techniques were utilized, including a 1-month preculture prior to construct assembly, to determine the most appropriate cellular context for implantation.

5.3.1 Fabrication of Electrospun Scaffolds with Varying Alignment and Porosity

To create electrospun scaffolds, two separate solutions (14.3% w/v poly(ε-caprolactone) (PCL, 80 kDa, Sigma-Aldrich, St. Louis MO) in a 1:1 mixture of tetrahydrofuran (THF, Fisher Chemical, Fairlawn NJ) and N,N-dimethylformamide (DMF, Fisher Chemical) and 10% polyethylene oxide (PEO, 200 kDa, Polysciences, Warrington PA) in 90%

EtOH) [107] were mixed overnight prior to electrospinning. Four scaffolds with distinct fiber architectures were created (**Figure 5-1A**) with two alignment schemes (disorganized, aligned) and 3 levels of PEO fiber fraction (0, 30%, 60%) to change the porosity. To create disorganized PCL scaffolds, a 20 mL syringe was filled with PCL electrospinning solution and fitted with a stainless steel 18G blunt-ended needle that served as a charged spinneret. A flow rate of 2.5 mL/h was maintained with a syringe pump (KDS100, KD Scientific, Holliston, MA). A power supply (ES30N-5W, Gamma High Voltage Research, Inc., Ormond Beach, FL) applied a +13 kV potential difference between the spinneret and the grounded mandrel located at a distance of 12 cm from the spinneret. Additionally, two aluminum shields charged to +10 kV were placed perpendicular to and on either side of the mandrel to better direct the electrospun fibers towards the grounded mandrel. The mandrel was rotated via a belt mechanism conjoined to an AC motor (Pacesetter 34R, Bodine Electric, Chicago, IL) at a speed of 0.34 m/sec, slow enough to limit any pronounced alignment.

To fabricate the remaining three aligned scaffolds, a custom trijet electrospinning device [147] was utilized to generate an intermingled composite of PCL and PEO fibers. Three syringes were fitted with needles, as described previously, and were directed at a single central rotating mandrel (10 m/s) equidistant from each other and separated by shields (+5 kV charge). The speed of the mandrel was sufficiently fast to align the collecting fibers into a single direction. A flow rate of 2 mL/h and a +15 potential difference between the needles and mandrel was utilized. The distance between the mandrel and the needle was 12 cm. The needles followed a reciprocating path using a custom fanner in order to better disperse the fibers along the length of the mandrel. As depicted in **Figure 5-1A**, the following configurations were used to create each of the three aligned scaffolds: 3 jets of PCL to create ‘Low Porosity’, 1 jet of PCL/1 jet of PEO to create

'Medium Porosity', and 1 jet of PCL/2 jets of PEO to create 'High Porosity' scaffolds. The resulting PCL content was 100%, 70%, and 30%, respectively. The grading (low, medium, high) indicates the relative porosity of the material after PEO removal. A total volume of 20 mL of spinning solution was used to generate each mat with a final thickness of ~1 mm prior to PEO removal. After fabrication, 4 mm discs were excised using a dermal punch and stored in a desiccator until use. The percent of PEO incorporation was verified by measurement of mass loss following exposure to aqueous solution.

5.3.2 Formation of Meniscus/Scaffold Constructs

Menisci were dissected from the knee joints of juvenile (3 months old) bovine limbs in a sterile manner. Cylinders (8 mm diameter x 3 mm thick) were excised centrally in the axial direction using a dermal punch (Miltex, Plainsboro, NJ). A smaller dermal punch (4 mm diameter) was used to remove a central core from the cylinder to form a ring, and an electrospun disc was press-fit into the meniscus ring as depicted in **Figure 5-1A** [128]. Prior to insertion, scaffolds were sterilized with UV light for 10 minutes.

5.3.3 Optimization of Scaffold Alignment and Porosity

Electrospinning was carried out as described above to generate disorganized low porosity, aligned low porosity, aligned medium porosity and aligned high porosity scaffolds (n=7-9/condition, all work performed in duplicate, one representative data set shown). In order to assess if the presence of tissue influenced scaffold maturation, tissue-free control scaffolds were cultured by seeding meniscus fibrochondrocytes (MFCs) directly onto both sides of the four types of scaffold discs at a density of 3333 MFCs/mm^2 scaffold per side (n=6-7/condition, work performed in duplicate, one representative data set shown). MFCs were extracted from a 5 mm radial slice of sterile

juvenile meniscus by mincing the tissue into 2 mm^3 pieces and allowing the cells to migrate out onto the tissue culture plastic (Corning, Sigma-Aldrich, St. Louis MO) to establish primary cultures over the course of a few weeks. For expansion, cells were cultured in basal media (Dulbecco's modified Eagles medium (DMEM) with 10% fetal bovine serum (FBS) and 1% penicillin/streptomycin/fungizone (PSF)). After formation, the tissue-free control scaffolds and scaffold/meniscus repair constructs were cultured in DMEM with 10% FBS, 1% PSF, 50 μg/mL ascorbate-2-phosphate (vitamin C) and 10 ng/mL TGF-β3. After 4 and 8 weeks, samples were removed from culture and prepared for histology (control scaffolds and repair constructs) or tested mechanically (repair constructs only). The mechanical integration strength between the scaffold and native meniscus tissue was measured using a custom push-through testing device [128]. Briefly, an Instron 5848 was outfitted with a 3.5 mm diameter indenter in series with a 50 N load cell. This indenter was placed above a plate with a 5 mm diameter hole. The construct was placed onto the plate, and the indenter progressed through the defect site at a rate of 0.0833 mm/sec. Integration strength was calculated using the following formula:

$$Integration\ Strength = \frac{Maximum\ force(N)}{2\pi r \cdot h}$$

The height (h) of the scaffold disc was measured using an OptoNCDT laser measuring device (Micro-Epsilon, Raleigh, NC) after pushout.

After testing, the native tissue was discarded and the scaffold was lyophilized and digested in a buffer containing 2% papain at 60°C. The resulting digest was used to assess DNA content (PicoGreen Assay, Invitrogen, Carlsbad, CA), glycosaminoglycan (GAG) content (DMMB assay [67]) and collagen content (OHP assay with a conversion factor of 7.14 [68]). Results were normalized to sample dry weight. To assess cell and

matrix distribution, 1-2 fresh constructs per condition were prepared for histology by fixing the samples in 4% paraformaldahyde overnight, embedding in OCT freezing media (Tissue-Tek, Fisher, Fairlawn, NJ) and cryosectioning onto glass slides (12 μm thick) perpendicular to the plane of the electrospun disc. Slides were stained with Alcian blue for proteoglycan, Picrosirius red for collagen and DAPI (Prolong Gold, Invitrogen, Carlsbad, CA) to identify cell nuclei.

5.3.4 Optimization of Scaffold Seeding Method

In order to assess the role of cell seeding (**Figure 5-1B**) on maturation and integration, juvenile bovine MFCs were seeded onto aligned Low and High porosity scaffolds as previously described. Scaffold discs were seeded and immediately implanted ('Cellular'), or seeded and cultured for 4 weeks prior to implantation ('Preculture'). Acellular scaffolds were also inserted as a control ('Acellular') (n=7-8/group, performed in duplicate, one representative data set shown). After 4 and 8 weeks, constructs were processed for histology and mechanical integration as previously described.

5.3.5 Statistical Analysis

For all work, 1 and 2-way ANOVAs were performed using SYSTAT software (Chicago, IL) to compare timepoints and conditions using Tukey's post-hoc test. Significance was set at $p \leq 0.05$.

5.4 Results

5.4.1 Optimization of Scaffold Architecture: Alignment and Porosity

Four types of electrospun scaffolds were created with various alignments and porosities. The disorganized scaffold had no prevailing fiber direction, whereas the aligned scaffolds

had a single predominant fiber direction (**Figure 5-2A**). When scaffolds were seeded with expanded MFCs and cultured for 8 weeks, histology revealed the formation of cell- and matrix-dense capsules around the scaffolds. While no differences were seen histologically between disorganized and aligned scaffolds, higher porosity scaffolds had better cell infiltration (**Figure 5-2B**) and more uniform matrix deposition (**Figure 5-2C**). Further, increasing porosity resulted in incrementally higher quantities of cells and matrix in the scaffold ($p < 0.05$) (**Figure 5-2D**).

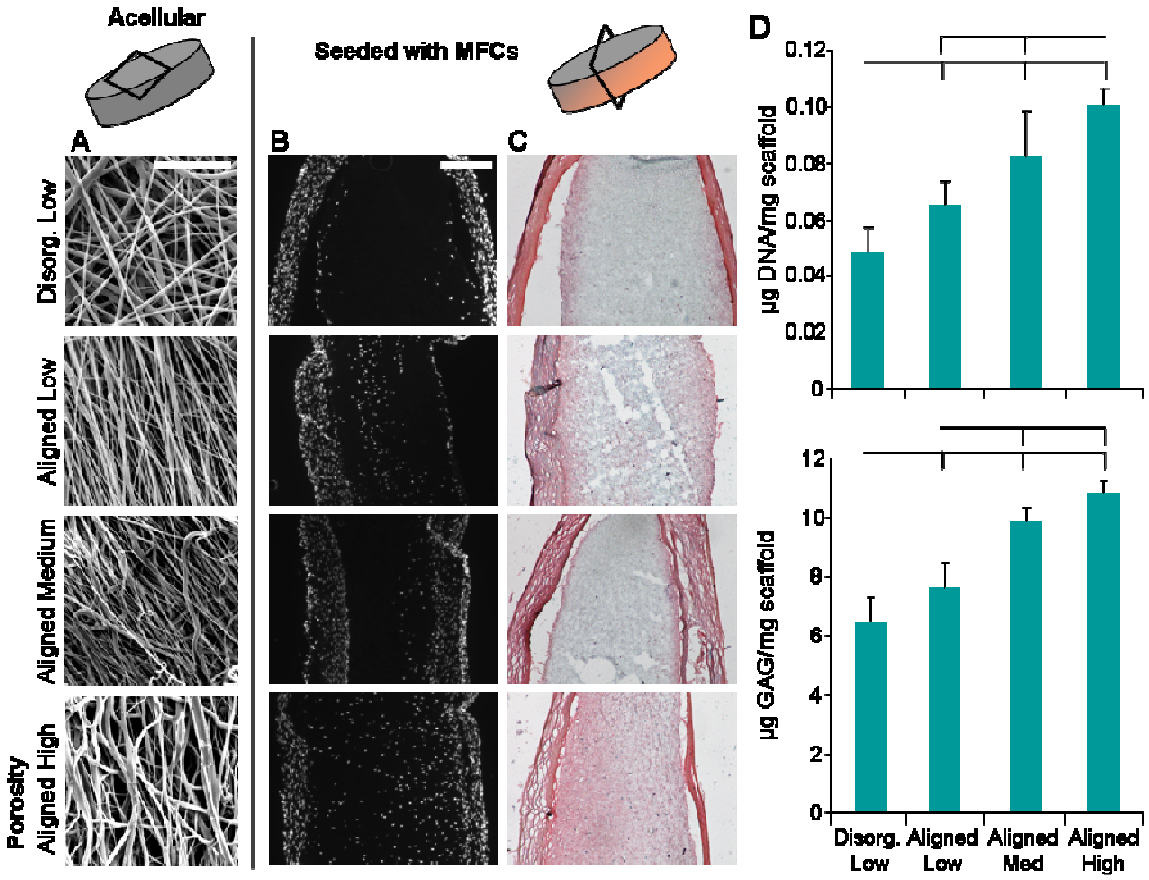

Figure 5-2 Tissue-free control scaffolds seeded with MFCs. (A) SEM images of scaffold fiber morphology (scale = 20 µm). Cross section of scaffolds with (B) DAPI staining for cell nuclei and (C) Picrosirius red / Alcian blue staining for matrix deposition indicates superior properties in high porosity scaffolds, with no difference based on alignment (scale = 200 µm). A thick capsule was observed around all scaffolds. (D) DNA (top) and GAG (bottom) content increased relative to scaffold weight with alignment and in higher porosity scaffolds. Line indicates significant difference, with $p < 0.05$; n=6-7/condition.

To test the impact of scaffold architecture and porosity on cell colonization directly from native tissue, we inserted discs of acellular scaffold into circular meniscus defects and evaluated infiltration into the scaffold and mechanical integration with the native tissue. This approach mimics the implantation of an acellular scaffold *in vivo*. We measured the force required to displace the inner scaffold disc from the outer meniscus ring, and calculated the integration strength based on the construct geometry at 4 and 8 weeks. High porosity scaffolds integrated with native tissue to a much greater degree than low porosity scaffolds, with a 3-fold improvements in integration strength at 8 weeks ($p < 0.05$) (**Figure 5-3A**). Fiber alignment did not modulate the integration capacity for the low porosity scaffolds. Scaffolds pushed out of meniscus rings were digested and the biochemical content measured after 8 weeks *in vitro*. Quantification confirmed that twice as many cells per weight of scaffold populated high porosity scaffolds compared to low porosity scaffolds ($p < 0.05$) (**Figure 5-3B**). Further, scaffold porosity strongly affected matrix deposition, with low, medium and high porosity scaffolds containing incrementally more matrix (**Figure 5-3C**).

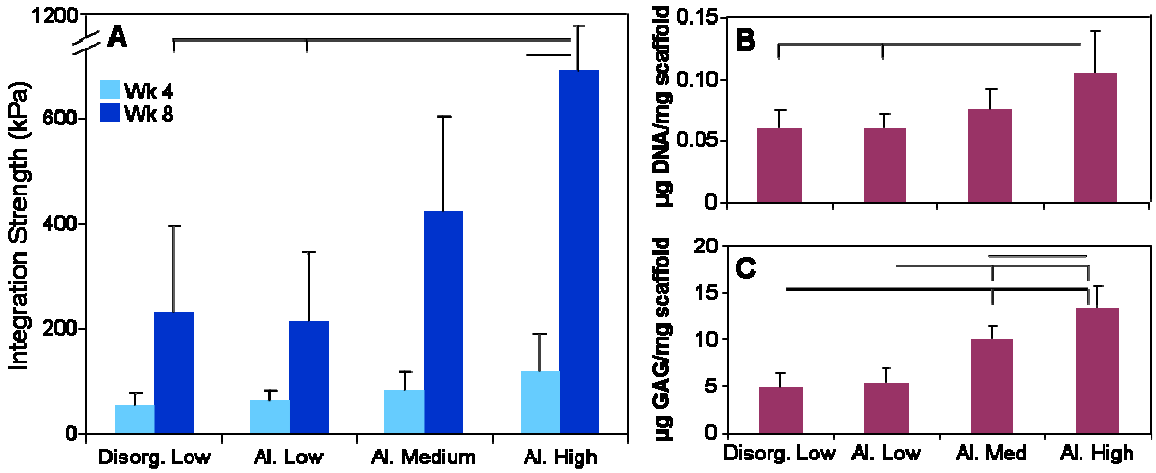

Figure 5-3 Optimization of scaffold architecture: Mechanical properties and biochemistry. (A) Integration with native tissue was greater for high porosity scaffolds than for disorganized or aligned low porosity scaffolds. (B) DNA content was higher in high porosity scaffolds compared to disorganized and aligned low porosity scaffolds after 8 weeks. (C) Scaffold porosity (but not alignment) influenced GAG deposition, with differences found between low, medium and high porosity scaffolds after 8 weeks. Line indicates significant difference, with $p < 0.05$; n = 7-8/condition.

Thin capsules of cells and matrix formed around the scaffold in this *in vitro* defect, but it was less pronounced than in tissue-free control scaffolds (**Figure 5-4A, B**). New ancillary tissue was deposited between the scaffold and native tissue, creating a bridge of matrix that influenced integration properties (**Figure 5-4A**). The ancillary tissue was more pronounced in high porosity scaffolds (*data not shown*). Furthermore, high porosity scaffolds showed the best cell distribution, with similar cell density to native meniscus tissue after 8 weeks in culture and almost uniform cell distribution throughout the material (**Figure 5-4B, lower-right image**).

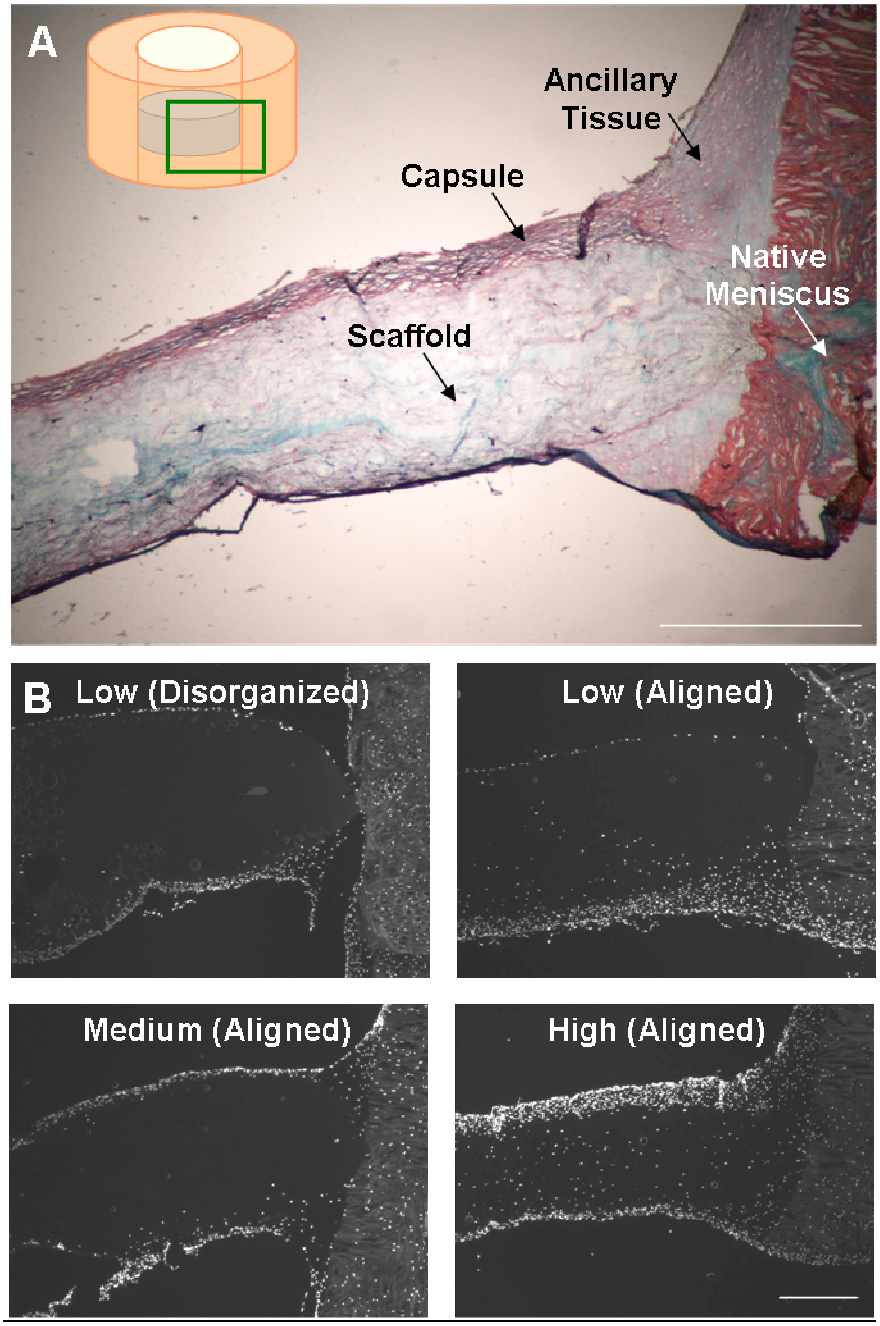

Figure 5-4 Optimization of scaffold architecture: Histology. (A) Alcian blue and Picrosirius red staining of high porosity scaffold discs cultured in meniscus defects for 8 weeks in vitro revealed significant matrix deposition in the scaffold and the formation of surrounding ancillary tissue (scale = 500 μm). (B) High porosity scaffolds had better cell distribution through the depth compared to low porosity scaffolds, and alignment did not affect cell infiltration (scale = 500 μm).

5.4.2 Optimization of Scaffold Seeding Method

Aligned low and high porosity scaffolds were next used to determine whether the seeding method influenced scaffold maturation and integration. While low porosity scaffolds are the easiest to fabricate and are most extensively tested, high porosity scaffolds demonstrate superior integration and maturation properties. Three different scaffold/meniscus repair constructs were formulated: acellular implantation, the addition of expanded MFCs immediately prior to insertion ('cellular'), and 4 weeks of preculture of seeded scaffolds prior to insertion ('preculture').

Mechanical testing revealed that, as previously shown, high porosity acellular scaffolds integrated to a greater extent than low porosity scaffolds after 8 weeks *in vitro* ($p < 0.05$) (**Figure 5-5A**). Seeding the scaffold immediately prior to implantation with a high density of expanded MFCs resulted in significantly better integration in low porosity scaffolds, but did not further improve high porosity scaffold integration capacity. Preculturing scaffolds for 4 weeks prior to implantation resulted in significantly lower integration strengths for both scaffold types compared to cellular conditions ($p < 0.05$).

Biochemical analysis of scaffolds revealed variable maturation based upon seeding technique. Seeding expanded MFCs onto the scaffold ('cellular' and 'preculture' conditions) resulted in lower cell densities in the scaffolds after 8 weeks compared to acellular controls, where MFCs populated the scaffold directly from the tissue (**Figure 5-5B**). One extra month of preculture did not bolster DNA content; however, it greatly increased GAG content in the scaffold, suggesting that the cells were steadily forming matrix that accumulated in the scaffold, with little proliferation, during the preculture period (**Figure 5-5C**).

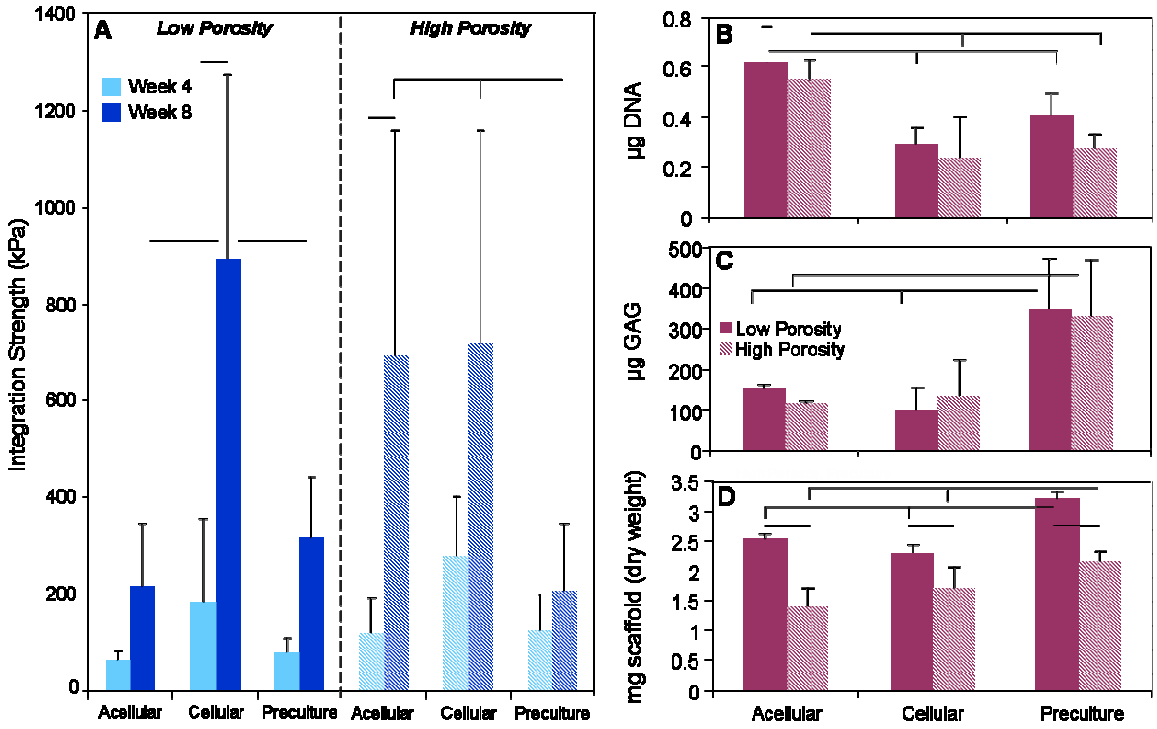

Figure 5-5 Optimization of seeding method: Mechanical properties and biochemistry. (A) For low porosity scaffolds, cellular scaffolds integrated significantly better than acellular or preculture scaffolds after 8 weeks. For high porosity scaffolds, acellular and cellular scaffolds had comparable integration strength. Both low and high porosity precultured scaffolds exhibited significantly lower integration strength with native tissue compared to cellular scaffolds. (B) Scaffolds seeded with expanded MFCs (cellular and preculture conditions) contained less DNA per dry weight than acellular scaffolds, which were populated by MFCs that migrated directly from the surrounding meniscus ring. (C) Precultured scaffolds contained more GAG overall than acellular or cellular scaffolds after 8 weeks. (D) High porosity scaffolds weighed less than low porosity scaffolds; preculture scaffolds were heavier than acellular and cellular scaffolds (dry weight). Line indicates difference, with $p > 0.05$.

Histologically, cellular and preculture constructs had incrementally thicker cell capsules surrounding the scaffold compared to acellular controls (**Figure 5-6B**). Examination of the scaffold/meniscus interface showed that the cellular capsule in precultured samples appeared to prevent integration with native tissue in preculture constructs. In contrast, cellular scaffolds had a tight connection with the native tissue (**Figure 5-6C,** arrows).

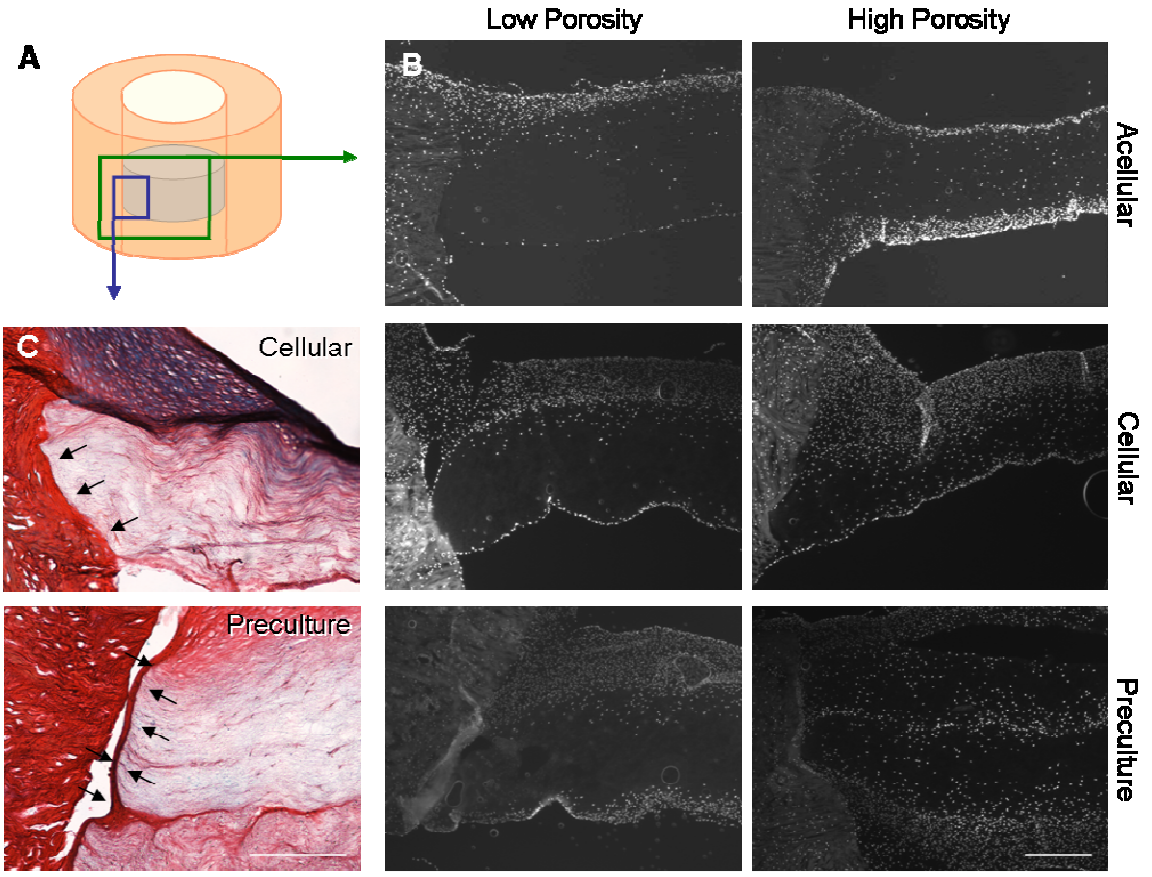

Figure 5-6 Optimization of seeding method: Histology. (A) Schematic of histology sectioning planes. (B) DAPI staining reveals better cell infiltration in high porosity scaffolds and thicker cell capsules in precultured samples (scale = 500 μm). (C) Alcian blue and Picrosirius red staining shows robust integration (arrows) between cellular scaffolds and native tissue. In contrast, limited integration was observed between the preculture scaffolds and native tissue, likely due to the formation of a cell capsule (arrows) during preculture (high porosity scaffold shown, scale = 250 μm).

5.5 Discussion

Electrospinning is an extremely versatile fabrication method that can produce scaffolds with a wide array of properties. By changing the collection surface, the type of polymer, and the number of spinnerets in the electrospinning apparatus, many different scaffold architectures can be created and evaluated. Over the years, our lab and others have explored a number of different types of electrospun scaffolds for use in fibrous tissue engineering. These tissues, such as the knee meniscus, suffer from low intrinsic repair capacity, low cell metabolic activity and density, and experience extremely high

mechanical stresses *in vivo*, so advanced materials must be used to engineer replacement tissues that can successfully promote repair and reestablish joint mechanics.

In this work, we employed a concentric explant model wherein a disc of electrospun scaffold was cultured inside a ring of bovine meniscus. We used this approach to assess both maturation (histology, biochemical content of the scaffold after 8 weeks) and integration of the scaffold to native tissue (mechanical integration strength after 4 and 8 weeks). Specifically, we explored the role of scaffold alignment, porosity and seeding technique on these outcomes. In this context, we found that scaffold alignment did not influence maturation or integration capacity. Also, the alignment of the fibers in the scaffold with respect to the alignment of the collagen fibers in the tissue did not influence integration (*data not shown*), although we hypothesize that it could influence the tensile load transmission under more physiologic loading scenarios. We also found that higher porosity scaffolds mature faster and integrated better with native tissue than their less porous counterparts. When considering different cell seeding techniques, the addition of cells immediately prior to implantation enhanced integration strength, particularly with low porosity scaffolds. While precultured scaffolds had the highest matrix content, integration with native tissue was markedly reduced. In future work, the outer rim of the precultured scaffolds might be removed to improve the integration properties of these more mature construct.

While the concentric explant model has been used by us and other groups to assess integration, it does not represent the most physiologically relevant damage force in the knee. A tissue engineering meniscus patch would primarily experience compressive forces and tensile forces, rather than shear extrusion. However, the technique does

provide us with comparative information on the relative integration potential between scaffold types, which can motivate other studies. While bioreactors and subcutaneous studies can mimic the *in situ* environment of the knee, direct implantation of the material into a meniscus defect will give us the best information on its repair potential. Indeed, preliminary data from an ovine implantation suggest that high porosity constructs integrate better than low porosity constructs *in situ* [148].

During *in vitro* testing, the composition of the culture media will influence the results of the experiment profoundly. All of the constructs in this study were cultured in the presence of fetal bovine serum, rather than in a chemically defined media, in order to more closely mimic the complexity of the *in vivo* environment. Notably, a thicker capsule was seen around the scaffolds and less pronounced matrix deposition was seen throughout the scaffolds compared to prior work that employed a pro-chondrogenic, chemically defined media [50, 129]. This capsule confounds the biochemical analysis, as we were unable to remove it prior to digestion. Also, we included TGF-β3 to the media in order to stimulate matrix production and a chondrogenic phenotype; without this growth factor, limited matrix would be deposited (*data not shown*). *In vivo*, local delivery of TGF-β3 could be accomplished through entrapped drug-delivering microspheres [114] or other delivery techniques from electropun fibers [53], in order to ensure that sufficient matrix is deposited to support the scaffold during compression and reinforce the fibers during tension.

Further, in this work, we employed two distinct cell populations. MFCs were either extracted from the tissue, expanded in monolayer and than added back to the scaffold at a high density, or acellular scaffolds were colonized by MFCs directly from the adjacent tissue. The expanded MFCs are likely phenotypically different from the native MFCs due

to dedifferentiation during monolayer expansion [149]. Thus, it is unclear if the maturation differences seen between tissue-free control scaffolds and scaffold-meniscus constructs are due to changes in cells themselves with passaging, or to the presence of the native tissue in the culture well. The tissue extracellular matrix is known to store a number of growth factors and those molecules could be released and alter cell behavior [150]. Alternatively, living MFCs within the meniscus ring may produce factors and signal to the adjacent scaffold [151].

While this work represents an important step towards identifying the optimal electrospun scaffold for meniscus tissue engineering, a few drawbacks exist. First, bovine meniscus rather than human meniscus was used. While bovine tissue has been used previously for *in vitro* meniscus work [107, 128, 152], differences in bovine MFC behavior compared to human MFCs has been identified [51]. Further, while the mechanical properties of meniscus from humans and domesticated animals like the cow are similar, the exact composition and the distribution of matrix elements are not identical [153]. Also, in this work, only one form of mechanical testing was explored. Lap testing or uni-axial tensile testing could all be explored by using different construct geometries, and could be related more closely to the specific mechanical challenges experienced by an implanted scaffold during normal knee motion; however, these constructs have proven challenging to test consistently in previous studies. Finally, young (0-3 month) tissue was used for this study. We have previously shown that this tissue is hypercellular and has a distinct matrix composition compared to mature bovine meniscus tissue, which is more clinically relevant to the aged human population that typically presents with meniscus tears. However, despite these differences, we can still learn a significant amount about how the different scaffolds mature and integrate with meniscus tissue.

5.6 Conclusions

In this work, we considered the effect of scaffold alignment, porosity and seeding technique on scaffold maturation and integration with native tissue. While *in vitro* techniques are valuable in assessing the relative potential of various scaffold architectures and implantation schemes, other key factors will need to be considered when implanting such materials *in vivo*, including the immune response, vascularization, and the response to the synovial environment. With this work, we identified several optimal material attributes that may further our efforts to replace resected meniscus in a manner that promote regeneration and reestablishes joint mechanics. These scaffolds may one day limit the development of cartilage erosion after meniscectomy, forestalling the onset of osteoarthritis and the need for total knee arthroplasty.

5.7 Acknowledgements

This work was done in collaboration with Robert Mauck. It will be submitted for publication in Tissue Engineering Part A. Funding was provided in part by the National Institutes of Health (AR056624) and the Veterans' Administration.

6: The Delivery of Molecules from Electrospun Scaffolds: A Review of Techniques and Biological Findings

6.1 Abstract

As previously shown, electrospun scaffolds are a versatile and promising material for fibrous tissue engineering. Multi-jet electrospinning and different seeding techniques, as well as exposure to various growth factors, can modulate the maturation of the scaffold and its integration with native tissue. However, these scaffolds would be more powerful if they could also harbor chemical cues that recruit cells, drive behavior or maintain appropriate cell phenotypes over time. Due to the large interest in electrospinning polymers, a wide range of drug delivery techniques have been developed. Many different kinds of molecules can be delivered, including antibiotics, analgesics, cancer therapeutics, and proteins. Recently, significant advances have been made in the encapsulation and release of growth factors, particularly useful in guiding cell behavior in tissue engineered materials. This review will assess the current landscape for drug delivery from electrospun scaffolds.

6.2 Delivery of Antibiotics

One of the first classes of molecules to be delivered from electrospun fibers are antibiotics, since scaffolds could be easily applied as wound dressings or formed into sutures and designed to release antibiotics slowly to prevent infection at the site of injury. Kenawy 2002 demonstrated for the first time the release of tetracycline hydrochloride (tet), a broad-spectrum antibiotic, from poly(lactic acid) (PLA), poly(ethylene-co-vinyl acetate) (PEVA) or a 50:50 blend of the two by adding tet to the

electrospinning solution and stabilizing the mixture with methanol. Drug release was seen over 5 days, with a significant burst release at day 1 [154].

The significant burst release has been observed by a number of groups mixing antibiotics directly into the electrospinning solution to form a blended fiber. Zong 2002 released Mefoxin from poly(L-lactic acid) (PLLA) fibers and demonstrated that the concentration and ionic salt addition had the largest influences on fiber morphology. However, they were unable to remove the large burst effect [155]. Similarly, Kim 2004 showed that Mefoxin released from poly(lactide-co-glycolide) (PLGA) fibers with a burst effect. However, this effect could be minimized by the addition of the amphiphilic block copolymer (PEG-b-PLA). Staphylococcus aureus cultures exposed to fibers demonstrated that the antibiotic remained bioactive upon release, with significant bacterial suppression at early timepoints [156].

However, it has been shown that the addition of molecules to the fibers can change the mechanical properties of the fibers. To combat this problem, Hong 2008 created nanofibrous sheets composed of two fiber populations. Biodegradable poly(ester urethane) urea (PEUU) fibers and PLGA fibers loaded with tet were co-electrospun into a single mat. Mechanical properties, such as breaking strengths, tensile strength and suture retention capacity, were greatly improved by the dual-scaffold over PLGA-tet fiber system alone. An *in vivo* study demonstrated that implantation of the tet-releasing scaffold could prevent abscess formation in a contaminated rat abdominal wall [157].

While significant effort has been made to incorporate tet, other antibiotics with variable properties have also been blended into electrospun scaffolds. Zeng 2003 found that adding surfactants or proteinase K decreased the burst release of the antibiotic rifampin

from PLLA fibers [158]. Also, Katti 2003 explored how fabrication parameters, such as needle gauge size, concentration, density and voltage influences loading of the antibiotic cefazolin [159].

Although adding the antibiotic directly to the electrospinning solution is a simple process, it would be desirable to decrease the burst release seen from most system. So, an alternate system of electrospinning a co-axial fiber, with an inner core containing the antibiotic and a protective outer shell modulating release properties. This method can decrease exposure of drugs to harsh fabrication conditions, as well as create a coating to decrease burst release and extend release times. He 2006 created nanofibers with a PLLA outer shell and tet encapsulated in the interior fiber. The resulting fibers showed a sustained release profile of tet, with almost no burst effect [160]. Huang 2006 compared the release of resveratrol (antioxidant) and gentamycin sulfate (antibiotic) from the inner core surrounded by a poly(capro-lactone) (PCL) shell. The degradation rate was found to be closely related to the hydrophilicity of the drug in the core, and the miscibility of the solvents used influenced mechanical properties of the fibers [161].

Some contest that a sustained release is ideal, but He 2009 argues that different release profiles have uses in unique applications. By fabricating fibers using either a blending or coaxial technique in order to create sutures, he found that the blended fibers with an initial burst could be applicable to antibacterial release, where the drug is needed more early on, whereas coaxial fabrication results in more sustained release appropriate for growth factor delivery or therapeutic agents [162].

6.3 Delivery of Analgesics

Analgesics have also been incorporated into electrospun fibers as well. Jiang 2004 demonstrated that by covalently conjugating ibuprofen with poly(ethylene glycol)-g-chitosan (PEG-g-CHN) and electrospinning with PLGA, sustained release of the drug could be attained over 16 days [163]. Also, Qi 2008 created acid-labile electrospun fibers that released an analgesic (paracetanol) more completely and at a faster rate when placed in acidic environments. Natural decreases in local pH often accompany inflammation, tumor growth, and myocardial ischemia, suggesting that such a system may provide sophisticated drug delivery capability [164]. The incorporation of paracetanol was also more closely explored [165], and it was determined that thicker fibers resulted in longer zero-order release profiles.

6.4 Delivery of Cancer Therapeutics

Another important class of molecules that have been incorporated and released from electrospun fibers treats cancer. Systemic administration of anti-cancer medications often leads to debilitating side-effects, suggesting that local delivery through a biodegradable patch may be less damaging to the patient. In a series of experiments, Zeng explored the incorporation of anticancer drugs into PLLA fibers. It was found that paclitaxel incorporated uniformly into the scaffolds, whereas doxorubicin hydrochloride, a hydrophilic drug, appeared to phase-separate onto the surface of the fibers, leading the scientists to propose that the solubility of the drug in the polymer/solvent liquid was essential for uniform fiber fabrication [166, 167]. Another interesting application by Xie 2006 incorporated paclitaxel into electrospun PLGA nanofibers and demonstrated cytotoxicity against C6 glioma cell lines for local applications in brain tumor destruction [168]. Also, Xu 2006 released BCNU (1,3-bis(2-chloroethyl)-1-nitrosourea from PEG–PLLA ultrafine fibers and demonstrated sustained release and decreased cell viability of

Glioma C6 cells over time [169]. Xu 2005 also demonstrated that doxorubicin hydrochloride could be loaded into amphiphilic poly (ethylene glycol)-poly (l-lactic acid) (PEG-PLLA) diblock copolymer at 1-5 wt% of the fibers, with release controlled by a combined diffusion mechanism and enzymatic degradation mechanism, that proved cytotoxic to Glioma C6 cells [170].

6.5 Delivery of Growth Factors

Recently, there have been significant advances in the ability to deliver growth factors from electropun scaffolds. This type of molecule is particularly challenging to deliver because it is prone to denaturation during the electrospinning process; growth factors are large and delicate molecules. To that end, a number of different techniques have been developed to release growth factors from electrospun materials, including the use of annealed fibers, blended fibers, coaxial fibers and multi-component scaffolds.

6.5.1 Annealed Fibers

One approach to functionalizing nanofibers is to modify the fibers after electrospinning in order to promote growth factor attachment. Growth factors can be immobilized on the fiber, reversibly attached via heparin bound to the fiber, or temporarily adsorbed to the fiber itself. Reversible attachment through heparin molecules seems to provide the highest loading and most sustained release over time.

The most extreme attachment of growth factors is via amine-conjugation of the proteins directly to the fibers. While this approach appears to maintain bioactivity of the growth factors, it limits exposure to cells directly attached to the fibers. One of the first approaches by Choi *et al* used a PEG-PCL amine-terminated block copolymer to improve wound healing in diabetic mice by binding EGF to the fibers using EDC/HOBt coupling

technique [171]. Later work by Cho *et al* released NGF bound to PEG-PCL fibers through EDC/NHS chemistry to promote a neuronal phenotype in mesenchymal stem cells, with clearly no release of growth factor over 1 week [172]. Also, simply soaking the fibers in NGF resulted in complete release after 1 day, suggesting that some chemical coupling is necessary to delivery growth factors in a sustained manner [172]. Futher, Tigli *et al* and Gumusderelioglu *et al* immobilized EGF via NHS on PCL and PCL/collagen electrospun scaffolds, and demonstrated improved cell spreading, proliferation and wound healing, with no proof of release over time [173, 174]. Interestingly, Lee *et al* first coated PLGA fibers with polypyrrole, a conductive material, and then attached NGF using EDC/NGF chemistry. A combination of NGF and electrical stimulated resulted optimal neutrite outgrowth, compared to NGF alone [175]. In another unique approach, Casper *et al* demonstrated that low molecular-weight heparin (LMWH) functionalized with PEG prior to electrospinning with PEO or PLGA improved bFGF retention over time compared to non-PEG LMWH [176].

While these approaches influence cell behavior, they only act upon cells in immediately contact with the fibers, thus limiting their influence. In order to release growth factors rather than immobilize them, similar chemistry can be used to immobilize heparin and heparin sulfate to fibers. Heparin is a glycosaminoglycan that reversibly binds a multitude of different growth factors [177]. By using EDC/NHS chemistry to attach heparin to electrospun fibers, growth factors can be reversibly attached, with sustained release over time. For example Kim *et al* found that heparin-conjugated PCL/gelatin fibers released more bFGF in a sustained manner than soaking the unmodified fibers in the growth factors, where release was low and abrupt. Further, heparin-fixed bFGF fibers stimulated proliferation in a number of different cell types for a longer amount of time than bFGF soaked fibers [130]. Similarly, Lam *et al* demonstrated that while PLLA

fiber/heparin-bound bFGF and EGF resulted in neural differentiation and axon growth, growth factor adsorption alone did not [178]. Rather than conjugating the PCL fibers after electrospinning, Ye *et al* conjugated prior to electrospinning and loaded bFGF, stimulating cell proliferation and cell adhesion *in vitro* better than growth-factor free controls [179]. Interestingly, molecules related to heparin can also be used to reversibly bind growth factors. For example, Casper *et al* demonstrated that attachment of perlecan was 10-fold better than heparin at attaching high concentrations of bFGF to collagen/gelatin fibers [180]. Further, one novel approach by Almodovar *et al* uses polyelectrolyte multilayer coating of heparin and chitosan to attach bFGF to fibers, rather than EDC/NHS chemistry. While the technique successfully attached the growth factor, it is unclear how it compares to the traditional method [181].

6.5.2 Blended Fibers

While surface modifications and coatings are a promising approach to protein delivery from electrospun fibers, another technique is to blend the proteins directly in the fibers. A major drawback to this technique is that many electrospinning solutions contain harsh organic solvents, so extra steps must be taken to prevent denaturing of growth factors. One of the first techniques was to include bovine serum albumin in the electrospinning solution. Chew *et al* was able to maintain bioactivity and sustained release for 3 months by electrospinning a mixture of BSA, NGF and copolymer of ε-caprolactone/ethyl ethylene phosphate (PCLEEP) [182]. Further, they improved bridging of a critical gap in rat neurons via glial cell-derived neurotrophic factor (GDNF) delivery compared to growth-factor free controls *in vivo* [183]. In contrast, Koh *et al* was unable to demonstrate clear benefit from delivery of NGF from BSA-containing PLGA electrospun fibrous bilayers *in vivo*. Specifically, encapsulated levels of NGF were low, perhaps due

to denaturing of the protein while interacting with the organic solvent or being exposed to high electric potentials during electrospinning [184, 185].

Another technique that has produced more consistent results is to create an oil/water emulsion prior to electrospinning that creates pockets of aqueous media for growth factors to reside. This technique is used to fabricate growth-factor laden polymeric microspheres with clear success [186]. Sahoo *et al* delivered bFGF from PLGA fibers by first emulsifying a mixture of an aqueous mixture of buffered bFGF and BSA with PLGA in HFIP. The resulting emulsion was then electrospun and the growth-factor laden scaffold stimulated BMSC proliferation over 2 weeks [187] and also demonstrated favorable properties for tendon/ligament tissue engineering applications [131]. Similarly, Valmikinathan *et al* electrospun an emulsion of aqueous NGF with PCL in HFIP. Inclusion of BSA in the emulsion improved release profiles over 1 month and helped maintained bioactivity as measured by a PC12 neurite outgrowth assay [188]. Li *et al* showed related results using poly(l-lactide-co-caprolactone) chloroform/Span80, and also found that the emulsion technique influence growth factor release properties from the fibers [189].

Certain polymers that can be electrospun in aqueous solutions can also be electrospun into growth factor delivery systems. Li *et el* electrospun mixtures of silk, poly(ethylene oxide) (PEO) and BMP-2 that resulted in higher calcium deposition and enhanced transcript levels of bone-specific markers than in the controls [190]. Madduri *et al* delivered NGF and GNDF from electrospun silk/PEO conduits over 28 days [191]. Because PEO fibers are instantly soluble, they can be used to enhance porosity in electrospun scaffolds [107] or to provide a quick release of drugs such as antibiotics [157]. Early work suggests that such fibers may be a valuable tool for other forms of drug

delivery. For example, Kluge *et al* released FGF from PEO/silk scaffolds stimulated cell infiltration in a subcutaneous rat model [192] and Qu *et al* delivered the enzyme trypsin from PEO fibers to degrade GAGs in cartilage *in vitro* [193].

6.5.3 Coaxial Fibers

Rather than creating a uniform fiber, coaxial electrospinning may offer additional protection to growth factors and prevent burst release by entrapping drugs in a central vein, although the technique is more technically challenging than regular fiber electrospinning. Early work by Liao *et al* encapsulated an aqueous mixture of PDGF and BSA in a PCL/PEG outer shell with zero-order release kinetics [132]. Both Liu *et al* and Sahoo *et al* elicited biological responses from a core-shell nanofiber scaffold with an aqueous core of NGF/solid shell of poly(lactic acid-caprolactone) (P(LLA-CL)) [194] and aqueous core of bFGF-BSA/solid shell of PLGA [187].

Recently, many investigators have utilized solid/solid coaxial structures rather than liquid/solid described above to extend the delivery period of the growth factor. For vascular tissue engineering, 28 days of bioactive release were demonstrated by Jia *et al* from the dextran-VEGF core/PLGA shell fibers [195] and by Li *et al* from dextran-PDGF core/PLCL shell fibers [196]. Yang *et al* promoted wound healing in diabetic rats by treating with cyclodextrin-bFGF core/PELA shell electrospin fibers [197]. Wang *et al* delivered NGF from an inner PEG core and an outer PLGA shell, and similar to Liu *et al* [194] found that nerve regeneration was comparable to autograph but better than control in a rat scientic nerve model [198].

In a different approach, Lu *et al* combined a number of different techniques to create an optimized fiber system. Specifically, they created a central core of PCL, to enhance

morphological stability and mechanical strength, with an outer shell of cationized gelatin which was amenable to heparin adsorption. Sustained release of VEGF was observed in the presence of adsorbed heparin, and release profiles were controllable through changes in cross-linking duration and pH [199].

6.5.4 Multi-Component Scaffolds

Another approach for growth factor delivery is to incorporate distinct delivery components into or between electrospun fibers. Early work by Dong demonstrated the feasibility of incorporating multiple microsphere populations into fibers [200]. A similar system by DeVolder *et al* was used to promote vascularity in chick embryos by releasing VEGF from PLGA microparticles contained inside PLA fibers [201]. Qi *et al* developed a modified form of emulsion electrospinning where large Ca-alginate bubbles in PLLA fibers released BSA, but most of the protein was released in the first day [202]. Rather than incorporating microspheres inside of fibers, Ionescu *et al* entrapped PLGA microspheres between PCL fibers to create a composite scaffold and demonstrated sustained release over 30 days of BSA and chondroitin sulfate [114], therefore decoupling the drug-deliver component from the fibers themselves.

Finally, nanofibers have been used to improve the behavior of drug-delivering hydrogels for tissue engineering. Specifically, nanofibers can promote tissue-like cell alignment and elongation, and promote the deposition of organized, anisotropic matrix [XXX]. Kolambkar *et al* delivered BMP from an alginate hydrogel embedded around an electrospun PCL nanofibrous tube and demonstrated synergistic effects of both drug delivery from the hydrogel and contact guidance by the fibers [203].

6.6 Delivery of Other Molecules

Moving beyond antibiotics, anticancer drugs and proteins, other unique molecules have been incorporated. Luu released plasmid DNA from a mixture of predominantly PLGA random copolymer and a PLA–PEG block copolymer. Release of plasmid DNA from the scaffolds was sustained over a 20-day study period with a significant burst release [204]. Also, Nie 2007 encapsulated DNA into chitosan nanoparticles that were electrospun into PLGA/hydroxylapetite fibers and optimized the system for cell attachment, viability and transfection efficiency [205]. Liang 2005 created a variation where the nanoparticles had a core-shell structure in order to better protect the contained DNA from the harsh electrospinning process [206]. Luong-Van 2005 created blended PCL-heparin fibers with applications in preventing vascular smooth muscle cell (VSMC) proliferation and graft occlusion. It was found that releasant from fibers prevented proliferation of VSMC in a bioassay in a concentration dependent manner over 6 days [207]. Also, Gandhi 2009 demonstrated that anti-integrin antibodies could be incorporated into PCL fibers and successfully transfect human umbilicial endothelial cells [208].

While most systems utilize biodegradable polymers, it may not be possible to incorporate some molecules into such systems. Verreck 2003 demonstrated that poorly water-soluble molecules such as the antifungal Itraconazole and the serotonin antagonist ketanserin could be released in a sustained manner from nonbiodegradable segmented polyurethane fibers [209].

Rather than incorporating the molecule into the fiber, some groups have looked at coating the fibers with the desired molecule. Casper functionalized PEG with low molecular weight heparin and demonstrated improved binding of b-FGF [176]. Casper when on to show that natural polymers, such as collagen or gelatin, could be

functionalized with the perlican domain I were 10 times as effective at binding b-FGF [180].

Finally, some groups have tried to better understand the physics drug release from electrospun fibers. Srikar 2008 proposed that the conventional belief that release occurs via solid-state diffusion of the encapsulated compound from the fibers into the surrounding aqueous bath may not be true, due to often seen incomplete release of molecules over time. Instead, they demonstrate that delivery of fluorescent dye rhodamine 610 chloride occurs via the desorption of the embedded compound from nanopores in the fibers or from the outer surface of the fibers in contact with the water bath [210]. Also, Gandhi 2009 extended this hypothesis to incorporate BSA as well [208].

6.7 Conclusions

Many different approaches have been developed to deliver a broad range of molecules from electrospun fibers. Each approach seeks to maintain the biological activity of the molecule during the electrospinning process or finds a way to integrate the molecule with the fibers without exposing it to electrostatic forces. Growth factors are an especially important class of molecules that can be used to drive cell behavior for tissue engineering applications. Recent work identifies a number of potential ways to incorporate these molecules; however, many of these approaches have significant drawbacks, including changing fiber morphology, suboptimal release profiles and complex manufacturing processes. In the next two chapters, we will present novel approaches to deliver growth factors from electrospun scaffolds for meniscus tissue engineering.

6.8 Acknowledgements

This work was published in “New Directions in Nanofibrous Scaffolds for Soft Tissue Engineering and Regeneration” (Expert Rev Med Devices. 2009 Sep;6(5):515-32). The growth factor section will be published in an invited upcoming review article in Advanced Drug Delivery Reviews.

7: An Anisotropic Nanofiber/Microsphere Composite with Controlled Release of Biomolecules for Fibrous Tissue Engineering

7.1 Abstract

Aligned nanofibrous scaffolds can recapitulate the structural hierarchy of fiber-reinforced tissues of the musculoskeletal system. While these electrospun fibrous scaffolds provide physical cues that can direct tissue formation when seeded with cells, the ability to chemically guide a population of cells, without disrupting scaffold mechanical properties, would improve the maturation of such constructs and add additional functionality to the system both in vitro and in vivo. In this study, we developed a fabrication technique to entrap drug-delivering microspheres within nanofibrous scaffolds. We hypothesized that entrapping microspheres between fibers would have a less adverse impact on mechanical properties than placing microspheres within the fibers themselves, and that the composite would exhibit sustained release of multiple model compounds. Our results show that microspheres ranging from 10~20 microns in diameter could be electrospun in a dose-dependent manner to form nanofibrous composites. When delivered in a sacrificial PEO fiber population, microspheres remained securely entrapped between slow-degrading PCL fibers after removal of the sacrificial delivery component. Stiffness and modulus of the composite decreased with increasing microsphere density for composites in which microspheres were entrapped within each fiber, while stiffness did not change when microspheres were entrapped between fibers. The release profiles of the composite structures were similar to free microspheres, with an initial burst release followed by a sustained release of the model molecules over 4 weeks. Further, multiple model molecules were released

from a single scaffold composite, demonstrating the capacity for multi-factor controlled release ideal for complex growth factor delivery from these structures.

7.2 Introduction

Fibrous tissues of the musculoskeletal system are characterized by aligned collagen bundles that impart non-linear and anisotropic mechanical properties, which enable load bearing functionality in demanding mechanical environments over a lifetime of use. Recapitulation of these fundamental structural and mechanical anisotropies is a key determinant in the development of successful engineered analogues for repair or replacement of these tissues. One scaffold fabrication technique, electrospinning, can produce nano- to micron-sized fibers, similar in length scale to native collagen, from a host of natural and synthetic polymers [52, 53, 211, 212]. Collection of these nanofibers onto a rotating mandrel [213-215] or implementation of specialized collection surfaces [216, 217] can further refine scaffolds by aligning fibers to create structural and mechanical anisotropy within the forming network. By modifying fiber elements such as composition, diameter, and organization, a wide range of mechanical properties can be achieved, which in turn can be tuned to tissue-specific applications. Indeed, such fibrous scaffolds have been used in a wide range of fibrous tissue engineering applications, including constructs for replacement of the knee meniscus [50], the annulus fibrosus [129, 218], tendons and ligaments [219], blood vessels [220] and articular cartilage [221, 222]. When seeded with cells, nanofibrous scaffolds have demonstrated excellent potential for directing ordered ECM deposition, resulting in improved mechanical properties of the engineered construct with time during *in vitro* culture [50, 51, 223].

Despite the potential of these aligned micropatterns to guide new tissue formation, further functionalization might be necessary to expand their general utility, both *in vitro* and with *in vivo* implantation. One key area for expansion is the ability of nanofibrous scaffolds to release select molecules in a controlled fashion. Previous work in other scaffold formats demonstrates the potential of such an approach, for example by promoting neo-vascularization of porous scaffolds through the dual release of pro-angiogenic factors (VEGF and PDGF) [123]. Recent work by several groups has demonstrated that nanofibrous scaffolds can be modified to achieve a degree of controlled release (as reviewed in [53, 224]). In most cases, molecules or biologic agents (i.e., antibiotic, growth factors) are delivered from the fibers themselves. This is a sensible approach, given the high surface area of fibers relative to the volume of the construct, and the close proximity of the fibers to seeded or infiltrating cells. Specific examples of delivery from nanofibrous scaffolds to date include antibiotics [155-158, 160, 225, 226], anticancer therapeutics [166-168, 170], proteins [227-231], DNA [204-206], and growth factors [232, 233]. These successes have been achieved either through direct blending of the molecule of interest into the polymer solution before electrospinning [226], or via the utilization of coaxial electrospinning, wherein a customized spinneret is employed to trap a secondary fluid layer (containing labile biofactors) within the core of the forming nanofiber [227]. For example, Li and coworkers electrospun silk fibroin fiber scaffolds containing a core of bone morphogenetic protein 2 (BMP-2) and demonstrated increased osteogenic differentiation after one month by seeded human mesenchymal stem cells [234].

Despite this progress, the incorporation of molecules into the electrospun fibers may have adverse consequences. For example, retinoic acid added at low levels increased the mechanical properties of single poly(caprolactone-co-ethyl ethylene phosphate) fibers,

while bovine serum albumin incorporated at higher concentrations decreased fiber properties [233]. In another study, Huang and co-workers co-axially electrospun two drugs into PCL fibers and demonstrated that, based on the limited miscibility of the two solvents, mechanical properties were significantly altered [235]. Still other issues may arise when release rates and mechanics are incompatible. For example, Hong and colleagues co-electrospun two populations of fibers, biodegradable poly(ester urethane) urea (PEUU) and poly(lactide-co-glycolide) (PLGA), where the PLGA fibers were loaded directly with the antibiotic tetracycline hydrochloride (PLGA-tet). The PLGA fibers alone had a modulus that was too high and a breaking strain that was too low for the intended application (wound closure in the abdomen). However, addition of a PEUU fiber family decreased the modulus and improved the breaking strain, resulting in more ideal mechanical properties. While promising, this work shows that the remnant fibers contribute to the overall scaffold mechanics, and that drug elution rates are dependent on the fiber properties.

If a fibrous scaffold is to serve the dual roles of load bearing and drug delivery simultaneously, then this issue is paramount and must be considered in the fabrication of scaffolds with defined mechanical characteristics. We report herein a new modification of the electrospinning system to allow for the decoupling of scaffold mechanics from biofactor delivery. This fabrication method is based on the well-established ability of microspheres to carry and deliver molecules of therapeutic interest [236]. In this system, drug releasing microspheres are delivered and entrapped within the fibrous network of the scaffold using sacrificial fibers that are removed upon hydration. We have previously demonstrated that removal of these sacrificial fibers, at the proper percentage [107], can act to increase cellular infiltration into these dense fibrous networks. We hypothesize that entrapping microspheres amongst these

sacrificial fibers, rather than releasing the drug from the fiber or placing the microspheres inside the fibers, will mitigate any major changes to scaffold properties. Further, this method will decouple the degradation rate of the fibers from microspheres, thus allowing for additional flexibility when designing optimal release profiles. The system is developed so that compatible solvent systems enable polymeric fiber formation from organic solvents, while the solvent for sacrificial fibers (water) can maintain PLGA microsphere in their native form. Finally, by including two populations of microspheres, we show that multiple factors can be released independently from one another, providing further design parameters for tissue-specific applications.

7.3 Materials and Methods

7.3.1 Materials

Polystyrene (PS) microspheres (MS) were from either Bangs Laboratories (diameters: 1.94 μm (fluorescent dragon green) and 8.31 μm, Fishers, IN) or Microsphere-Nanosphere (diameter: 15.7 μm, Cold Springs, NY). For nanofiber formation, polyethylene oxide (PEO, 200 kDa) was from Polysciences (Warrington, PA) and poly(ε-caprolactone) (PCL, 80 kDa) was from Sigma-Aldrich (St. Louis MO). Tetrahydrofuran (THF) and N,N-dimethylformamide (DMF), used to dissolve PCL, were from Fisher Chemical (Fairlawn, NJ). Poly lactide co-glycolide 50:50 (PLGA, inherent viscosity: 0.61 dL/g in HFIP) for microsphere fabrication was from DURECT Corp (Pelham, AL). Dichloromethane for microsphere fabrication, bovine serum albumin (BSA, Cohen V fraction), chondroitin 6-sulfate sodium salt (CS), poly vinyl alcohol (PVA, 87-89% hydrolyzed), and fluorescein (free acid) were all from Sigma-Aldrich (Allentown, PA). The bicinchoninic acid (BCA) assay kit was purchased from Pierce Protein Research

Products (Thermo Scientific, Rockford, IL). Dulbecco's phosphate-buffered saline (PBS) was purchased from Gibco (Invitrogen, Grand Island, NY).

7.3.2 Electrospinning Nanofibrous Scaffolds using Pre-Fabricated Microspheres

To electrospin fibers containing pre-fabricated microspheres, a high concentration of PS microspheres (1^9-10^9 MS/mL) was dispersed in 10% PEO in 90% ethanol or in 35.7% w/v PCL in a 1:1 mixture of THF and DMF. The suspension was sonicated for 3 minutes to disperse the MS and electrospun as in [50]. Briefly, a 10 mL syringe was filled with the electrospinning solution and fitted with a stainless steel 18G blunt-ended needle that served as a charged spinneret. A flow rate of 2.5 mL/h was maintained with a syringe pump (KDS100, KD Scientific, Holliston, MA). A power supply (ES30N-5W, Gamma High Voltage Research, Inc., Ormond Beach, FL) applied a +15 kV potential difference between the spinneret and the grounded mandrel located at a distance of 12 cm from the spinneret. The mandrel was rotated via a belt mechanism conjoined to an AC motor (Pacesetter 34R, Bodine Electric, Chicago, IL). Additionally, two aluminum shields charged to +10 kV were placed perpendicular to and on either side of the mandrel to better direct the electrospun fibers towards the grounded mandrel.

7.3.3 Fabrication and Electrospinning of PLGA Microsphere-Laden Nanofibrous Scaffolds

Degradable PLGA microspheres were fabricated using a double-emulsion water/oil/water technique based on [236]. Briefly, 0.5 grams of 75:25 PLGA was dissolved in 1 to 4 ml of DCM. The solution was further supplemented with 0.5 ml of 10%

BSA and homogenized at Speed 5 for 30 seconds using a Homogenizer 2000 (Omni International, Kennesaw GA). One to 2 mL of 1% PVA was then added and the entire mixture re-emulsified by homogenization for 1 minute at Speed 1. Hardened microspheres were collected after gentle stirring for 3 hours in 100 ml of 0.1% PVA. The collected microsphere solution was then passed through a 70 μm nylon filter (BD Biosciences, Bedford, MA), centrifuged, and washed 3 times in water. Fabricated microspheres were lyophilized and stored at -20°C until use. Light microscope images were taken after fabrication, after filtration, and before lyophilization, and diameters determined using a custom MATLAB program. Microsphere density in formed nanofibers was determined after electrospinning from solutions containing 0.01, 0.03, 0.05, 0.07 and 0.09 g MS/mL PEO solution onto a glass slide for 5 seconds (n=3). For each condition, three light microscope images were obtained with similar fiber density per slide, and microspheres were counted in each image.

7.3.4 Fabrication of PCL/MS Composite Nanofibrous Scaffolds

Composite nanofibrous scaffolds (PCL/PCL and PCL/PEO) containing PS microspheres (15.7 micron diameter) were formed by dual-electrospinning from two opposing spinnerets onto a common rotating mandrel as in [107]. In one configuration, a PCL jet (2.5 mL, +15 kV, 12 cm) and a PCL jet with microspheres (2.5 mL/hr, +11 to +16 kV, 6 cm) were electrospun together. In the second configuration, a PCL jet and a PEO jet with microspheres (2 mL/hr, +16 kV, 6 cm) were electrospun together. Microsphere densities in the spinning solutions were 0, 0.05, 0.1 and 0.2 g PS microspheres/mL electrospinning solution. After fabrication, scaffold samples containing PEO were taken along the length of the scaffold, weighed, hydrated in 50% ethanol for 10 minutes to remove PEO, lyophilized and reweighed to determine PEO content as a function of

position. Scaffolds were imaged via SEM (Philips XL20 by FEI, Hillsboro, Oregon) before and after PEO elution to visualize MS inclusions.

7.3.5 Mechanical Properties of PCL/MS Composite Nanofibrous Scaffolds

For mechanical testing, 30 x 5 mm strips of scaffold were excised with their long axes oriented in the fiber direction (along the circumference of the collecting mandrel). For PCL/PEO-MS scaffolds, strips containing ~15% PEO were utilized. Prior to mechanical testing, all samples were soaked in 50% ethanol for 10 minutes, and then stored in PBS until testing. The cross-sectional area of each sample was measured using an OptoNCDT laser measuring device (Micro-Epsilon, Raleigh, NC) combined with a custom Matlab program [237]. Samples were loaded into an Instron 5848 Microtester equipped with serrated vise grips and a 50 N load cell (Instron, Canton, MA). Strips were pre-loaded for 2 minutes to 0.5N, after which the gauge length was noted. Samples were then preconditioned with extension to 0.5% of the gauge length at a frequency of 0.1 Hz for 10 cycles. Finally, samples were extended to failure at a rate of 0.1% of the gauge length per second. Stiffness was determined from the linear portion of the force-elongation curve, and modulus calculated by considering sample cross-sectional area and gauge length.

7.3.6 Dual Release from Composite Nanofibrous Scaffolds

PLGA microspheres were formed containing two representative molecules, bovine serum albumin (BSA) and chondroitin sulfate (CS). BSA-containing microspheres were prepared as above with a 10% mass/volume BSA solution encapsulated in 50:50 PLGA. CS-containing microspheres were prepared from a 20% mass/volume CS solution that

was mixed with 100 µl of 1% PVA with encapsulation in 50:50 PLGA. The initial encapsulation efficiency of BSA was determined by dissolving 50 mg of fresh MS in 0.1N NaOH containing 5% SDS with vigorous agitation for 16 hours. The supernatant was assessed via the BCA assay, with standards containing 0.1N NaOH with 5% SDS. To determine CS encapsulation efficiency, 50 mg of MS were dissolved in 8 mL of a 1:1 solution of DCM and H_2O with vigorous agitation for 4 hours. After overnight phase separation, the aqueous phase was removed and CS content determined using the DMMB assay [67].

Long term release of CS or BSA from PLGA microspheres was evaluated via incubation in PBS (30 mg MS per 1 mL PBS) at 37°C on a 3-D mini-rocker (Denville Scientific, South Plainfield, NJ). At defined intervals over 5 weeks, microspheres were pelleted by centrifugation and the supernatant tested for CS content (via the DMMB assay) or BSA content (via the BCA assay) as above. At each sampling, fresh PBS was added and MS re-dispersed by gentle vortexing. Next, composites were formed to evaluate release from MS when entrapped in a PCL network. In preliminary studies, to image the composite, PCL was doped with fluorescein and PLGA microspheres were fabricated with rhodamine B. Fluorescent and light micrographs were overlaid to identify each component within the composite system. Subsequently, three microsphere-laden nanofibrous composites were constructed: one with CS-containing microspheres, one with BSA-containing microspheres, and one with a 1:1 mixture of CS- and BSA-containing microspheres. For these studies, rectangles of scaffold (80 mg) were cut across the length of the mandrel to ensure sample uniformity. Scaffolds were soaked in 5 ml of 50% ethanol for 10 minutes and washed in PBS to remove PEO. Scaffolds were then transferred to PBS (1 mL) and incubated as above for the MS release study. At set intervals, the supernatant was removed and CS and BSA quantified as above.

7.3.7 Statistical Analyses

One-way analysis of variance (ANOVA) was carried out using GraphPad Prism software (Graphpad Software, La Jolla, CA) with Bonferonni's *post-hoc* tests (n=3 for characterization of MS density, n=5 for mechanical testing, n=5 for evalution of release kinetics), with significance set at $p < 0.05$.

7.4 Results

7.4.1 Formation of Nanofibers with Microspheres

Electrospinning from a solution of PEO and pre-fabricated fluorescent polystyrene microspheres resulted in the formation of fibers with embedded microspheres (**Figure 7-1A**). Similar findings were noted when PS microspheres were electrospun from a PCL solution, with thickened regions of PCL visible around the microsphere via SEM (**Figure 7-1B**).

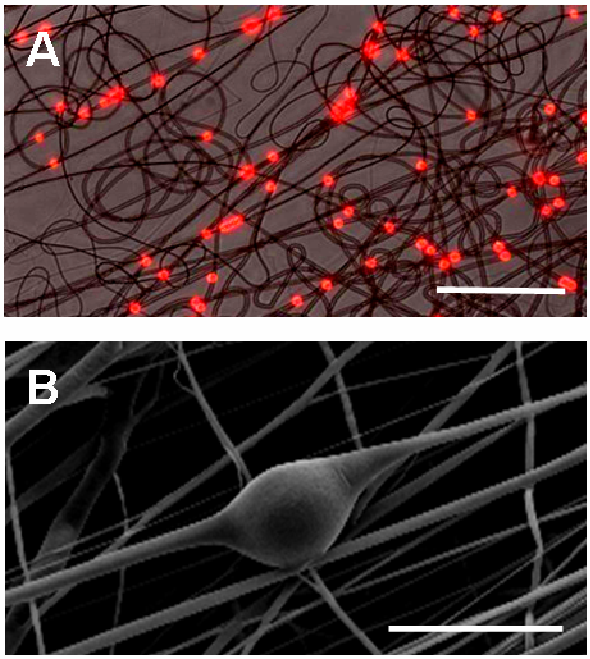

Figure 7-1 Fabrication of microsphere-laden nanofibrous scaffolds. (A) Composite light and fluorescent micrograph showing electrospun PEO fibers with embedded PS microspheres (diameter 2 microns) distributed along the fiber length (Scale bar = 50 μm). (B) SEM micrograph demonstating alterations in PCL fiber morphology local to the inclusion of an 15.7 micron diameter PS microsphere (Scale bar = 25 μm).

PLGA microspheres were fabricated via the water/oil/water double emulsion process (**Figure 7-2A**). Microsphere diameters were on the order of 10-20 microns (**Figure 7-2B**), with little change through the washing process (data not shown). Increasing the density of PLGA microspheres in the PEO electrospinning solution increased the density of microspheres in the resulting fibers (Figure **7-2C,D**). Microsphere numerical density within the fibrous scaffold was higher for solutions starting with microspheres at 0.07 and 0.09 g/mL compared to those starting with lower microsphere concentrations (**Figure 7-2C**, $p<0.05$).

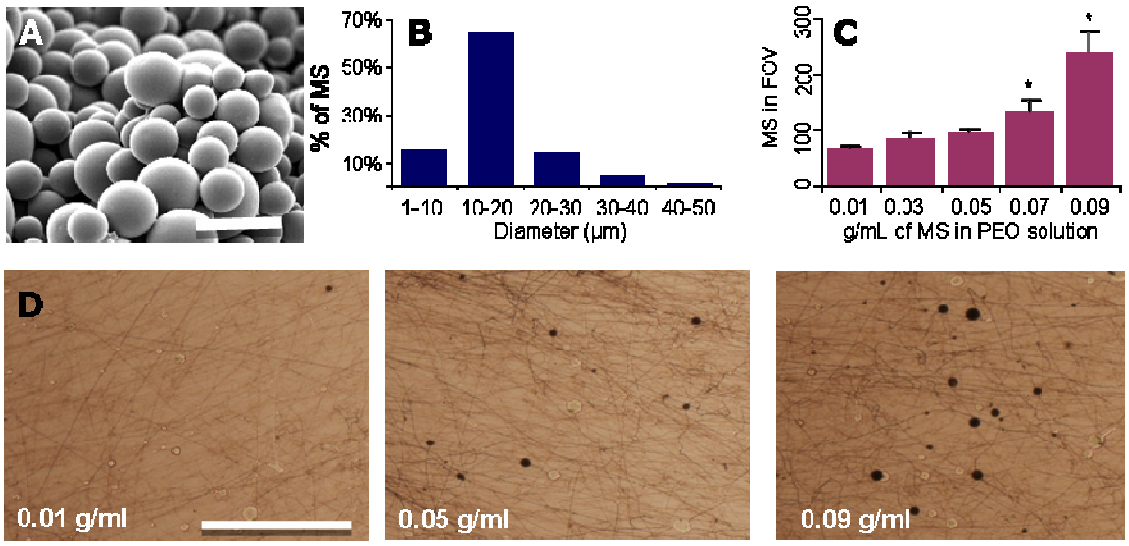

Figure 7-2 Dose-dependent inclusion of PLGA microspheres in nanofibrous mats. (A) SEM micrograph showing PLGA microspheres fabricated by the double emulsion technique (Scale bar = 50 µm). (B) Histogram of microsphere diameter. (C) PLGA microsphere density with a field of view (FOV) of a PEO fiber mat increases with increasing microsphere density in the electrospinning solution. *indicates significant difference compared with lower values, $p<0.05$. (D) Bright-field images of PEO fiber mats formed from solutions of increasing PLGA MS density (Scale bar = 500 µm).

7.4.2 Fabrication and Electrospinning of Microsphere-Laden Nanofibrous Scaffolds

As described above, and shown schematically in **Figure 7-3**, a fabrication system was developed to entrap microspheres within a fibrous scaffold. In this technique, the sacrificial PEO fiber population containing microspheres is co-electrospun with PCL fibers onto a common rotating mandrel. Fluorescent labeling of PCL fibers (green) and microspheres (blue), while the PEO component remained unlabelled, identifies the blend of the three components (**Figure 7-4A**). Upon hydration, the sacrificial PEO fibers dissolve away, resulting in a structure in which microspheres are entrapped between aligned PCL fibers. SEM images of composites before (**Figure 7-4B**) and after (**Figure 7-4C,D**) PEO removal shows that microspheres remain entrapped between the aligned fibers throughout the fabrication process. Notably, this dispersion is seen through the thickness of the composite when cross sections are viewed end on (**Figure 7-4D**).

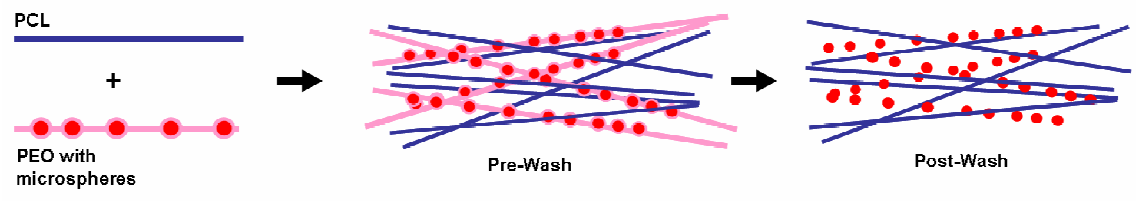

Figure 7-3 An approach for decoupling drug delivery from scaffold mechanics. Composite scaffolds are formed from microspheres delivered through a sacrificial PEO fiber fraction coupled with a stable PCL fiber fraction (Pre-Wash). With dissolution of the PEO (After-Wash), MS remain entrapped within the slow degrading and surrounding fibrous PCL fibrous network.

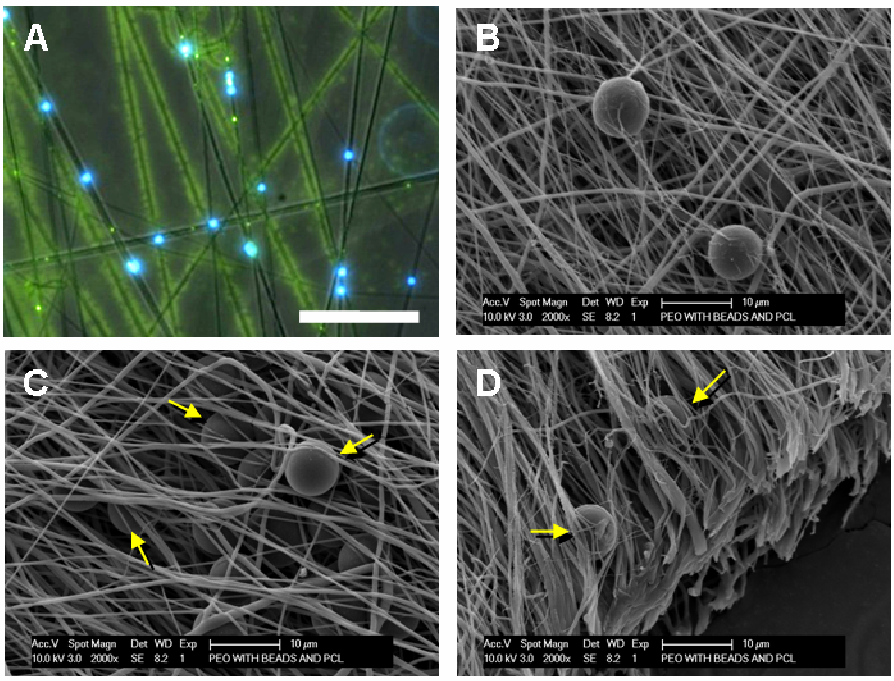

Figure 7-4 Realization of composite MS-laden scaffolds with sacrificial content. Bright-field with overlaid fluorescent image (A, 4X, Scale bar = 50 μm) and SEM (B, Scale bar = 20 μm) of PEO/PCL/MS composite. In (A), blue shows MS, green shows PCL fibers, and black shows sacrificial PEO fibers within the composite structure. After PEO removal, microspheres remain entrapped and distributed between the remaining PCL fibers (C and D, arrows, Scale bar = 10 μm).

7.4.3 Mechanical Properties of Composite Scaffolds as a Function of Microsphere Inclusion

To better understand the mechanical consequences of microsphere inclusion, networks were formed in which a graded concentration of polystyrene microspheres was entrapped either within or between the nanofibers of the scaffold. PS microspheres (15.7 μm diameter) were used here because PLGA microspheres would dissolve when mixed into the solvents employed for electrospinning PCL. Scaffolds were fabricated as depicted in **Figure 7-5A and 7-5D**, with one jet used to produce a PCL fiber population, and a second jet used to produce a microsphere-containing fiber population of either PCL or PEO. Tensile testing showed that when microspheres were included within the PCL fiber population, both the stiffness and modulus decreased with each step of increasing microsphere density (**Figure 7-5B and C**). Conversely, in composites where the microspheres were entrapped between fibers after sacrificial fiber removal, no change in stiffness was observed at any microsphere density (**Figure 7-5E**). Likewise, modulus in these composites did not differ from control values at Low microsphere densities.

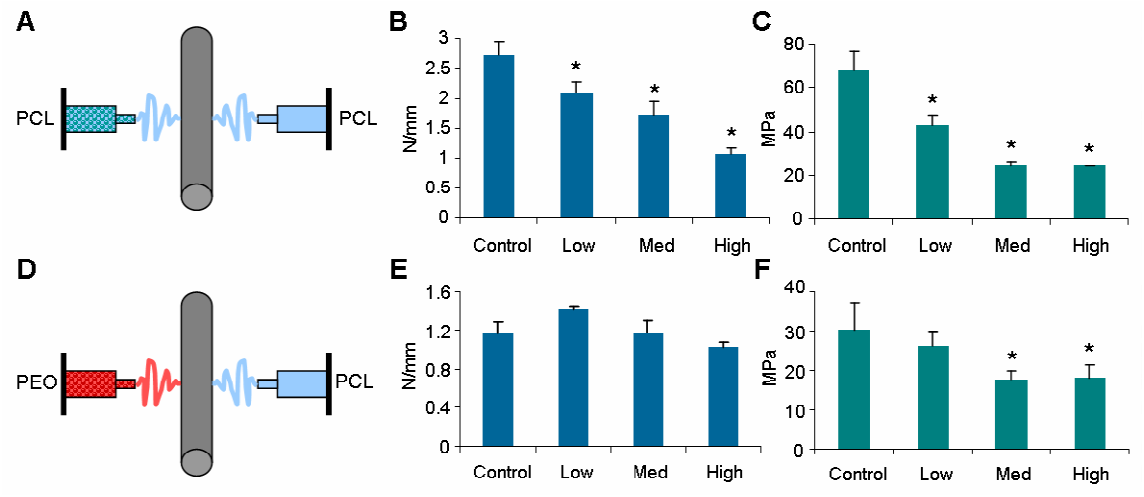

Figure 7-5 Construction and mechanical analysis of composite MS-laden scaffolds. (A) Schematic of electrospinning PCL/PCL-MS scaffold. (B) Stiffness of scaffold decreases with increasing MS density (Control = 0, Low = 0.05, Med = 0.1, High = 0.2 g MS/mL electrospinning solution). (C) Modulus decreases with increasing MS density. (D) Schematic of electrospinning PCL/PEO-MS scaffold. (E) Stiffness does not change with increasing MS density. (F) Modulus decreases at medium and high density MS inclusion, but not at low inclusion density. *indicates $p < 0.05$ from control.

7.4.4 Controlled Release from Microsphere-Laden Nanofibrous Composites

To determine if molecules could be released from the composite in a controlled fashion, BSA- and CS-containing PLGA microspheres were fabricated and release rates determined for both free microspheres and microspheres entrapped within the composite structures. The encapsulation rate for each molecule was 13% and 11%, respectively, with a burst release occurring over the first day for free microspheres, followed by a sustained release over 27 days (**Figure 7-6B**). The initial burst release was larger from the CS-containing microspheres compared to BSA-containing microspheres. By day 27, free microspheres had degraded to the point where clumping of the polymer was apparent (*data not shown*). When either BSA- or CS-containing microspheres were electrospun into the composite, a slightly-more gradual release profile was observed over the first 5 days, with sustained released occurring thereafter (**Figure 7-6C**) perhaps due to washing steps that occurred during PEO removal. Contrary to free microspheres,

microspheres entrapped in nanofibrous scaffolds remained distinct, most likely due to physical protection and isolation when media was changed (data not shown). When the microsphere populations were mixed 1:1 and electrospun into a single nanofibrous composite (**Figure 7-6D**, black = CS, red = BSA), a similar graded release profile for each molecule was observed over 35 days.

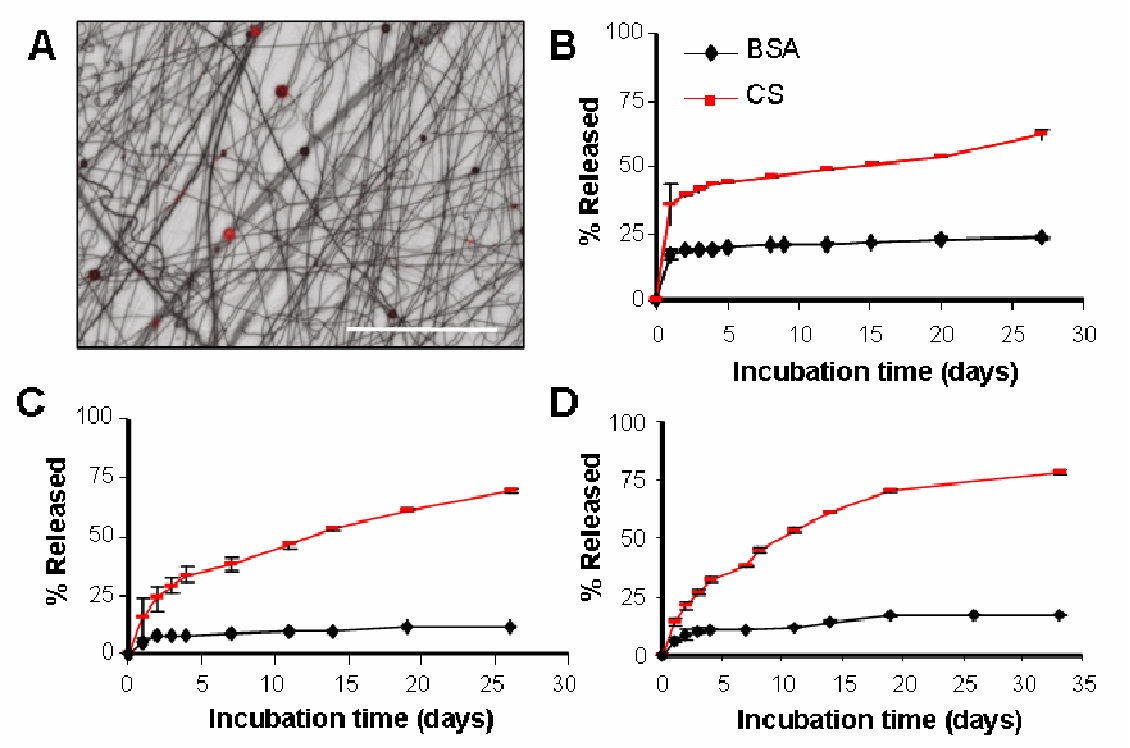

Figure 7-6 Controlled release from composite MS-laden scaffolds. (A) Overlay of light and fluorescent micrographs showing mixed MS population (BSA MS = red, CS MS = black, scale bar = 250 μm). (B) Sustained release of bovine serum albumin (BSA) or chondroitin sulfate (CS) from PLGA microspheres with time in physiologic conditions. (C) Sustained release of BSA and CS from composite PCL/PEO-MS scaffold containing either BSA or CS microspheres. (D) Sustained release of both BSA and CS from a single composite system containing both BSA and CS microspheres at a 1:1 ratio.

7.5 Discussion

Electrospun nanofibrous scaffolds are a promising tool for fibrous tissue engineering as they provide excellent structural cues and can foster development of anisotropic mechanical properties similar to native tissues [50]. Indeed, we have grown constructs *in vitro*, under chemically defined conditions and with the addition of matrix-promoting growth factors that reach 50-100% of the tensile properties of native meniscus and annulus fibrosus [53, 129]. Simply providing a guided micropattern for tissue formation may not be enough, however, as both tissue development and regeneration occur in the context of a host of biologic factors whose timing and doses vary considerably. Moreover, upon implantation of a scaffold, our ability to control the chemical environment (i.e., the provision of pro-matrix forming growth factors in culture medium) is lost. Further functionalization of these scaffolds to enable delivery of drugs, growth factors or other chemicals would further our ability to both guide construct maturation and dictate cell behavior *in vivo* and *in vitro*.

Several recent reports have shown that micro-and nano-particles can be incorporated into electrospun nanofibers. In one report, Lim and colleagues demonstrated that silica particles ranging in size from 100-1000 nanometers could be electrospun from a solution of polyacrylimide to create a 'bead on a string' fiber morphology [238]. Also, Dong et al. incorporated two distinct populations of nanospheres into electrospun polyurethane fibers, suggesting the ability to multiplex delivered factors, but did not evaluate release [200]. Towards drug delivery, Melaiye et al. incorporated silver(I)-imidazole cyclophane gem-diol complexes into tecophilic polymer electrospun fibers, and demonstrated that release of this molecule from particles within the fibers could prevent microbial growth [239]. Finally, Qi et al. fabricated BSA-loaded Ca-alginate microspheres and emulsion

electrospun the spheres within PLLA fibers. In this context, BSA released at a slower rate and with a lower initial burst than from free Ca-alginate microspheres [202]. While these previous studies represent early efforts to protect a molecule during fabrication and release it from a particle in a fiber, they did not address the mechanical characteristics of the system or how to decouple the fiber function, degradation, and microsphere release kinetics.

Given the mechanical roles these scaffolds must play upon *in vivo* placement (where the tensile moduli of fiber reinforced tissues are on the order of 100 MPa [240]), we endeavored to create a system where microspheres could be delivered without significantly disrupting the overall scaffold mechanics. The inclusion of particles within fibers disrupts individual fiber architecture (**Figure 7-1B**) and creates local stress concentrations, thereby modifying the overall mechanical properties of the scaffold. When the microspheres were included within the load-bearing PCL fibers, scaffold stiffness decreased even at low microsphere concentrations (**Figure 7-5B**). Conversely, in our composite system that contains particles between the fibrous network but not the fibers themselves, stiffness remained unchanged (**Figure 7-5E**) at all microsphere densities explored. Of note, while stiffness did not change in our composite, the modulus did decrease at the medium and high microsphere concentrations. This result was due to a slight increase in scaffold cross sectional area with microsphere inclusion caused by decreased fiber packing, and may be considered a limitation of our design.

Spatial and temporal control of growth factor presentation is an important consideration in directing cell behavior during development and repair. Delivery of particles within a fiber may complicate release by coupling molecular diffusion within a fiber and/or fiber degradation with the release kinetics of the factor from the particle itself. Our approach

delivers particles via a sacrificial fiber population that is removed immediately upon hydration. When particles are of sufficient size (20 microns, in this case), they remain entrapped within the fibrous network but are exposed directly to the aqueous environment. This approach decouples the release kinetics of the microspheres from the degradation kinetics of the fibers themselves. Furthermore, using PEO allows for a compatible solvent system (water) for sacrificial fiber production, such that the PLGA microsphere structure is not disrupted with exposure to organic solvents (i.e., the DMF/THF solution used to dissolve PCL). When two model agents, BSA and CS, were included in microspheres in the composite, release kinetics were independent from one another and comparable to free microspheres, suggesting that release is indeed independent of the surrounding fiber population (**Figure 7-6**).

The potential applications of a composite nanofibrous system that can deliver multiple factors in a controlled fashion while maintaining mechanical functionality are enumerable. For example, a cascade of growth factors (i.e., PDGF followed by VEGF) might be delivered to promote vascularization of the implanted construct [123]. This would be particularly suited for the knee meniscus, whose dense structure and limited vascularity does not allow for endogenous repair. Alternatively, one might engineer the system to provide for instantaneous release of mitogenic (i.e., FGF) or migratory factors, followed by a delayed release of a pro-matrix forming compound (i.e., TGF-β). This construction would promote cell infiltration from surrounding tissue and division during an initial period of repair, followed by transition towards a matrix deposition phase of development. Delivered factors also need not be solely anabolic/growth promoting. For example, microparticles might be designed to deliver proteases locally to engender local matrix disruption to enhance bridging of new matrix between the host tissue and the implanted material. Similarly, the distribution of particles need not be homogenous,

with gradients of local release established both through the depth and along the fiber plane.

While the results of this study are promising, and the system meets our stated design criteria, some issues remain to be optimized. First, it is not clear how microsphere size influences mechanical properties; in this work, microspheres were on the order of 20-30 microns. Larger microsphere sizes might further disrupt mechanical properties, while smaller particles could be lost from the scaffold through the porous structure. Additional studies are required to examine this variable. Another point of optimization involves the steric and biologic influence of the particles themselves. We have previously demonstrated that both meniscus fibrochondrocytes and mesenchymal stem cells attach to and infiltrate electrospun PCL scaffolds [50, 107, 129, 218]. While the microspheres in this formulation are composed of a biocompatible material (PLGA), local pH changes with PLGA degradation might influence cellular activity. Further, sacrificial fibers were used here to deliver microspheres. We previously utilized these sacrificial fibers (at a level of ~40-60% of the composite) to increase scaffold porosity and enhance cell infiltration into the depth of the aligned nanofibrous structure [107]. For microsphere inclusion, our highest PEO content was on the order of 15%. It remains to be determined how this low level of sacrificial fibers (and the potential decrease in fiber packing due to the microspheres themselves) influences cell infiltration. Future iterations may utilize a multiple spinneret system comprised of one source jet delivering PCL or another slow-degrading structural fiber population, one source jet delivering PEO fibers, and the final jet delivering microspheres through additional sacrificial PEO fibers. Such a multi-jet system would also allow for the provision of additional mechanical functionality via variation in the mechanical properties of the PCL or slow eroding component [241]. A final point of optimization is the microspheres themselves. We used a traditional

fabrication technique (water/oil/water emulsions) to entrap model compounds in order to demonstrate multi-factor release. While sufficient for proof of principle, we did observe the commonly seen burst release with each compound. Others have shown that microsphere fabrication methods can be tuned to enable release with a multitude of profiles, including constant, early burst, and late burst [242]; such methods would be useful in further tuning towards the intended biologic applications described above.

7.6 Conclusions

Overall, this study describes an approach for the creation of drug-delivering anisotropic nanofibrous scaffolds for fibrous tissue engineering. In this fabrication method the inclusion of microspheres does not significantly modify the mechanical properties of the scaffold or the release properties of the microspheres entrapped within the composite. Importantly, multiple populations of microspheres releasing unique factors can be incorporated, allowing for the complex control of cellular behavior through spatially and temporally-tuned release. Vascular recruitment, cellular phenotype and matrix elaboration may all be dictated via the proper release of single or multiple factors from these composites. Rather than creating a simple template for new ECM deposition, this advanced composite provides higher order functionality for mechanical and biologic guidance of tissue regeneration.

7.7 Acknowledgements

This work was performed in collaboration with Gregory C. Lee, Brian J. Sennett, Jason A. Burdick, and Robert L. Mauck. It was published in Biomaterials (2010 May;31(14):4113-20). Funding was provided in part by the National Institutes of Health (R01 AR056624 and T32 AR007132), the Penn Center for Musculoskeletal Disorders, the University Of Pennsylvania Department Of Orthopaedic Surgery, and the Department of Veterans Affairs (VA).

8: Vascularization of VEGF-Loaded Electrospun Scaffolds for Fibrous Tissue Repair Using Sacrificial Fibers and Entrapped Microspheres

8.1 Abstract

Aligned electrospun scaffolds provide an instructive environment for fibrous tissue engineering. Additional functionalization, such as the ability to deliver growth factors from these materials, would further guide cell behavior and expand the clinical applications of such materials. Because biofactor inclusion can alter the mechanics of the scaffold fibers, our goal was to identify alternative delivery techniques for applications in orthopedic tissues, where scaffold mechanics are important. In this work, composite, aligned fibrous scaffolds composed of both slow-degrading poly(ε-caprolactone) (PCL) fibers and sacrificial poly(ethylene oxide) (PEO) fibers were formed via multi-jet electrospinning. PEO fibers within the composite scaffold were used to directly deliver biologic factors (burst release) or to entrap poly(lactide-co-glycolide) (PLGA) microspheres containing these same factors (controlled release). Composites delivering basic fibroblast growth factor (bFGF) stimulated the proliferation of meniscus fibrochondrocytes (MFCs) *in vitro*. When evaluated *in vivo*, delivery of vascular endothelial growth factor (VEGF) from these composites enhanced blood vessel density in the peri-implant space in a dose-dependent manner. This system has the potential to deliver different combinations of growth factors, inflammatory regulators, antibiotics and other chemical cues to create a regenerative environment at the site of injury, restoring tissue function in situations where endogenous repair capacity is limited.

8.2 Introduction

Tissue engineering of dense fibrous structures of the musculoskeletal system, such as the knee meniscus and annulus fibrous, presents a particularly difficult challenge. Not only must the temporary scaffold architecture provide a defined anisotropic mechanical environment, but the scaffold must also drive the ordered behavior of cell populations that typically have low density and metabolic activity [52]. Many orthopedic structures, such as the knee meniscus, exist in challenging environments typified by little vascular support, high mechanical loads, and consequently, minimal repair potential [119]. Successful repair in this context requires that natural and synthetic scaffolds recruit and/or maintain a highly active cell population to infiltrate the material and to deposit organized matrix that regenerates the original tissue structure. *In situ* cell recruitment is simpler and more cost effective than implanting scaffolds already loaded with expanded cells. Significant progress has been made towards matching the mechanical environment of such fibrous tissues with engineered materials; however, the ability to direct cells, activate differentiation and promote cell recruitment in these settings is also of paramount importance [14].

Electrospinning is a simple method to generate polymeric nano- to micron-sized fibers via electrostatic forces [53]. Various synthetic and biological polymers can be employed that create a permanent structure or degrade over defined timescales [52, 53, 211, 243]. Fibers can be collected on a variety of surfaces to control organization and alignment, and multiple fibers can be spun into a single composite scaffold from multiple polymer sources [52, 107, 213-215]. Electrospinning has been used in many tissue engineering applications, including blood vessels, tendons, meniscus, annulus fibrosus, and cartilage [50, 129, 218-222].

Previously, we have developed a number of different electrospun scaffolds with unique benefits for orthopedic tissues. We have created scaffolds composed of 100% poly(ε-caprolactone) (PCL) fibers that possess relevant anisotropic mechanical properties and long-term degradation profiles (**Figure 8-1A**). When seeded with meniscus fibrochondrocytes (MFCs) or mesenchymal stem cells and cultured *in vitro* under defined conditions, the tensile modulus of the neotissue formed was close to that of native meniscus tissue, with robust matrix deposition and cell distribution throughout the structure [50, 51]. To further improve the properties of this structure, a multi-jet apparatus was developed, where multiple fiber populations were collected onto a single rotating mandrel to generate an aligned, composite scaffold (**Figure 8-1B**) [107, 147]. In one illustration, scaffolds containing a blend of PCL fibers and poly(ethylene oxide) (PEO) fibers resulted in a more porous structure upon hydration, as PEO fibers instantly dissolved away. Dissolution of the PEO fibers created voids between the PCL fibers, and with this additional porosity, composite scaffolds were better infiltrated and had increased matrix deposition with time *in vitro* compared to scaffolds containing PCL fibers alone [107]. While extensive *in vitro* work has been performed, it is not yet clear how these scaffolds will perform *in vivo*. In this work, we hypothesized that electrospun scaffolds containing PCL and PEO would be well tolerated *in vivo* and would be populated by cells from the subcutaneous space. Also, we posited that composite scaffolds containing both PCL and PEO fibers would be better infiltrated than those containing only PCL fibers, due to the increase in porosity [148].

In addition to fostering cell infiltration, scaffolds should promote cell recruitment and activation at the repair site. Interestingly, many of the polymers used in electrospinning have also been used in drug delivery applications as well, suggesting that such scaffolds

could provide biologic as well as structural cues. Unfortunately, electrospinning utilizes harsh organic solvents that can denature large molecules such as growth factors [244]. Direct addition of growth factors to the polymer solution prior to electrospinning does not consistently produce bioactive scaffolds, with several groups demonstrating a marked loss of activity after spinning [183-185]. In order to overcome this limitation, alterations to the fabrication process can be implemented, for example through an initial water/oil emulsion step prior to electrospinning [187, 188], or through post-fabrication chemical modification of the fibers [130, 171]. Alternatively, specialized coaxial electrospinning devices can be employed that protect growth factors within a central channel in the fiber, although the equipment needed can be complex to build and use [132, 195, 196].

As another option to the approaches mentioned above, we developed two distinct methods to deliver active biologic factors from aligned nanofibrous scaffolds. The first, most direct method involved modifying to our sacrificial fibers to enable electrospinning of PEO in water, without the use of organic solvents or alcohol. We hypothesized that this all-aqueous formulation would uniquely harbor and release functional growth factors without any additional fabrication steps (**Figure 8-1C**). This method represents a simple technique to release growth factors with an immediate 'burst' from sacrificial fibers.

An alternative approach for delivering bioactive growth factors from fibers is to incorporate secondary structures in or between the fibers that protect these delicate molecules during the fabrication process. Approaches include the use of bubbles, microparticles and microspheres [114, 200-202]. Previously, we developed a technique to entrap degradable poly(lactide-co-glycolide) (PLGA) microspheres (MS) between

electrospun PCL fibers by loading the MS into the sacrificial PEO fiber population. The result is a MS-composite scaffold containing distinct PCL fibers and PLGA microspheres after PEO removal through hydration (**Figure 8-1D**) [114]. This technique limits the mechanical perturbations to the scaffold as the microspheres reside outside the structural elements, while also creating drug delivery capabilities that are materially distinct from the structural fibers. PLGA microspheres are FDA approved for use in humans, and can deliver a broad range of chemicals with diverse release profiles, including growth factors [245-250]. Multiple microsphere populations can be mixed into the scaffold, a useful property when delivering time- and dose-sensitive molecules that work best in concert [123, 251, 252]. Previously, we simultaneously delivered the small molecules bovine serum albumin (BSA) and chondroitin sulfate (CS) over a month from a single MS-composite scaffold with distinct release profiles [114].

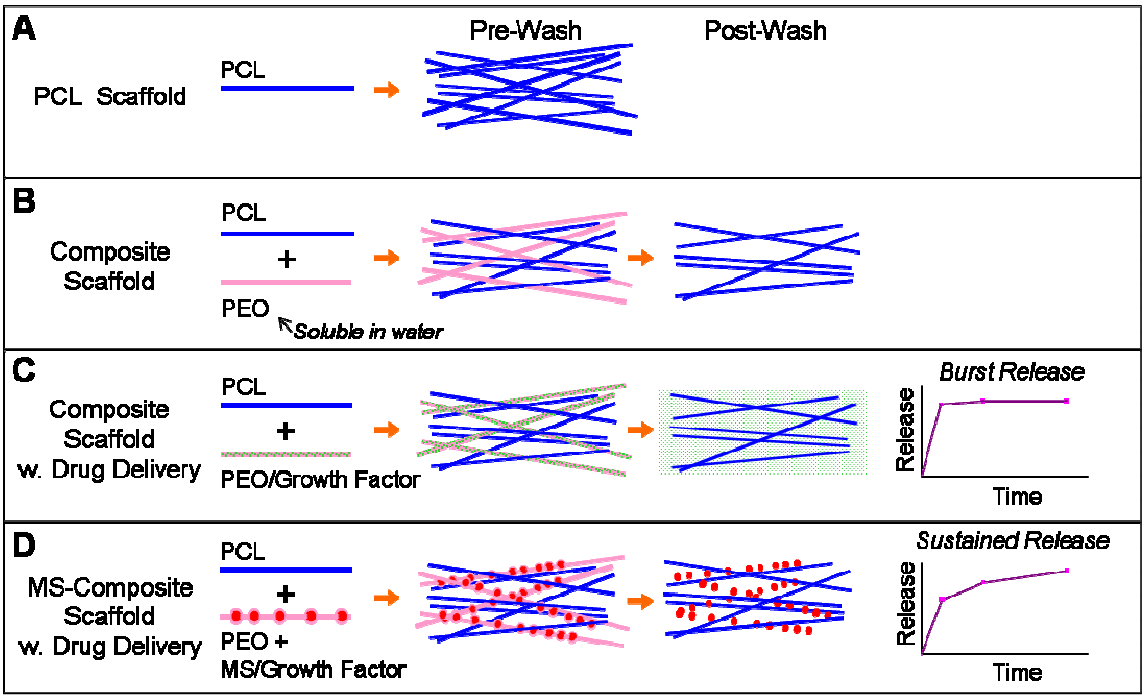

Figure 8-1 Schematics of the fiber populations, pre- and post-wash scaffold structures, and hypothetical drug release profiles for scaffolds capable of delivery. (A) PCL scaffold. (B) Composite scaffold. (C) Composite scaffold with drug delivery. (D) MS-composite scaffold with drug delivery.

Having established this delivery framework, the current study sought to deliver growth factors from the novel MS-composite scaffolds in order to elicit biologic responses both *in vitro* and *in vivo*. Because shear forces and phase separation during microsphere fabrication, and electrostatic forces during electrospinning, can all result in growth factor degradation [253], we first assayed for bioactivity *in vitro*. To do so, basic fibroblast growth factor (bFGF) was delivered from MS alone and MS-composite scaffolds. bFGF has a strong mitogenic effect on MFCs and is relatively inexpensive for optimization studies [10, 111]. Upon confirmation of bioactivity and a favorable response *in vivo* for composite scaffolds and MS-composite scaffolds, we next focused on the delivery of vascular endothelial growth factor (VEGF) from both sacrificial fibers and microspheres in composite scaffolds, hypothesizing that this growth factor would improve vascularization of scaffolds *in vivo*. VEGF is an important factor in the molecular cascade that controls angiogenesis [254-256], and could play a vital role in healing and integration after scaffold or neotissue implantation [117, 118]. Previously, VEGF has been shown to improve vascularity in engineered materials [123, 257-259], with an optimal release profile similar to that of our MS-composite scaffolds [260]. We hypothesized that the two techniques (delivery from sacrificial fibers and from entrapped MS) would result in distinct delivery profiles; while sacrificial PEO fibers dissolve instantly, PLGA microspheres degrade over weeks or months. Further, the effect of dosage was explored by including different fiber fractions of PEO-VEGF fibers within the composite scaffolds, and we hypothesized that vascularization would occur in a dose-dependent manner. The effects of VEGF were assessed via semi-quantitative histological analysis inside macropores that transit the scaffolds and serve as vascular conduits. Results from this work validate this technology as a multifunctional scaffold capable of both mechanical and biologic instruction for fibrous tissue engineering.

8.3 Materials and Methods

8.3.1 Fabrication and Characterization of Microspheres

Microspheres (MS) were fabricated using a double emulsion technique [114]. Briefly, 0.5g 75:25 DL-lactide/glycolide copolymer (Purasorb PDLG 7502, generously provided by Purac Biomaterials, Gorinchem, Netherlands) was dissolved in 1 mL dichloromethane (DCM, Sigma-Aldrich, Allentown, PA). Next, this solution was combined with 0.5 mL 10% bovine serum albumin containing 0 or 20 μg basic fibroblast growth factor (bFGF, Peprotech, Rocky Hill, NJ) and sonicated for 5 seconds at speed 10 to form a primary emulsion. Polyvinyl alcohol (1 mL 1%, PVA, Sigma-Adrich, St. Louis, MO) was added, and the mixture sonicated again, and subsequently poured into 100 mL 0.1% PVA to stir gently for 3 hours while hardening. Afterwards, microspheres were filtered to below 70 μm in diameter, centrifuged, lyophilized and frozen until ready for use. The microspheres were visualized using a scanning electron microscope (SEM, Philips XL20 by FEI, Hillsboro, Oregon) to confirm round, smooth spheres. The average microsphere diameter was 20 μm [114]. To characterize release from microspheres, 1.5 mL tubes containing 50 μg microspheres and 1 mL phosphate-buffered saline (PBS) were incubated at 37°C on a rocker for 7 days. At set timepoints, the tubes were centrifuged, and the supernatant was removed, stored, and replaced. bFGF concentration in the supernatant was measured with an ELISA kit (Quantikine, R&D Systems, Minneapolis, MN). The assay work was performed in triplicate over several distinct fabrications to ensure consistency of release profile (n=3).

To determine if bFGF remained bioactive after encapsulation, a meniscus fibrochondrocyte (MFC) proliferation assay was employed. Briefly, 0-3 month old bovine meniscus tissue was dissected in a sterile fashion, with care taken to remove all surrounding synovial tissue. The meniscus was minced and plated on tissue-culture

plastic (Corning, Sigma-Aldrich, St. Louis, MO) in basal media (Dulbecco's modified Eagle's medium containing 10% fetal bovine serum and 1% penicillin/streptomysin/fungizone). MFCs emerged onto the plate and proliferated over the course of 2 weeks. For the proliferation assay, 40,000 MFCs were cultured in basal media (control), plus 50 ng/mL of aqueous FGF, plus 50 mg control microspheres, or plus 50 mg bFGF microspheres. The microspheres were suspended above the cells with a hanging cell culture insert (Millicell, Millipore, Billerica, MA). After 3 days, the relative cell density was determined using the colorimetric MTT assay ((3-(4,5-dimethylthiazol-2-yl)-2,5-diphenyltetrazolium bromide), Invitrogen, Carlsbad, CA) by normalizing to the control condition (n=3/group, 3 replicates, one representative data set shown).

8.3.2 Fabrication and Characterization of Scaffolds, Composite Scaffolds and MS-Composite Scaffolds containing bFGF

To fabricate composite scaffolds, three electrospinning solutions were prepared and mixed overnight prior to fabrication: 14.3% w/v poly(ε-caprolactone) (PCL, 80 kDa, Sigma-Aldrich, St. Louis MO) in a 1:1 mixture of tetrahydrofuran (THF, Fisher Chemical, Fairlawn NJ) and N,N-dimethylformamide (DMF, Fisher Chemical), 10% poly(ethylene oxide) (PEO, 200 kDa, Polysciences, Warrington PA) in 90% ethanol (EtOH), and 10% PEO in ddH_2O. A custom-built trijet electrospinning device was used that forms an interpenetrating mesh of distinct polymer fibers [147]. A total of 20 mL of electrospinning solution was added to syringes that were fixed with 18G needles and loaded into syringe pumps (2 mL/hr). The needles were charged (+15kV) and reciprocated using custom fanners to better disperse the fiber jets. A vertical, centrally-located rotating mandrel (10 m/s) was placed between 3 vertical metallic shields (+5kV), which helped to guide fibers onto the mandrel. Composite scaffolds with different fiber fractions were produced with the following configurations: three jets of PCL to form a

'PCL Scaffold', 1 jet of PCL and 2 jets of PEO in EtOH to form a 'Composite Scaffold', 1 jet of PCL and 2 jets of PEO with 0.05g MS/mL PEO solution in ddH_2O to form a 'MS-Composite Scaffold'. The PEO fibers constituted 50% of the composite scaffold and 25% of the MS-composite scaffold weight immediately after electrospinning, as measured by mass loss following incubation in an aqueous environment. The difference in PEO content was attributed to the mass of microspheres remaining in the MS-composite scaffold after PEO removal, as well as differences in the width of the fiber cloud extruded from the needles due to the inclusion of microspheres. Both control and bFGF microspheres were formed into composite scaffolds. After fabrication, all scaffolds were stored at -20°C. SEM images were captured (Philips XL20 by FEI, Hillsboro, Oregon) after incubation in 90% alcohol for 2 hours to remove the soluble PEO. Bioactivity was assessed as described above, using the following conditions: basal media (control), plus 50 ng/mL of aqueous bFGF, plus 80 mg PCL of scaffold, plus 80 mg of blank composite scaffold, or plus 80 mg of bFGF MS-composite scaffold (n=3/group, 2 replicates, one representative data set shown).

8.3.3 In Vivo Implantation of Composite Scaffolds and MS-Composite Scaffolds containing bFGF

PCL scaffolds, composite scaffolds, blank MS-composite scaffolds and bFGF MS-composite scaffolds were implanted subcutaneously in the dorsum of Sprague-Dawley rats, with approval from the VA Animal Use Committee. All scaffolds underwent 15 minutes of UV sterilization prior to implantation. Each scaffold was placed within a distinct pouch, and the anatomic location was randomized. After 2 weeks, rats were sacrificed and the samples dissected with care to maintain the surrounding tissue capsule (n=3/scaffold type/time point, 2 replicates). Samples were frozen in OCT media, sectioned onto glass slides and stained for DAPI (Prolong Gold, Invitrogen, Carlsbad,

CA) to identify cell nuclei. Blood vessels and proliferating cells were identified via immunohistochemical detection of alpha smooth muscle actin (aSMA, 1:200 dilution, Abcam, Cambridge, MA) and anti-phospho-histone H3 (PHH3, 1:500 dilution, Sigma-Aldrich, Saint Louis, MO), respectively, using the rabbit SuperPicture kit (Invitrogen, Carlsbad, CA). The PHH3 samples were counterstained with hematoxylin.

8.3.4 In Vivo Implantation of Composite Scaffolds and MS-Composite Scaffolds containing VEGF

The previously described MS-composite scaffolds were fabricated to contain recombinant rat VEGF 165 (R&D Systems), at either 0 or 16 μg VEGF added per 0.5g PLGA. Composite scaffolds with PEO fibers containing VEGF were also fabricated to assess the effect of immediate VEGF release (at differing dosages). The following configurations were employed with the multijet electrospinner: 2 jets of PEO in 90% EtOH and 1 jet of PCL to form a 'Control Composite Scaffold', 1 jet of PEO in 90% EtOH and 1 jet of PEO containing 2.2 μg VEGF/mL PEO in ddH2O and 1 jet of PCL to form a 'Low VEGF Composite Scaffold', and 2 jets of PEO containing 2.2 μg VEGF/mL PEO in ddH2O and 1 jet of PCL to form a 'High VEGF Composite Scaffold' (see **Figure 8-4A**). To determine release profiles, 10-20 mg of composite scaffold (control, low VEGF and high VEGF), microspheres alone, and MS-composite scaffold (control and VEGF) were maintained in 1 mL of PBS at 37°C for 1 week. At set timepoints, the tubes were centrifuged, supernatant removed and fresh PBS was added back. Growth factor release was determined with a rat VEGF ELISA Quantikine Kit (R&D Systems, Minneapolis, MN), and normalized to starting biomaterial weight (n=3/group, performed in duplicate, one representative data set shown).

After fabrication, rectangles (1mm x 10mm x 15mm) of scaffold were prepared for implantation. Blood vessel pores were created by cutting 8 equally-spaced 1 mm holes using a biopsy punch as shown in **Figure 8-5B** [261]. Constructs were implanted subcutaneously into rats for 2 weeks as previously described. Upon sacrifice, samples were excised, embedded in OCT and sectioned *en face*. Samples were stained for Picrosirius red for collagens and DAPI for cell nuclei, as described above, as well as with von Willebrand factor (vWF, 1:1000 dilution, Abcam, Cambridge, MA) using the SuperPicture Kit to identify blood vessels, as previously described.

In order to semi-quantitatively assess vessel formation in the constructs, samples were stained with aSMA (n=4-7 pores/construct, 3 constructs/scaffold type; or 12-21 pores/scaffold type total). Using GIMP image software (GNU Image Manipulate Program, www.gimp.org), the scaffold and background color was removed using the 'Color Threshold' function, leaving only the aSMA stain as shown in **Figure 8-6A**. 'Positive' staining was defined as greater than 0.05% color in a given field of view, which included 1 pore per image. Also, the number of lumens per pore were counted manually in triplicate (per pore) and averaged across samples.

8.3.5 Statistical Analysis

Significance was determined via 1-way ANOVA for the MTT proliferation assay and lumen quantification with $p < 0.05$, followed by Tukey's post-hoc test. When analyzing the percent of pores staining positively for aSMA, Fisher's exact test was used with $p < 0.005$ to account for 10 direct comparisons possible in the data set. All calculations were performed SYSTAT software (Chicago, IL).

8.4 Results

8.4.1 Fabrication and Characterization of Microspheres, Composite Scaffolds and MS-Composite Scaffolds containing bFGF

PLGA microspheres encapsulating bFGF were fabricated using the double-emulsion technique. Microspheres were smooth and round in shape (**Figure 8-2A**), with a similar size profile to prior studies (~20 μm diameter) [114]. bFGF was released in a sustained manner over 7 days (**Figure 8-2B**). When cocultured with MFCs for three days, bFGF MS stimulated cell proliferation, with a 40% increase in cell density that was comparable to the addition of 50 ng/mL aqueous bFGF ($p < 0.001$) (**Figure 8-2C**). Next, the microspheres were mixed with PEO electrospinning solution and simultaneously electrospun with PCL to form a MS-composite scaffold. Also, PCL scaffolds and composite scaffolds were fabricated to serve as controls. SEM images revealed increased porosity in composites after PEO removal, consistent with previous findings [107], and microspheres were entrapped between the PCL fibers in the MS-composite scaffolds (**Figure 8-2D**) [114]. The proliferation rate of MFCs did not change with 3 days of exposure to PCL or composite scaffolds (**Figure 8-2E**). In contrast, MS-composites scaffolds containing bFGF increased MFC density by 50%, to levels comparable to the direct addition of aqueous bFGF ($p < 0.001$) (**Figure 8-2E**). This study demonstrated that bFGF encapsulated in microspheres and MS-composite scaffolds remained bioactive, despite the fabrication procedures used to create the biomaterials.

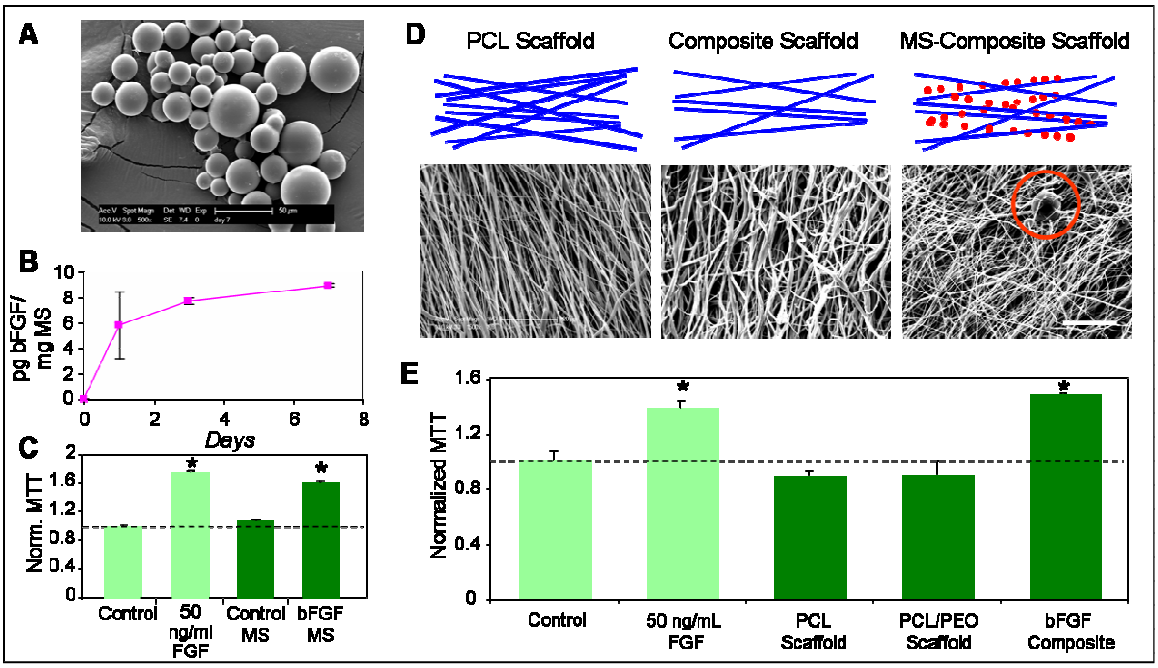

Figure 8-2 Characterization and in vitro bioactivity of microspheres and MS-composite scaffolds. (A) SEM image of PLGA microspheres (scale bar = 50 μm). (B) Cumulative release of bFGF from microspheres over 7 days, as measured by ELISA. (C) Exposure to aqueous bFGF and bFGF MS result in higher cell density after 3 days, as measured by normalized MTT. (D) Schematic and SEM images of PCL scaffolds, composite scaffolds and MS-composite scaffolds containing microspheres (circle) (scale bar = 20 μm). (E) Cell density increased after 3 days in conditions containing bFGF, demonstrating the maintenance of growth factor bioactivity through the fabrication process. * indicates significant difference from control, $p < 0.001$.

8.4.2 In Vivo Implantation of Composite Scaffolds and MS-Composite Scaffolds containing bFGF

PCL scaffolds, composite scaffolds, blank MS-composite scaffolds and bFGF MS-composite scaffolds were implanted subcutaneously in rats for 2 weeks. Upon sacrifice, all samples were well integrated with the adjacent tissue and surrounded by a thin vascularized capsule (**Figure 8-3A**). DAPI staining showed sparse infiltration of the PCL scaffolds by cells from the subcutaneous space after 2 weeks. Increased scaffold infiltration was seen for composite scaffolds and MS-composite scaffolds, both of which contain sacrificial PEO fibers that increased porosity (**Figure 8-3C**). This finding was consistent with our past observation that increased porosity improves infiltration *in vitro* [107]. Of note, the composite scaffold and MS-composite scaffold appeared to be

slightly compressed compared to PCL scaffolds (double arrows, **Figure 8-3C**), despite all groups starting with the same thickness at implantation. Also, sacrificial PEO was not removed from the scaffold prior to implantation. In order to assess the effects of bFGF delivery from MS-composite scaffolds, the proliferation marker PHH3 was used. Histology revealed an increased number of proliferating cells within the bFGF MS-composite scaffolds compared to other groups, demonstrating the bioactivity of the encapsulated growth factor *in vivo* (**Figure 8-3D**). Also, vascularity was confirmed in the capsule via aSMA staining (**Figure 8-3E,** arrows). Notably, vessels did not penetrate the scaffold under any condition.

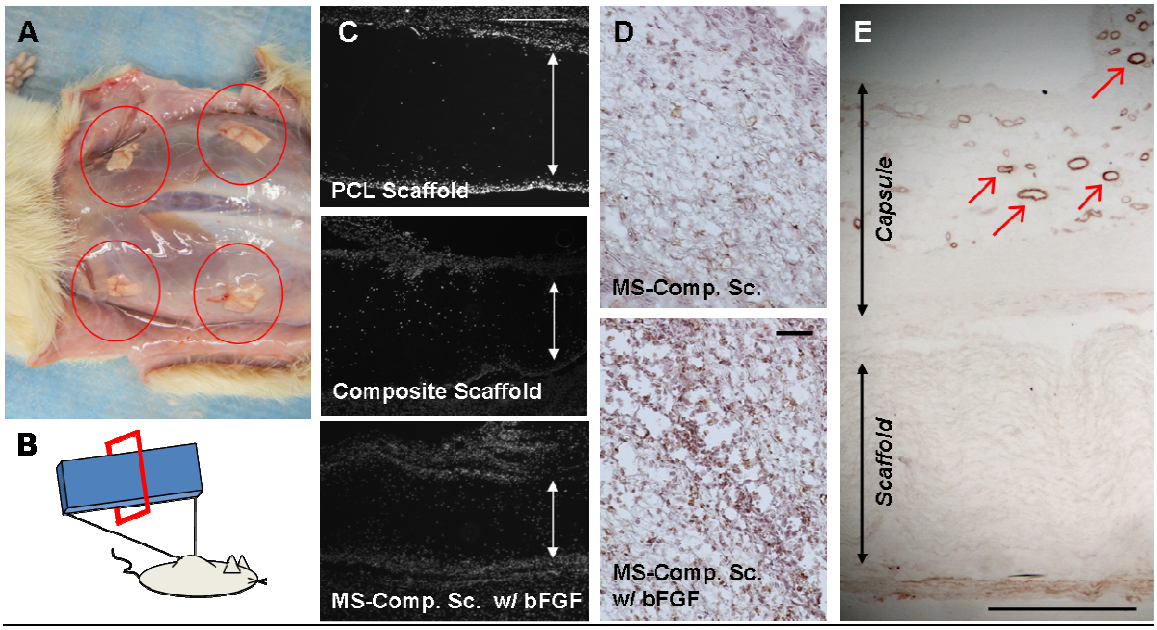

Figure 8-3 *In vivo* response to MS-composite scaffolds containing bFGF. (A) All scaffolds were well integrated with the adjacent tissue and surrounded by a thin, vascularized capsule. (B) Schematic of histological sections from the materials. (C) Cells were better distributed through composite scaffolds (which contain sacrificial PEO) than PCL scaffolds after 2 weeks (scale = 100 μm). (D) More cells stained for the proliferation marker PHH3 in the bFGF composite scaffold compared to blank composite scaffolds (PHH3 - brown, hematoxylin counterstain - purple, scale = 50 μm). (E) Blood vessels were identified in the capsules of all samples (aSMA staining, scale = 500 μm).

8.4.3 In Vivo Implantation of Composite Scaffolds and MS-Composite Scaffolds containing VEGF

We next investigated the effect of incorporating VEGF in composite scaffolds and MS-composite scaffolds on vascularization. For this, we utilized delivery from both the sacrificial PEO fibers (using 2 distinct doses) and from entrapped MS (**Figure 8-4A**). When electrospun into PEO fibers, the majority (85-93%) of VEGF was released on the first day (Low = 50 and High = 175 pg VEGF/mg scaffold). In contrast, the release profiles from the MS-composite scaffolds (as well as the microspheres alone) exhibited a slower, more sustained release over 7 days to a total of 400 pg/mg (for MS alone) and 5 pg/mg (for MS-composite scaffolds) (**Figure 8-4B**), with attenuation of release in the MS-composite scaffold compared to the microspheres alone, as previously observed [114].

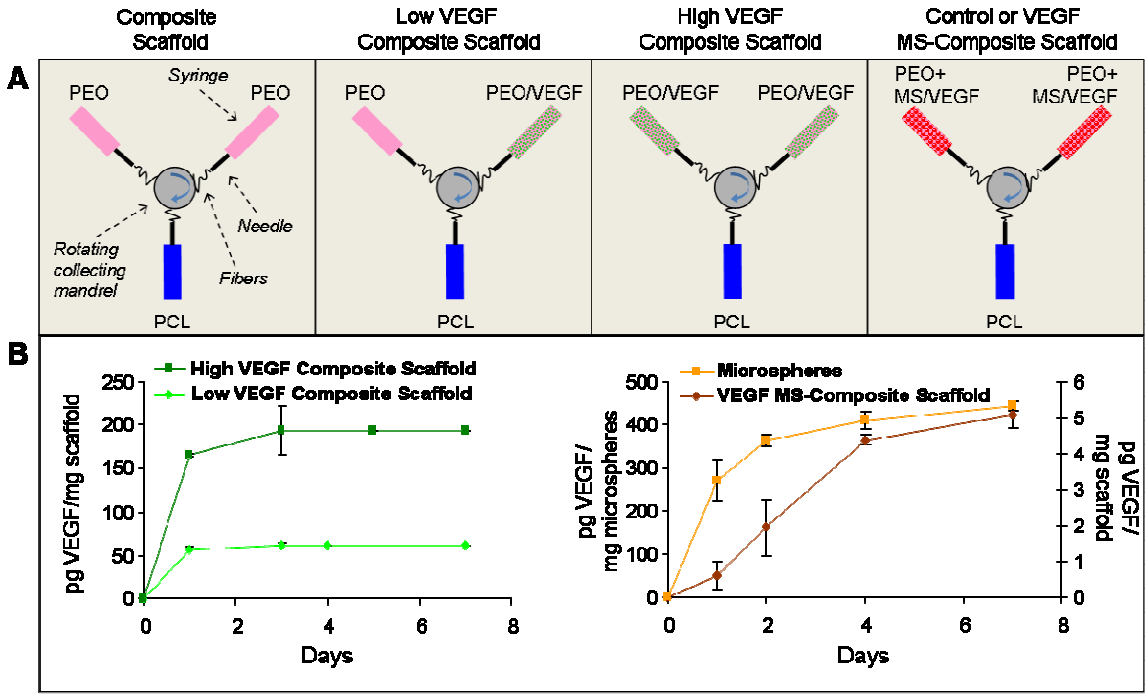

Figure 8-4 Delivery of VEGF from composite scaffolds and MS-composite scaffolds. (A) Schematic depicting contents for each jet in the electrospinner that collect on a rotating mandrel to form an intermingled mesh for each type of scaffold fabricated. (B) Cumulative VEGF release over 7 days as measured by ELISA from composite scaffolds (left), and both microspheres alone and MS-composite scaffolds (note differences in scale for y-axes) (right).

Four types of composites containing VEGF were implanted subcutaneously (**Figure 8-5A**). After 2 weeks, cells colonized the macropores created as vascular conduits and deposited collagen (**Figure 8-5C,D**). Cells and collagen decreased in density with increasing depth into the scaffold, from both the outer edge of the scaffold and from the pore perimeter (solid and dashed arrows, respectively, **Figure 8-5D**). A greater amount of vWF staining was observed in VEGF-containing scaffolds compared to control scaffolds, demonstrating the stimulation of blood vessel formation with VEGF delivery (**Figure 8-5F,G**). Within the pore, cell organization changed with increased VEGF delivery, with circular structures reminiscent of lumens identified at high VEGF doses (arrows, **Figure 8-5H**). aSMA staining confirmed the presence of blood vessels, with more lumens present in VEGF composite scaffolds compared to control composite scaffolds (**Figure 8-5I)**. Similar staining patterns were observed in VEGF MS-composite scaffolds (**Figure 8-5J**), where VEGF scaffolds exhibited significantly more staining for aSMA than control scaffolds.

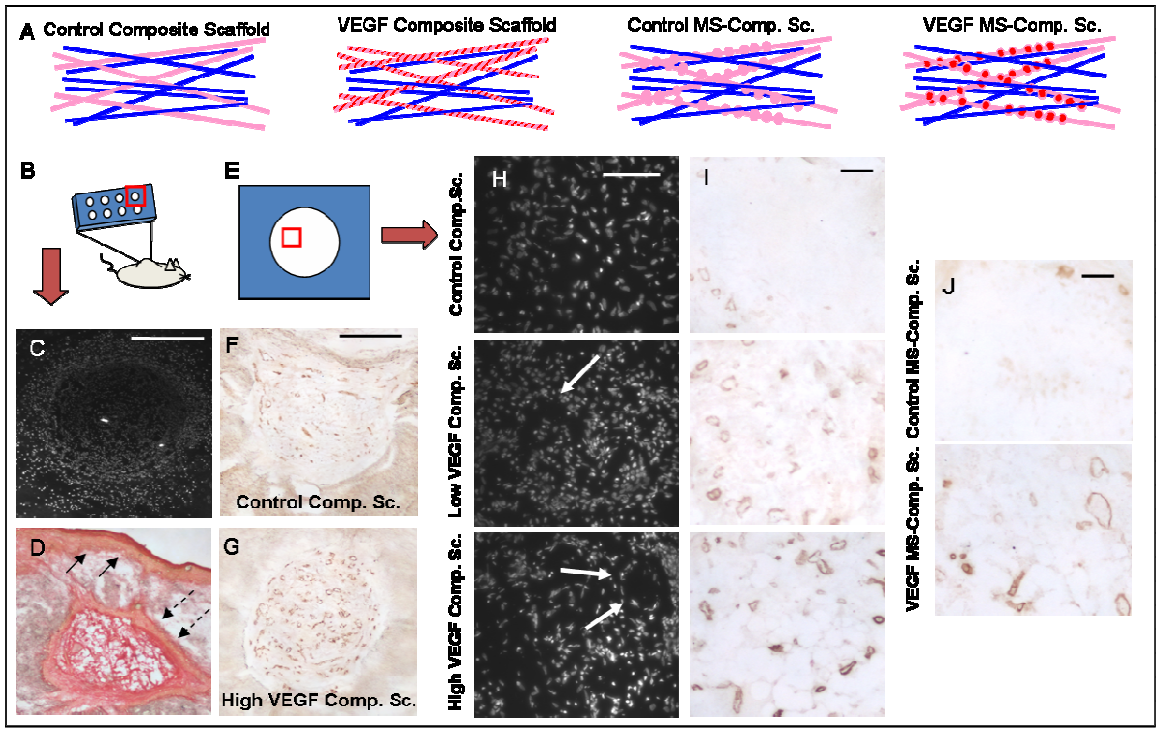

Figure 8-5 *In vivo* response to MS-composite scaffolds containing VEGF. (A, B) Schematics of different electropun materials, and the areas that were analyzed histologically in C-D, F-G. (C) DAPI staining and (D) Picrosirius red staining of a pore in the scaffold, showing cells and collagen, respectively (scale = 500 μm). (E) Schematic of the area analyzed histologically in H-J. (F, G) vWF staining of pores show improved vascularity in the composite scaffolds containing VEGF. (H) DAPI staining shows progressively more organization of cells into lumen-like structures (arrows) with increased VEGF delivery (scale = 100 μm). (I, J) aSMA staining of pores show significantly more vessels in VEGF-containing scaffolds (scale = 100 μm).

Image analysis was used to quantify the aSMA staining prevalence and the number of lumens per pore (**Figure 8-6A**). While there was variability in the magnitude of vascularization between animals, the trends were similar (**Figure 8-6B**). 'Positive staining' was defined as >0.05% color per image, which included a single pore. For control composite scaffolds, only 30% of pores stained positively for aSMA. Conversely, 60% of pores for low VEGF composite scaffolds and 100% of pores from high VEGF composite scaffolds stained positively for aSMA, demonstrating a dose-dependent response in vessel recruitment after 2 weeks *in vivo*. Similarly, VEGF MS-composite scaffolds resulted in 95% of pores staining positively for aSMA, compared to only 54% for control MS-composite scaffolds (**Figure 8-6C**). The aSMA stain identified both early

capillary formation, seen as non-distinct shapes within the pore, as well as organized circular lumens, representing competent blood vessels. Significantly more lumens were found in the presence of both high VEGF composite scaffolds and VEGF MS-composite scaffolds, demonstrating the efficacy of VEGF delivery from both fibers and microspheres (**Figure 8-6D**).

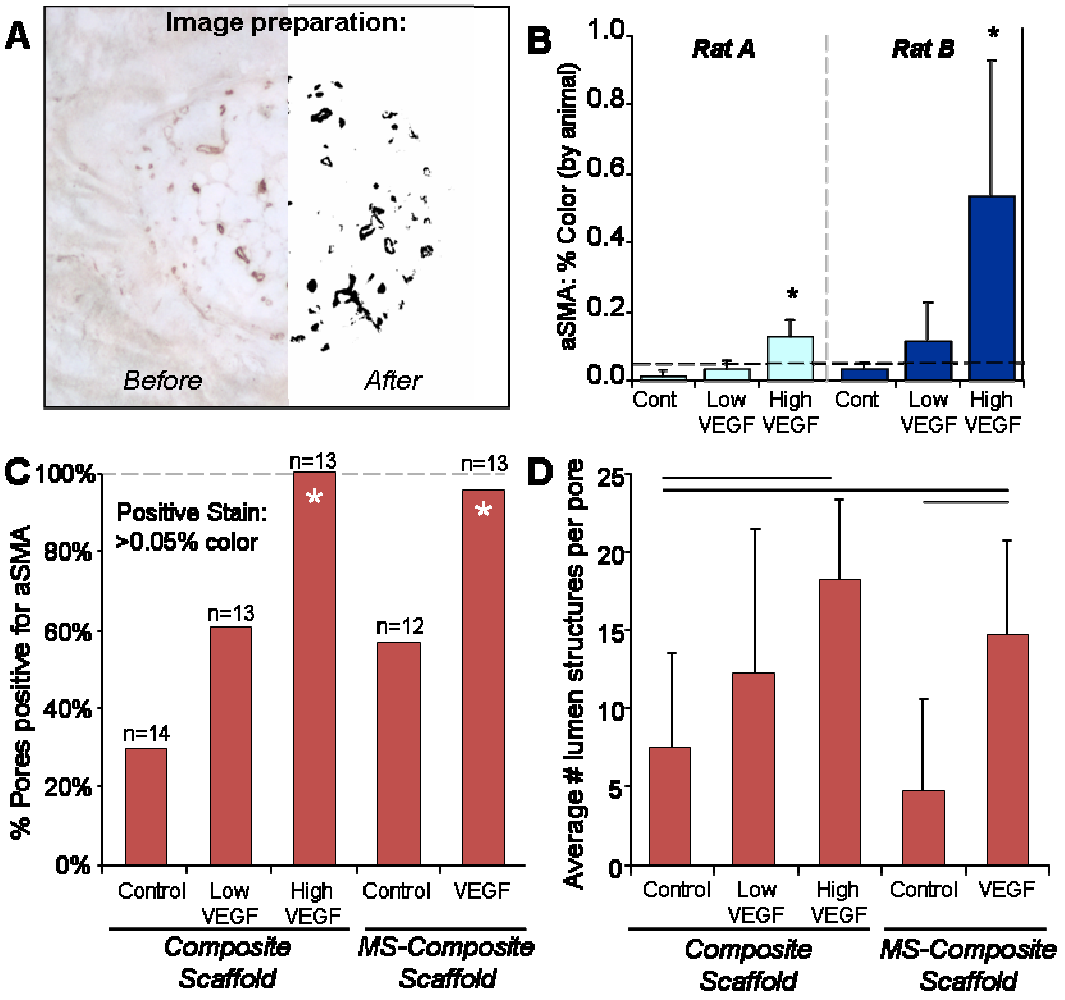

Figure 8-6 Quantification of enhanced vascularization through VEGF delivery. (A) Representative image demonstrating the image processing used to clarify the aSMA staining. (B) The amount of aSMA staining in composite scaffolds varied in magnitude between animals, but followed a similar pattern (2 representative animals shown). (C) High VEGF composite scaffolds and VEGF MS-composite scaffolds stimulated vascularity compared to other groups (positive stain threshold > 0.05% color, * indicates difference from respective control, $p < 0.005$). (D) Similarly, high VEGF composite scaffolds and VEGF MS-composite scaffolds had more lumens per pore compared to control conditions (line indicates difference, $p < 0.05$).

8.5 Discussion

The ability to control cell behavior in engineered tissues may be critical to successful tissue regeneration. This is particularly true in fibrous tissues, where extreme mechanical forces, reduced metabolic activity, and little access to blood supply pose significant challenges. Further, mechanical cues alone from the surrounding environment may not be sufficient to control cell fate. For example, mesenchymal stem cells, which are easily accessible and possess a number of appealing properties, may need significant chemical guidance to develop a stable and appropriate phenotype [262]. With this work, we present a range of techniques for delivery of bioactive growth factors from electrospin fibrous scaffolds (**Figure 8-1**) that do not affect the overall mechanical properties of the scaffold, and that can be tuned to deliver different types of factors with time-varying release profiles.

Because only small molecules were previously delivered from electrospun MS-composite scaffolds [114], we first demonstrated that active growth factors could be encapsulated and released from the materials, eliciting a biological response both *in vitro* and *in vivo*. Exposure to microspheres and MS-composite scaffolds containing bFGF stimulated MFC proliferation to similar levels as the addition of 50 ng/mL aqueous bFGF, despite differences in dosage (**Figure 8-2**). Further, while previous work washed out the PEO fibers prior to cell seeding, we did not remove PEO prior to use, further simplifying the scaffold preparation process. Allowing the PEO to dissolve *in situ* did not adversely affect cell proliferation or morphology, or affect *in vivo* behavior (*data not shown*). In contrast, while control PLGA microspheres did not affect cell behavior *in vitro*, PLGA microspheres caused a heightened immune response *in vivo*, stimulating in a slight increase in vascularity for all MS-containing scaffolds, perhaps due to the acidic by-products of PLGA degradation. An increased number of immune cells were identified

using H&E in MS-composite scaffolds compared to composite scaffolds without MS (*data not shown*). Finally, we demonstrated that similar to prior *in vitro* work, scaffolds containing sacrificial PEO fibers resulted in better cell infiltration *in vivo* due to an increase in the porosity of the scaffold.

Interestingly, the doses of VEGF that stimulated vessel formation were significantly lower than previous reports [123, 263, 264]. While we attempted to encapsulate comparable levels of VEGF to prior work, a significant proportion of the growth factor dosage was either excluded during fabrication or denatured, according to ELISA measurements. Despite the low quantity of VEGF delivered from both sacrificial fibers and entrapped microspheres, the angiogenic response *in vivo* was robust for all conditions, suggesting that either the ELISA results were misleading or that significantly lower doses of VEGF are needed to stimulate a vascular response than previously reported. Indeed, many reports only describe the theoretical VEGF loading prior to biomaterial fabrication, and they may also experience similar decreases in growth factor dosage after material fabrication.

Two distinct release profiles elicited similar responses *in vivo*. A relatively large initial burst of VEGF from composite scaffolds resulted in similar vascularization as a much smaller, sustained release of VEGF from MS-composite scaffolds (a 40-fold difference in dosage). Aside from minimizing growth factor expense, the materials used here present unique opportunities for designing delivery schemes that closely resemble natural biological cascades *in vivo*. For example, a burst of VEGF could be followed by a sustained release of platelet-derived growth factor, which demonstrated improved vessel maturation compared to VEGF alone [123, 265]. Or, an initial burst of antibiotic could help prevent infections associated with surgery [266].

While this work presents a number of interesting new techniques to deliver growth factors from electrospun fibers with distinct release profiles, some limitations do exist. First of all, it is unclear whether the vessels present at 2 weeks would continue to mature or recede with time *in vivo*. Using our system, we could deliver additional growth factors that promote vessel maturation, such as the VEGF/PDGF combination mentioned earlier. Further, it is unclear if the 1 mm pores would be sufficient to sustain the metabolic needs of the cells in the scaffold, and more testing must be conducted to understand the effect of such pores on the mechanical properties of the material. Another approach to promote vascular invasion would be to include a large-diameter sacrificial fiber population that creates pores wide enough to harbor capillaries and other blood vessels. Finally, the subcutaneous space is significantly different from the synovial environment of the knee, so biomaterial degradation, release profiles and biological response will also need to be studied in that context. Large animal studies are on-going to assess the role of both composite scaffolds and growth factor delivery from such scaffolds.

8.6 Conclusions

Growth factors are a powerful tool to control cell behavior in tissue engineering materials. Because fibrous tissues are especially challenging to engineer, incorporating the capability to deliver growth factors from electrospun scaffolds without compromising mechanical properties will improve the success of such materials. Two novel approaches, one simple method that allows for a burst release and a more complex method that allows for sustained release, can be combined in a wide array of ways to generate unique delivery schemes that mimic natural cascades or promote regenerative behavior in the

neotissue. With this work, we hope to bring electrospun scaffolds closer to a clinically successful therapy for fibrous tissue repair.

8.7 Acknowledgements

This work was done in collaboration with Matthew B. Fisher, Mara L. Schenker, Kevin L. Huang, John L. Esterhai, and Robert L. Mauck. It will be submitted for publication in Biomaterials. This work was funded in part by the NIH (AR056624), the Department for Veteran's Affairs, and the Penn Center for Musculoskeletal Disorders.

9: Conclusions and Future Work

Meniscus repair remains elusive in medicine today. Since meniscus tears are one of the most prevalent injuries in orthopedics, a successful meniscus treatment will prove extremely valuable and lucrative, and will have a significant impact on the orthopedic field. However, despite major efforts by many researchers around the world, we have not been able to engineer a structure that mimics the complexity of the native tissue itself or regenerates the tissue in a functional way. Not only is the meniscus composed of various specialized cell populations, multiple layers of uniquely-oriented collagen fibers, and distinct regions of proteoglycan that all blend seamlessly together, but also the overall shape of the tissue features curves and arches that must precisely match the overlaying femoral condyles and underlying tibial plateau in order to successfully balance joint mechanics, creating an architectural challenge on many levels.

Three potential repair schemes exist for a degradable tissue engineering meniscus therapy. In the simplest case, a tear is filled with a degradable material (**Figure 9-1A**) that restores continuity of the tissue across the injury region, either through the material itself or by delivering chemical cues locally. In cases where complex tears require entire regions to be resected, a patch of material would be inserted (**Figure 9-1B**) that can harbor cells and also match the surrounding physiological characteristics. Finally, in the most extreme situations, the entire meniscus can be removed and replaced (**Figure 9-1C**) by a complete meniscus construct, complete with insertion sites to the bone.

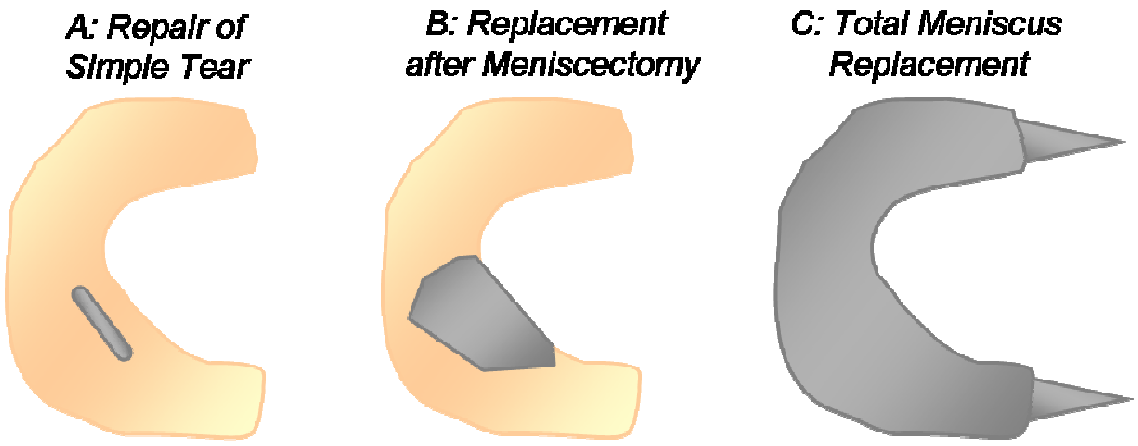

Figure 9-1 Potential treatments after a meniscus injury. (A) A material is used to promote integration across a clean meniscus tear. (B) After meniscectomy, the removed tissue is replaced with new material, capable of recapitulating the function of the resected tissue. (C) In extreme cases, complete meniscus replacement is required, with insertions into the tibial plateau at the meniscus horns.

We believe that the most promising approach is to create a meniscus patch (**Figure 9-1B**), due to the prevalence of meniscectomy after injury. By maintaining a majority of the original tissue, joint mechanics are minimally changed, and guide patch insertion and geometry. Based on the work described in this thesis, as well as other work performed in the lab, we recommend the repair procedure described in **Figure 9-2**. Specifically, an electrospun patch should include sacrificial fibers to increase porosity, which promote maturation and result in better integration properties with native tissue. Hastening these properties will decrease the amount of time a patient is non-weight bearing after implantation. Also, drug-delivering microspheres should be entrapped between the fibers in the scaffold, and vascular conduits formed to support cell metabolism during regeneration. The addition of expanded cells to the exterior of the scaffold will further improve integration, although the cost associated with isolating and expanding autologous cells may outweigh this benefit. Based on current work, we also recommend that a cocktail of growth factors are delivered from the electrospun material. These

chemicals should promote the properties of immature, healing meniscus in the neotissue, and create a regenerative environment that stimulates optimal tissue formation. Specifically, we propose a short-term release of bFGF (to increase cell density around the repair site) and VEGF (to stimulate early vascularization that supports regeneration) from sacrificial fibers, along with delivery of both TGF-β (to stimulate matrix production) and PDGF (to mature /sustain existing blood vessels) from entrapped microspheres. With this approach, vasculature would be continuously present from early timepoints, and integration/maturation properties would slowly improve over time. Eventually, as the original tissue is regenerated through matrix deposition, the scaffold and associated vascularity will recede, leaving a tissue that is functionally similar to the original tissue.

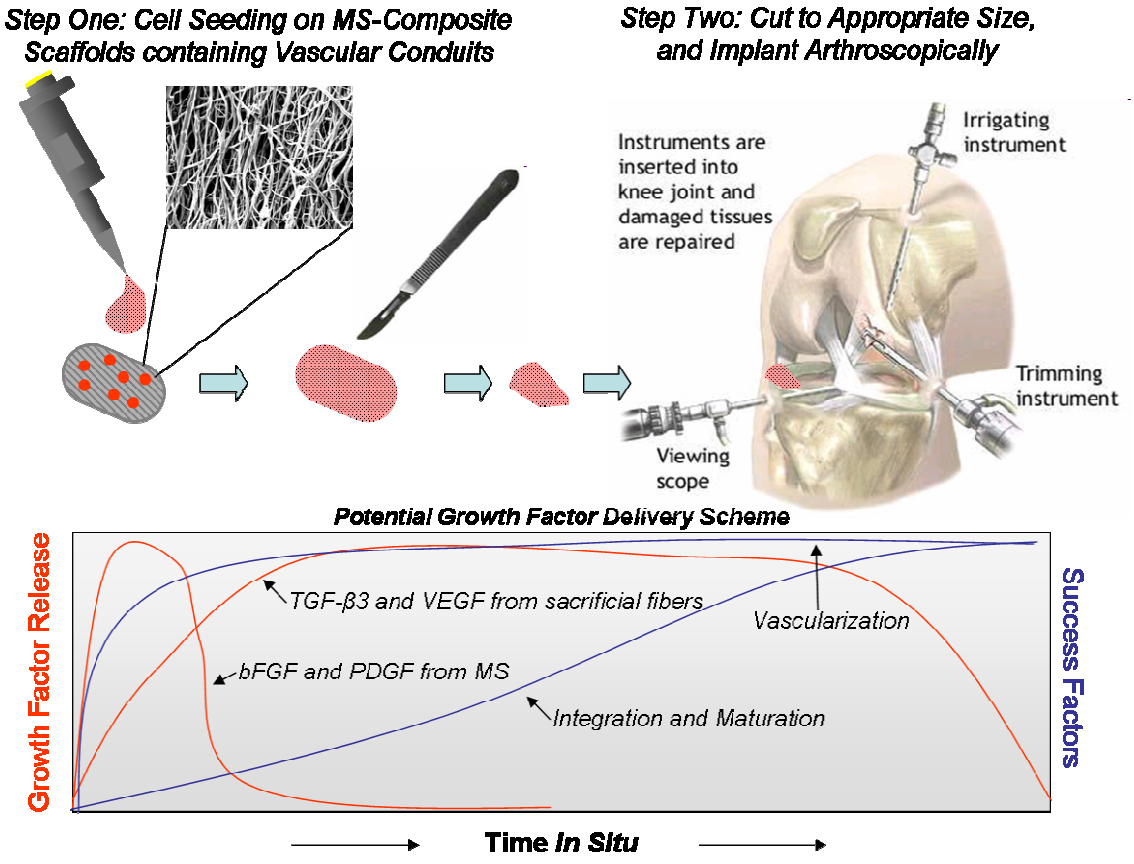

Figure 9-2 A potential meniscus repair scheme.

Future work can explore the delivery of other types of molecules from electropun scaffolds to promote meniscus repair. For example, early work suggests that enzymes such as hyalurodinase could be used to decrease matrix density at the repair site [267], allowing for more cell migration and new matrix deposition that spans the injury region. Further, regulators of the immune response, such as dexamethasone, could be delivered locally, tempering inflammatory processes that might inhibit regenerative behavior. Because both short- and long-term delivery schemes are possible, with multiple fibers and microsphere populations in a single scaffold, this biomaterial provides a significant amount of flexibility in terms of delivery of different factors that support regeneration.

Despite the progress that has been made to date in creating a meniscus repair patch, a number of challenges remain. Specifically, our current fabrication technique creates thin, flat sheets of scaffold, and it is unclear how these can be formed into the 3-sided c-shape of the meniscus. Once we have identified a way to create the overall architecture, other surgical realities must be tackled. Current technology allows for measurement of the exterior rim of a resected region using an arthroscopic measuring tape (used in the Menaflex procedure), but a new device would be needed to measure the radial thickness. Further, we need to develop a way to cut the scaffold to the correct dimensions, with minimal damage to the remaining scaffold. The material currently requires delicate handling, which is unlikely in an orthopedic OR. It ideally must also be inserted arthroscopically, as opening the knee is costly and time-consuming, and will significantly limit the use of such a therapy. Finally, while we have demonstrated that new matrix will interface the scaffold and native tissue, temporary sutures or a glue may help ensure scaffold stability prior to maturation and must be thoroughly tested.

Prior to human studies, a number of large animal studies will be crucial in understanding the potential for success. The *in vitro* work performed in this thesis provides a significant amount of information for designing *in vivo* studies. However, the synovial environment is very different from both the *in vitro* culture conditions and the subcutaneous space in a rat, so we must test the behavior of cells on these scaffolds in the knee, as well as the effects on the material properties and degradation rates of the polymers that are used. Preliminary studies in an ovine model show some cell infiltration into the scaffolds, but that the scaffolds become dislodged over time [148]. Further, we will need to test if local growth factor delivery stimulates cell behavior in ways similar to *in vitro* and subcutaneous *in vivo* studies, which is not a liquid environment like the knee.

Finally, while a patch may restore joint mechanics and minimize pain to the patient, the ultimate goal is to extend the period of time before a patient must receive a knee replacement, ideally removing the need for that surgery entirely. While total knee arthroplasty (TKA) is relatively routine and has a high success rate, it is a major surgery with large associated costs both in medical expenses as well as in lost wages during recovery. Also, revision surgeries are tricky and expensive, and with the population aging, so we must delay the need for such extreme surgeries as much as possible. Delaying the onset of osteoarthritis, and subsequent TKA surgery, by maintaining joint mechanics through the use of such a patch will make this therapy a success, and will likely result in the therapy being embraced by both surgeons who would finally have a clinical option for their patients beyond resection, and payers who would be happy to decrease the number of expensive TKAs.

Overall, I must believe that successful meniscus regeneration will some day exist, because we have been able to conquer many other challenging conditions. The problem is lofty: meniscus repair requires a mix of architectural, chemical and biological optimization and design. It is evident that the solution will not be straightforward, but the successful design and implementation of such a therapy will certainly revolutionize the field of orthopedics.

10: References

1. Hsieh, H.H. and P.S. Walker, *Stabilizing mechanisms of the loaded and unloaded knee joint.* J Bone Joint Surg Am., 1976. **58**(1): p. 87-93.

2. Walker, P.S. and M.J. Erkman, *The role of the menisci in force transmission across the knee.* Clin Orthop Relat Res, 1975. **109**: p. 184-92.

3. Ghosh, P. and T.K. Taylor, *The knee joint meniscus: a fibrocartilage of some distinction.* Clin Orthop Relat Res, 1987. **224**: p. 52-63.

4. Fithian, D.C., M.A. Kelly, and V.C. Mow, *Material properties and structure-function relationships in the menisci.* Clin Orthop Relat Res, 1990. **252**: p. 19-31.

5. Sweigart, M.A. and K.A. Athanasiou, *Toward Tissue Engineering of the Knee Meniscus.* Tissue Eng, 2001. **7**(2): p. 111-29.

6. Chia, H.N. and M.L. Hull, *Compressive moduli of the human medial meniscus in the axial and radial directions at equilibrium and at a physiological strain rate.* J Orthop Res, 2008. **26**(7): p. 951-6.

7. Sweigart, M.A. and K.A. Athanasiou, *Biomechanical characteristics of the normal medial and lateral porcine knee menisci.* Proc Inst Mech Eng H, 2005. **219**(1): p. 53-62.

8. Tissakht, M. and A.M. Ahmed, *Tensile stress-strain characteristics of the human meniscal material.* J Biomech, 1995. **28**(4): p. 411-22.

9. Herwig, J., E. Egner, and E. Buddecke, *Chemical changes of human knee joint menisci in various stages of degeneration.* Ann Rheum Dis, 1984. **43**(4): p. 635-40.

10. Webber, R.J., M.G. Harris, and A.J. Hough, *Cell culture of rabbit meniscal fibrochondrocytes: proliferative and synthetic response to growth factors and ascorbate.* J. Orthop. Res., 1985. **3**: p. 36.

11. Bullough, P.G., et al., *The strength of the menisci of the knee as it relates to their fine structure.* J Bone Joint Surg Br., 1970. **52**(3): p. 564-7.

12. Adams, M.E. and H. Muir, *The glycosaminoglycans of canine menisci.* Biochem. J., 1981. **197**: p. 385.

13. Balazs, E.A., ed. *Chemistry and Molecular Biology of the Intercellular Matrix.* 1970, Academic Press: New York. 1231-1240.

14. Buma, P., et al., *Tissue engineering of the meniscus.* Biomaterials, 2004. **25**: p. 1523-1532.

15. Arnoczky, S.P. and R.F. Warren, *Microvasculature of the human meniscus.* Am J Sports Med., 1982. **10**(2): p. 90-5.

16. Finerman, G.A.M. and F.R. Noyes, *Biology and Biomechanics of the Traumatized Synovial Joint: The Knee as a Model.* 1992, Rosemont: American Academy of Orthopaedic Surgeons.

17. Garrett, W.E., et al., *American Board of Orthopaedic Surgery Practice of the Orthopaedic Surgeon: Part-II, Certification Examination Case Mix* The Journal of Bone and Joint Surgery (American), 2006. **88**: p. 660-667.

18. King, D., *The healing of semilunar cartilages. 1936.* Clin Orthop Relat Res, 1990. **252**: p. 4-7.

19. Shapiro, F. and M.J. Glimcher, *Induction of osteoarthritus in the rabbit knee joint: Histological changes following meniscectomy and meniscal lesions.* Clin. Orthop., 1980. **147**: p. 287.

20. Lufti, A.M., *Morphological changes in the articular cartilage after meniscectomy.* J. Bone Joint Surg, 1975. **57B**: p. 525.

21. Hoshikawa, Y., et al., *The prognosis of meniscectomy in athletes. The simple meniscus lesions without ligamentous instabilities.* Am J Sports Med, 1983. **11**: p. 8-13.

22. Yoo, J.C., et al., *Suturing complete radial tears of the lateral meniscus.* Arthroscopy, 2007. **23**(11): p. 1249.

23. Farng, E. and O. Sherman, *Meniscal repair devices: a clinical and biomechanical literature review.* Arthroscopy., 2004. **20**(3): p. 273-86.

24. Rodkey, W.G., et al., *Comparison of the collagen meniscus implant with partial meniscectomy. A prospective randomized trial.* J Bone Joint Surg Am, 2008. **90**(7): p. 1413-26.

25. Verdonk, R. and D. Kohn, *Harvest and conservation of meniscal allografts.* Scand J Med Sci Sports, 1999. **9**: p. 158-9.

26. Arnoczky, S.P. and R.F. Warren, *The microvasculature of the meniscus and its response to injury. An experimental study in the dog.* Am J Sports Med, 1983. **11**(3): p. 131-41.

27. Gershuni, D.H., et al., *Experimental models to promote healing of tears in the avascular segment of canine knee menisci.* J Bone Joint Surg Am, 1989. **71**(9): p. 1363-70.

28. Huang, T.L., et al., *Healing potential of experimental meniscal tears in the rabbit. Preliminary results.* Clin Orthop Relat Res, 1991(267): p. 299-305.

29. Okuda, K., et al., *Meniscal rasping for repair of meniscal tear in the avascular zone.* Arthroscopy., 1999. **15**(3): p. 281-6.

30. van Trommel, M.F., et al., *Arthroscopic meniscal repair with fibrin clot of complete radial tears of the lateral meniscus in the avascular zone.* Arthroscopy., 1998. **14**(4): p. 360-5.

31. Clark, C.R. and J.A. Ogden, *Development of the menisci of the human knee joint. Morphological changes and their potential role in childhood meniscal injury.* J Bone Joint Surg Am, 1983. **65**(4): p. 538-547.

32. Petersen, W. and B. Tillmann, *Age-related blood and lymph supply of the knee menisci. A cadaver study.* Acta Orthop Scand, 1995. **66**(4): p. 308-12.

33. Andrish, J.T., *Meniscal Injuries in Children and Adolescents: Diagnosis and Management.* J Am Acad Orthop Surg, 1996. **4**(5): p. 231-237.

34. Ishida, K., et al., *The regenerative effects of platelet-rich plasma on meniscal cells in vitro and its in vivo application with biodegradable gelatin hydrogel.* Tissue Eng, 2007. **13**(5): p. 1103-12.

35. McNulty, A.L. and F. Guilak, *Integrative repair of the meniscus: lessons from in vitro studies.* Biorheology, 2008. **45**(3-4): p. 487-500.

36. McNulty, A.L., et al., *Enhanced integrative repair of the porcine meniscus in vitro by inhibition of interleukin-1 or tumor necrosis factor alpha.* Arthritis Rheum, 2007. **6**(9): p. 3033-42.

37. McNulty, A.L., J.B. Weinberg, and F. Guilak, *Inhibition of matrix metalloproteinases enhances in vitro repair of the meniscus.* Clin Orthop Relat Res, 2009. **467**(6): p. 1557-67.

38. Wilusz, R.E., et al., *Inhibition of integrative repair of the meniscus following acute exposure to interleukin-1 in vitro.* J Orthop Res, 2008. **26**(4): p. 504-12.

39. Hennerbichler, A., et al., *Interleukin-1 and tumor necrosis factor alpha inhibit repair of the porcine meniscus in vitro.* Osteoarthritis Cartilage, 2007. **15**(9): p. 1053-60.

40. Langer, R. and J.P. Vacanti, *Tissue Engineering*. Science, 1993. **260**(5110): p. 920-6.

41. Cook, J.L., et al., *Evaluation of small intestinal submucosa grafts for meniscal regeneration in a clinically relevant posterior meniscectomy model in dogs*. J Knee Surg, 2006. **19**(3): p. 159-67.

42. Welch, J.A., et al., *Evaluation of small-intestinal submucosa implants for repair of meniscal defects in dogs*. Am J Vet Res, 2002. **63**(3): p. 427-31.

43. Tan, Y., Y. Zhang, and M. Pei, *Meniscus reconstruction through coculturing meniscus cells with synovium-derived stem cells on small intestine submucosa--a pilot study to engineer meniscus tissue constructs*. Tissue Eng Part A, 2010. **16**(1): p. 67-79.

44. Cook, J.L., et al., *In vitro and in vivo comparison of five biomaterials used for orthopedic soft tissue augmentation*. Am J Vet Res, 2008. **69**(1): p. 148-56.

45. Tienen, T.G., et al., *Replacement of the knee meniscus by a porous polymer implant: a study in dogs*. Am J Sports Med, 2006. **34**(1): p. 64-71.

46. Ramrattan, N.N., et al., *Assessment of tissue ingrowth rates in polyurethane scaffolds for tissue engineering*. Tissue Eng, 2005. **11**(7-8): p. 1212-23.

47. Aufderheide, A.C. and K.A. Athanasiou, *Assessment of a bovine co-culture, scaffold-free method for growing meniscus-shaped constructs*. Tissue Eng, 2007. **13**(9): p. 2195-205.

48. Ballyns, J.J., et al., *Image-guided tissue engineering of anatomically shaped implants via MRI and micro-CT using injection molding*. Tissue Eng Part A., 2008. **14**(7): p. 1195-202.

49. van Tienen, T.G., G. Hannink, and P. Buma, *Meniscus replacement using synthetic materials*. Clin Sports Med., 2009. **28**(1): p. 143-56.

50. Baker, B.M. and R.L. Mauck, *The effect of nanofiber alignment on the maturation of engineered meniscus constructs*. Biomaterials, 2007. **28**(11): p. 1967-77.

51. Baker, B.M., et al., *Tissue engineering with meniscus cells derived from surgical debris*. Osteoarthr Cartilage, 2009. **17**(3): p. 336-45.

52. Mauck, R.L., et al., *Engineering on the Straight and Narrow: The Mechanics of Nanofibrous Assemblies for Fiber-Reinforced Tissue Regeneration*. Tissue Eng Part B Rev., 2009. **15**(2): p. 171-193.

53. Baker, B.M., et al., *New directions in nanofibrous scaffolds for soft tissue engineering and regeneration.* Expert Rev Med Devices., 2009. **6**(5): p. 515-32.

54. Namba, R.S., et al., *Spontaneous Repair of Superficial Defects in Articular Cartilage in a Fetal Lamb Model.* J Bone Joint Surg, 1998. **80**(1): p. 4.

55. al-Qattan, M.M., et al., *Fetal tendon healing: development of an experimental model.* Plast Reconstr Surg., 1993. **92**(6): p. 1155-60.

56. Favata, M., et al., *Regenerative properties of fetal sheep tendon are not adversely affected by transplantation into an adult environment.* J Orthop Res, 2006. **24**(11): p. 2124-32.

57. Stalling, S.S. and S.B. Nicoll, *Fetal ACL fibroblasts exhibit enhanced cellular properties compared with adults.* Clin Orthop Relat Res, 2008. **466**(12): p. 3130-7.

58. Brink, H.E., et al., *Serum-dependent effects on adult and fetal tendon fibroblast migration and collagen expression.* Wound Repair Regen., 2006. **14**(2): p. 179-86.

59. Tran-Khanh, N., et al., *Aged bovine chondrocytes display a diminished capacity to produce a collagen-rich, mechanically functional cartilage extracellular matrix.* J Orthop Res, 2005. **23**(6): p. 1354-62.

60. Adkisson, H.D., et al., *In vitro generation of scaffold independent neocartilage.* Clin Orthop Relat Res, 2001. **391 Supplement**: p. S280-94.

61. Brink, H.E., S.S. Stalling, and S.B. Nicoll, *Influence of serum on adult and fetal dermal fibroblast migration, adhesion, and collagen expression.* In Vitro Cell Dev Biol Anim, 2005. **41**(8-9): p. 252-7.

62. Brink, H.E., J. Bernstein, and S.B. Nicoll, *Fetal dermal fibroblasts exhibit enhanced growth and collagen production in two- and three-dimensional culture in comparison to adult fibroblasts.* J Tissue Eng Regen Med, 2009. **3**(8): p. 623-33.

63. Shah, M., D.M. Foreman, and M.W. Ferguson, *Neutralisation of TGF-beta 1 and TGF-beta 2 or exogenous addition of TGF-beta 3 to cutaneous rat wounds reduces scarring*. J Cell Sci, 1995. **108**(3): p. 985-1002.

64. Chen, W., et al., *Ontogeny of expression of basic fibroblast growth factor and its receptors in human fetal skin.* Chin J Traumatol., 2005. **8**(6): p. 332-8.

65. Mauck, R.L., et al., *Regional multilineage differentiation potential of meniscal fibrochondrocytes: implications for meniscus repair*. Anat Rec., 2007. **290**: p. 48-58.

66. Huang, A.H., et al., *Tensile properties of engineered cartilage formed from chondrocyte- and MSC-laden hydrogels*. Osteoarthritis Cartilage, 2008. **16**(9): p. 1074-82.

67. Farndale, R.W., D.J. Buttle, and A.J. Barrett, *Improved quantitation and discrimination of sulphated glycosaminoglycans by use of dimethylmethylene blue*. Biochim Biophys Acta, 1986. **883**(2): p. 173-7.

68. Stegemann, H. and K. Stalder, *Determination of hydroxyproline*. Clin Chim Acta, 1967. **18**(2): p. 267-73.

69. Hess, A., *Reactions of mammalian fetal tissues to injury. I. Surgical technique.* Anat Rec., 1954. **119**(1): p. 35-51.

70. Hess, A., *Reactions of mammalian fetal tissues to injury. II. Skin*. Anat Rec., 1954. **119**(4): p. 435-447.

71. Longaker, M.T., et al., *Fetal fracture healing in a lamb model.* Plast Reconstr Surg., 1992. **90**(2): p. 161-171.

72. Mastrangelo, A.N., et al., *Immature animals have higher cellular density in the healing anterior cruciate ligament than adolescent or adult animals*. J Orthop Res., 2010.

73. Melrose, J., et al., *Comparative spatial and temporal localisation of perlecan, aggrecan and type I, II and IV collagen in the ovine meniscus: an ageing study*. Histochem Cell Biol., 2005. **124**(3-4): p. 225-35.

74. Webber, R.J., T. Zitaglio, and A.J. Hough, *In vitro cell proliferation and proteoglycan synthesis of rabbit meniscal fibrochondrocytes as a function of age and sex*. Arthritis Rheum, 1986. **29**: p. 1010-6.

75. Ionescu, L.C., et al., *In Vitro Meniscus Integration is Age Dependent - 0927*, in *Orthopedic Research Society*. 2010: New Orleans, LA.

76. Ionescu, L.C., et al., *In vitro meniscus integration potential is inversely correlated with tissue maturation state*, in *American Society of Mechanical Engineerings - Bioengineering Devision*. 2010.

77. Barry, F.P. and J.M. Murphy, *Mesenchymal stem cells: clinical applications and biological characterization*. Int J Biochem Cell Biol., 2004. **36**(4): p. 568-84.

78. Vavken, P., F.A. Saad, and M.M. Murray, *Age dependence of expression of growth factor receptors in porcine ACL fibroblasts*. J Orthop Res, 2010. **In Press**.

79. Verdonk, P.C., et al., *Characterisation of human knee meniscus cell phenotype*. Osteoarthritis Cartilage, 2005. **13**(7): p. 548-60.

80. Collier, S. and P. Ghosh, *Effects of transforming growth factor beta on proteoglycan synthesis by cell and explant cultures derived from the knee joint meniscus*. Osteoarthr Cartilage. , 1995. **3**(2): p. 127-38.

81. Gruber, H.E., et al., *Three-dimensional culture of human meniscal cells: extracellular matrix and proteoglycan production*. BMC Biotechnol, 2008. **8**(54).

82. Tanaka, T., K. Fujii, and Y. Kumagae, *Comparison of biochemical characteristics of cultured fibrochondrocytes isolated from the inner and outer regions of human meniscus*. Knee Surg Sports Traumatol Arthrosc, 1999. **7**(2): p. 75-80.

83. Varga, J., J. Rosenbloom, and S.A. Jimenez, *Transforming growth factor beta (TGF beta) causes a persistent increase in steady-state amounts of type I and type III collagen and fibronectin mRNAs in normal human dermal fibroblasts*. Biochem J. , 1987. **247**(3): p. 597-604.

84. Overall, C.M., J.L. Wrana, and J. Sodek, *Independent regulation of collagenase, 72-kDa progelatinase, and metalloendoproteinase inhibitor expression in human fibroblasts by transforming growth factor-beta*. J Biol Chem, 1989. **264**(3): p. 1860-9.

85. Beredjiklian, P.K., et al., *Regenerative versus reparative healing in tendon: a study of biomechanical and histological properties in fetal sheep*. Ann Biomed Eng, 2003. **31**(10): p. 1143-52.

86. Barry, F., et al., *Chondrogenic differentiation of mesenchymal stem cells from bone marrow: differentiation-dependent gene expression of matrix components*. Exp Cell Res., 2001. **268**(2): p. 189-200.

87. Rolfe, K.J., et al., *Differential gene expression in response to transforming growth factor-beta1 by fetal and postnatal dermal fibroblasts*. Wound Repair Regen., 2007. **15**(6): p. 897-906.

88. Webber, R.J., T. Zitaglio, and A.J. Hough, *Serum-free culture of rabbit meniscal fibrochondrocytes: proliferative response*. J Orthop Res, 1988. **6**(1): p. 13-23.

89. Cicuttini, F.M., et al., *Rate of knee cartilage loss after partial meniscectomy*. J Rheumatol, 2002. **29**(9): p. 1954-6.

90. Verdonk R, K.D., *Harvest and conservation of meniscal allografts*. Scand J Med Sci Sports, 1999. **9**: p. 158-9.

91. Cox, J.S., et al., *The degenerative effects of partial and total resection of the medial meniscus in dogs' knees*. Clin Orthop Relat Res, 1975. **109**: p. 178-83.

92. Webber, R.J., et al., *An organ culture model for assaying wound repair of the fibrocartilaginous knee joint meniscus*. Am J Sports Med, 1989. **17**(3): p. 393-400.

93. Kobayashi, K., et al., *Regional differences in the healing potential of the meniscus-an organ culture model to eliminate the influence of microvasculature and the synovium*. Knee, 2004. **11**(4): p. 271-8.

94. van de Breevaart Bravenboer, J., et al., *Improved cartilage integration and interfacial strength after enzymatic treatment in a cartilage transplantation model*. Arthritis Res Ther, 2004. **6**(5): p. R469-76.

95. Hennerbichler, A., et al., *Repair response of the inner and outer regions of the porcine meniscus in vitro*. Am J Sports Med., 2007. **35**(5): p. 754-62.

96. DiMicco, M.A., et al., *Integrative articular cartilage repair: dependence on developmental stage and collagen metabolism*. Osteoarthritis Cartilage, 2002. **10**(3): p. 218-25.

97. Giurea, A., et al., *Development-associated differences in integrative cartilage repair: roles of biosynthesis and matrix*. J Orthop Res, 2002. **20**(6): p. 1274-81.

98. Provenzano, P.P., et al., *Healing of subfailure ligament injury: comparison between immature and mature ligaments in a rat model*. J Orthop Res, 2002. **20**(5): p. 975-83.

99. Tognana, E., et al., *Adjacent tissues (cartilage, bone) affect the functional integration of engineered calf cartilage in vitro*. Osteoarthritis Cartilage, 2005. **13**(2): p. 129-38.

100. Obradovic, B., et al., *Integration of engineered cartilage*. J Orthop Res, 2001. **19**(6): p. 1089-97.

101. Maher, S.A., et al., *A nanofibrous cell-seeded hydrogel promotes integration in a cartilage gap model*. J Tissue Eng Regen Med, 2010. **4**(1): p. 25-9.

102. Kon, E., et al., *Tissue engineering for total meniscal substitution: animal study in sheep model*. Tissue Eng Part A, 2008. **14**(6): p. 1067-80.

103. Ionescu, L.C., et al., *Differential Regenerative Potential of Fetal and Adult Meniscus Fibrochondrocytes*. Tissue Eng and Regen Med, 2010. **In review.**

104. Mauck, R.L., X. Yuan, and R.S. Tuan, *Chondrogenic differentiation and functional maturation of bovine mesenchymal stem cells in long-term agarose culture*. Osteoarthr Cartilage, 2006. **14**: p. 179–189.

105. Farndale RW, B.D., Barrett AJ, *Improved quantitation and discrimination of sulphated glycosaminoglycans by use of dimethylmethylene blue*. Biochim Biophys Acta, 1986. **883**(2): p. 173-7.

106. Erickson, I.E., et al., *In Vitro Cartilage Integration of MSC-Seeded Hyaluronic Acid Constructs*. The 56th Annual Meeting of the Orthopaedic Research Society, 2010. **New Orleans, Louisiana**.

107. Baker, B.M., et al., *The potential to improve cell infiltration in composite fiber-aligned electrospun scaffolds by the selective removal of sacrificial fibers*. Biomaterials, 2008. **29**(15): p. 2348-2358.

108. Englund, M., A. Guermazi, and L.S. Lohmander, *The meniscus in knee osteoarthritis*. Rheum Dis Clin North Am., 2009. **35**(3): p. 579-90.

109. Stärke, C., et al., *Meniscal repair*. Arthroscopy., 2009. **25**(9): p. 1033-44.

110. Chen, A.C., W.M. Wong, and R.L. Sah. *Maturation Dependent Biomechanical Properties of Bovine Meniscus - 0074*. in *Orthopedic Research Society Annual Conference*. 2002.

111. Imler, S.M., A.N. Doshi, and M.E. Levenston, *Combined effects of growth factors and static mechanical compression on meniscus explant biosynthesis*. Osteoarthr Cartilage, 2004. **12**(9): p. 736-44.

112. Wilson, C.G., J.F. Nishimuta, and M.E. Levenston, *Chondrocytes and meniscal fibrochondrocytes differentially process aggrecan during de novo extracellular matrix assembly*. Tissue Eng Part A, 2009. **15**(7): p. 1513-22.

113. Wilson, C.G., et al., *Aggrecanolysis and in vitro matrix degradation in the immature bovine meniscus: mechanisms and functional implications*. Arthritis Res Ther, 2009. **11**(6): p. R173.

114. Ionescu, L.C., et al., *An Anisotropic Nanofiber/Microsphere Composite with Controlled Release of Biomolecules for For Fibrous Tissue Engineering*. Biomaterials, 2010. **31**(14): p. 4113-20.

115. Arendt, E.A., *Orthopaedic Knowledge Update: Sports Medicine 2*. 1999: Rosemont, Ill: American Academy of Orthopaedic Surgeons.

116. Petersen, W., et al., *Locally applied angiogenic factors--a new therapeutic tool for meniscal repair*. Ann Anat, 2005. **187**(5-6): p. 509-19.

117. Kopf, S., et al., *Local treatment of meniscal lesions with vascular endothelial growth factor*. J Bone Joint Surg Am, 2010. **92**(16): p. 2682-91.

118. Petersen, W., et al., *The effect of locally applied vascular endothelial growth factor on meniscus healing: gross and histological findings*. Arch Orthop Traum Su, 2007. **127**(4): p. 235-240.

119. Makris, E.A., P. Hadidi, and K.A. Athanasiou, *The knee meniscus: Structure-function, pathophysiology, current repair techniques, and prospects for regeneration*. Biomaterials, 2011. **32**(30): p. 7411-7431.

120. Forriol, F., *Growth factors in cartilage and meniscus repair*. Injury, 2009. **40**(Supplement 3): p. S12-S16.

121. Adesida, A.B., et al., *The matrix-forming phenotype of cultured human meniscus cells is enhanced after culture with fibroblast growth factor 2 and is further stimulated by hypoxia*. Arthritis Res Ther., 2006. **8**(3): p. R61.

122. Kasemkijwattana, C., et al., *The use of growth factors, gene therapy and tissue engineering to improve meniscal healing*. Mater Sci Eng C, 2000. **13**(1-2): p. 19-28.

123. Richardson, T.P., et al., *Polymeric system for dual growth factor delivery*. Nat Biotechnol, 2001. **19**(11): p. 1029-34.

124. Lieb, E., et al., *Effects of transforming growth factor beta1 on bonelike tissue formation in three-dimensional cell culture. II: Osteoblastic differentiation.* Tissue Eng, 2004. **10**(9-10): p. 1414-25.

125. Byers, B.A., et al., *Transient exposure to transforming growth factor beta 3 under serum-free conditions enhances the biomechanical and biochemical maturation of tissue-engineered cartilage.* Tissue Eng Part A, 2008. **14**(11): p. 1821-34.

126. Lima, E.G., et al., *The beneficial effect of delayed compressive loading on tissue-engineered cartilage constructs cultured with TGF-[beta]3*. Osteoarthr and Cartilage, 2007. **15**(9): p. 1025-1033.

127. Huang, A.H., et al., *Transient exposure to transforming growth factor beta 3 improves the mechanical properties of mesenchymal stem cell-laden cartilage constructs in a density-dependent manner*. Tissue Eng Part A, 2009. **15**(11): p. 3461-72.

128. Ionescu, L.C., et al., *Maturation state-dependent alterations in meniscus integration: implications for scaffold design and tissue engineering*. Tissue Eng Part A, 2011. **14**(1-2): p. 193-204.

129. Nerurkar, N.L., et al., *Nanofibrous biologic laminates replicate the form and function of the annulus fibrosus*. Nat Mater, 2009. **8**(12): p. 986-92.

130. Kim, M.S., et al., *Release Kinetics and in vitro Bioactivity of Basic Fibroblast Growth Factor: Effect of the Thickness of Fibrous Matrices*. Macromol Biosci, 2011. **11**(1): p. 122-130.

131. Sahoo, S., et al., *Bioactive nanofibers for fibroblastic differentiation of mesenchymal precursor cells for ligament/tendon tissue engineering applications*. Differentiation, 2010. **79**(2): p. 102-110.

132. Liao, I.C., S.Y. Chew, and K.W. Leong, *Aligned core-shell nanofibers delivering bioactive proteins*. Nanomedicine, 2006. **1**(4): p. 465-71.

133. Kato, Y. and D. Gospodarowicz, *Sulfated proteoglycan synthesis by confluent cultures of rabbit costal chondrocytes grown in the presence of fibroblast growth factor*. J Cell Biol, 1985. **1002**(2): p. 477-85.

134. Gunja, N.J. and K.A. Athanasiou, *Additive and synergistic effects of bFGF and hypoxia on leporine meniscus cell-seeded PLLA scaffolds*. J Tissue Eng Regen M, 2009. **4**(2): p. 115-122.

135. Kalpakci, K.N., E.J. Kim, and K.A. Athanasiou, *Assessment of growth factor treatment on fibrochondrocyte and chondrocyte co-cultures for TMJ fibrocartilage engineering*. Acta Biomater, 2011. **7**(4): p. 1710-1718.

136. Pangborn, C.A. and K.A. Athanasiou, *Growth factors and fibrochondrocytes in scaffolds*. J Orthop Res, 2005. **23**(5): p. 1184-90.

137. Zhong, S.P., Y.Z. Zhang, and C.T. Lim, *Tissue scaffolds for skin wound healing and dermal reconstruction*. Wiley Interdiscip Rev Nanomed Nanobiotechnol., 2010. **2**(5): p. 510-25.

138. Xie, J., et al., *Electrospun nanofibers for neural tissue engineering*. Nanoscale, 2010. **2**(1): p. 35-44.

139. Sell, S.A., et al., *Electrospinning of collagen/biopolymers for regenerative medicine and cardiovascular tissue engineering*. Adv Drug Deliv Rev, 2009. **61**(12): p. 1007-19.

140. Jang, J.H., O. Castano, and H.W. Kim, *Electrospun materials as potential platforms for bone tissue engineering*. Adv Drug Deliv Rev, 2009. **61**(12): p. 1065-83.

141. Baker, B.M., et al., *Meniscus tissue engineering on the nanoscale: from basic principles to clinical application*. J Knee Surg, 2009. **22**(1): p. 45-59.

142. Pittenger, M.F., et al., *Multilineage potential of adult human mesenchymal stem cells*. Science, 1999. **284**(5411): p. 143-7.

143. Baker, B.M., et al., *The influence of an aligned nanofibrous topography on human mesenchymal stem cell fibrochondrogenesis*. Biomaterials, 2010. **31**(24): p. 6190-6200.

144. Mandal, B.B., et al., *Multilayered silk scaffolds for meniscus tissue engineering*. Biomaterials, 2011. **32**(2): p. 639-651.

145. Warnock, J.J., et al., *Evaluation of in vitro growth factor treatments on fibrochondrogenesis by synovial membrane cells from osteoarthritic and nonosteoarthritic joints of dogs*. American Journal of Veterinary Research, 2011. **72**(4): p. 500-511.

146. Nerurkar, N.L., et al., *Dynamic culture enhances stem cell infiltration and modulates extracellular matrix production on aligned electrospun nanofibrous scaffolds*. Acta Biomaterialia, 2011. **7**(2): p. 485-491.

147. Baker, B.M., et al., *Fabrication and modeling of dynamic multipolymer nanofibrous scaffolds*. J Biomech Eng, 2009. **131**(10): p. 101-12.

148. Schenker, M.L., et al., *Dynamic Nanofibrous Scaffolds Improve In Vivo Colonization and Implant Fixation in a Meniscus Defect Model*. Orthopedic Research Society Annual Conference, 2011: p. San Francisco, CA.

149. Gunja, N.J. and K.A. Athanasiou, *Passage and reversal effects on gene expression of bovine meniscal fibrochondrocytes*. Arthritis Res Ther, 2007. **9**(5): p. R93.

150. Gentili, C. and R. Cancedda, *Cartilage and bone extracellular matrix*. Curr Pharm Des, 2009. **15**(12): p. 1334-48.

151. Tan, A.R., et al., *Coculture of engineered cartilage with primary chondrocytes induces expedited growth*. Clin Orthop Relat Res, 2011. **469**(10): p. 2735-43.

152. Baker, B.M., et al., *Dynamic tensile loading improves the functional properties of mesenchymal stem cell-laden nanofiber-based fibrocartilage*. Tissue Eng Part A, 2011. **17**(9-10): p. 1445-55.

153. Arnoczky, S.P., et al., *Translational models for studying meniscal repair and replacement: what they can and cannot tell us.* Tissue Eng Part B Rev., 2010. **16**(1): p. 31-9.

154. Kenawy el-R, B.G., Mansfield K, Layman J, Simpson DG, Sanders EH, Wnek GE, *Release of tetracycline hydrochloride from electrospun poly(ethylene-co-vinylacetate), poly(lactic acid), and a blend.* J Control Release, 2002. **17**(81): p. 57-64.

155. Zong, X., et al., *Structure and process relationship of electrospun bioabsorbable nanofiber membranes.* Polymer, 2002. **43**(16): p. 4403-4412.

156. Kim, K., et al., *Incorporation and controlled release of a hydrophilic antibiotic using poly(lactide-co-glycolide)-based electrospun nanofibrous scaffolds.* J Control Release, 2004. **98**(1): p. 47-56.

157. Hong, Y., et al., *Generating Elastic, Biodegradable Polyurethane/Poly(lactide-co-glycolide) Fibrous Sheets with Controlled Antibiotic Release via Two-Stream Electrospinning*. Biomacromolecules, 2008. **9**(4): p. 1200-1207.

158. Zeng, J., et al., *Biodegradable electrospun fibers for drug delivery*. J Control Release, 2003. **92**(3): p. 227-231.

159. Katti DS, et al., *Bioresorbable nanofiber-based systems for wound healing and drug delivery: Optimization of fabrication parameters.* Journal of Biomedical Materials Research Part B: Applied Biomaterials, 2004. **70B**(2): p. 286-296.

160. He, C.L., et al., *Coaxial Electrospun Poly(Lactic Acid) Ultrafine Fibers for Sustained Drug Delivery*. J Macromol Sci Phys, 2006. **45**: p. 515-524.

161. Huang ZM, et al., *Encapsulating drugs in biodegradable ultrafine fibers through co-axial electrospinning*. Journal of Biomedical Materials Research Part A, 2006. **77A**(1): p. 169-179.

162. He, C.-L., Z.-M. Huang, and X.-J. Han, *Fabrication of drug-loaded electrospun aligned fibrous threads for suture applications*. Journal of Biomedical Materials Research Part A, 2009. **89A**(1): p. 80-95.

163. Jiang, H., et al., *Preparation and characterization of ibuprofen-loaded poly(lactide-co-glycolide)/poly(ethylene glycol)-g-chitosan electrospun membranes.* Journal of Biomaterials Science, Polymer Edition, 2004. **15**: p. 279-296.

164. Cui, W., et al., *Electrospun fibers of acid-labile biodegradable polymers with acetal groups as potential drug carriers.* International Journal of Pharmaceutics, 2008. **361**(1-2): p. 47-55.

165. Cui, W., et al., *Investigation of Drug Release and Matrix Degradation of Electrospun Poly(dl-lactide) Fibers with Paracetanol Inoculation.* Biomacromolecules, 2006. **7**(5): p. 1623-1629.

166. Zeng, J., et al., *Influence of the drug compatibility with polymer solution on the release kinetics of electrospun fiber formulation.* J Control Release, 2005. **105**(1-2): p. 43-51.

167. Zeng, J., et al., *Poly(vinyl alcohol) Nanofibers by Electrospinning as a Protein Delivery System and the Retardation of Enzyme Release by Additional Polymer Coatings*. Biomacromolecules, 2005. **6**(3): p. 1484-1488.

168. Xie, J. and C.H. Wang, *Electrospun Micro- and Nanofibers for Sustained Delivery of Paclitaxel to Treat C6 Glioma in Vitro.* Pharm Res., 2006. **23**(8): p. 1817-1826.

169. Xu, X., et al., *BCNU-loaded PEG-PLLA ultrafine fibers and their in vitro antitumor activity against Glioma C6 cells*. J Control Release, 2006. **114**(3): p. 307-316.

170. Xu, X., et al., *Ultrafine medicated fibers electrospun from W/O emulsions.* J Control Release, 2005. **108**(1): p. 33-42.

171. Choi, J.S., K.W. Leong, and H.S. Yoo, *In vivo wound healing of diabetic ulcers using electrospun nanofibers immobilized with human epidermal growth factor (EGF).* Biomaterials, 2008. **29**(5): p. 587-596.

172. Cho, Y.I., et al., *Nerve growth factor (NGF)-conjugated electrospun nanostructures with topographical cues for neuronal differentiation of mesenchymal stem cells*. Acta Biomaterialia, 2010. **6**(12): p. 4725-4733.

173. Tığlı, R.S., et al., *Cellular Behavior on Epidermal Growth Factor (EGF)-Immobilized PCL/Gelatin Nanofibrous Scaffolds.* J Biomater Sci Polym Ed, 2010.

174. Gümüşderelioğlu, M., et al., *A novel dermal substitute based on biofunctionalized electrospun PCL nanofibrous matrix.* Journal of Biomedical Materials Research Part A, 2011. **98A**(3): p. 461-472.

175. Lee, J., et al., *Nerve Growth Factor-Immobilized Electrically Conducting Fibrous Scaffolds for Potential Use in Neural Engineering Applications.* NanoBioscience, IEEE Transactions on, 2010. **PP**(99): p. 1-1.

176. Casper, C.L., et al., *Functionalizing Electrospun Fibers with Biologically Relevant Macromolecules*. Biomacromolecules, 2005. **6**(4): p. 1998-2007.

177. Ishihara, M., et al., *Heparin-carrying polystyrene (HCPS)-bound collagen substratum to immobilize heparin-binding growth factors and to enhance cellular growth*. Journal of Biomedical Materials Research, 2001. **56**(4): p. 536-544.

178. Lam, H.J., et al., *In vitro regulation of neural differentiation and axon growth by growth factors and bioactive nanofibers*. Tissue Eng Part A, 2010. **16**(8): p. 2641-8.

179. Ye, L., et al., *Heparin-Conjugated PCL Scaffolds Fabricated by Electrospinning and Loaded with Fibroblast Growth Factor 2*. J Biomater Sci Polym Ed, 2010.

180. Casper, C.L., et al., *Coating Electrospun Collagen and Gelatin Fibers with Perlecan Domain I for Increased Growth Factor Binding*. Biomacromolecules, 2007. **8**(4): p. 1116-1123.

181. Almodóvar, J. and M.J. Kipper, *Coating Electrospun Chitosan Nanofibers with Polyelectrolyte Multilayers Using the Polysaccharides Heparin and N,N,N-Trimethyl Chitosan*. Macromolecular Bioscience, 2010. **11**(1): p. 72-76.

182. Chew, S.Y., et al., *Sustained release of proteins from electrospun biodegradable fibers*. Biomacromolecules, 2005. **6**(4): p. 2017-24.

183. Chew, S.Y., et al., *Aligned Protein–Polymer Composite Fibers Enhance Nerve Regeneration: A Potential Tissue-Engineering Platform*. Adv Funct Mater, 2007. **17**(8): p. 1288-1296.

184. Koh, H.S., et al., *In vivo study of novel nanofibrous intra-luminal guidance channels to promote nerve regeneration*. J Neural Eng., 2010. **7**(4): p. 046003.

185. Koh, H.S., et al., *Enhancement of neurite outgrowth using nano-structured scaffolds coupled with laminin*. Biomaterials, 2008. **29**(26): p. 3574-3582.

186. van der Walle, C.F., G. Sharma, and M. Ravi Kumar, *Current approaches to stabilising and analysing proteins during microencapsulation in PLGA*. Expert Opin Drug Deliv, 2009. **6**(2): p. 177-86.

187. Sahoo, S., et al., *Growth factor delivery through electrospun nanofibers in scaffolds for tissue engineering applications*. J Biomed Mater Res A, 2010. **93A**(4): p. 1539-1550.

188. Valmikinathan, C.M., S. Defroda, and X. Yu, *Polycaprolactone and bovine serum albumin based nanofibers for controlled release of nerve growth factor*. Biomacromolecules, 2009. **10**(5): p. 1084-9.

189. Li, X., et al., *Encapsulation of proteins in poly(l-lactide-co-caprolactone) fibers by emulsion electrospinning*. Colloids and Surfaces B: Biointerfaces, 2010. **75**(2): p. 418-424.

190. Li, C., et al., *Electrospun silk-BMP-2 scaffolds for bone tissue engineering*. Biomaterials, 2006. **27**(16): p. 3115-3124.

191. Madduri, S., M. Papaloïzos, and B. Gander, *Trophically and topographically functionalized silk fibroin nerve conduits for guided peripheral nerve regeneration*. Biomaterials, 2010. **31**(8): p. 2323-2334.

192. Kluge, J.A., et al. *Delivery of Active FGF-2 from Mechanically-Stable Biological Nanofibers Accelerates Cell Ingress into Multifiber Composites*. in *Proceedings of ASME 2011 Summer Bioengineering Conference*. 2011. Farmington, PA.

193. Qu, F., et al. *Enzymatic Delivery from Functionalized Sacrificial Nanofibers for Tissue Repair and Regeneration*. in *Orthopaedic Research Society Annual Meeting*. 2011. Long Beach, CA.

194. Liu, J.-J., et al., *Peripheral nerve regeneration using composite poly(lactic acid-caprolactone)/nerve growth factor conduits prepared by coaxial electrospinning*. Journal of Biomedical Materials Research Part A, 2010. **96A**(1): p. 13-20.

195. Jia, X., et al., *Sustained release of VEGF by coaxial electrospun dextran/PLGA fibrous membranes in vascular tissue engineering*. J Biomater Sci Polym Ed, 2011. **22**(13): p. 1811-27.

196. Li, H., et al., *Controlled Release of PDGF-bb by Coaxial Electrospun Dextran/Poly(L-lactide-co--caprolactone) Fibers with an Ultrafine Core/Shell Structure*. J Biomat Sci-Polym E, 2010. **21**(6-7): p. 803-819.

197. Yang, Y., et al., *Promotion of skin regeneration in diabetic rats by electrospun core-sheath fibers loaded with basic fibroblast growth factor*. Biomaterials, 2011. **32**(18): p. 4243-4254.

198. Wang CY, L.J., Fan CY, Mo XM, Ruan HJ, Li FF., *The Effect of Aligned Core-Shell Nanofibres Delivering NGF on the Promotion of Sciatic Nerve Regeneration*. J Biomater Sci Polym Ed, 2010.

199. Lu, Y., et al., *Mild immobilization of diverse macromolecular bioactive agents onto multifunctional fibrous membranes prepared by coaxial electrospinning*. Acta Biomaterialia, 2009. **5**(5): p. 1562-1574.

200. Dong, B., M.E. Smith, and G.E. Wnek, *Encapsulation of Multiple Biological Compounds Within a Single Electrospun Fiber*. Small, 2009. **5**(13): p. 1508-12.

201. DeVolder, R.J., et al., *Directed Blood Vessel Growth Using an Angiogenic Microfiber/Microparticle Composite Patch*. Adv Mater, 2011. **23**(28): p. 3139-3143.

202. Qi, H., et al., *Encapsulation of Drug Reservoirs in Fibers by Emulsion Electrospinning: Morphology Characterization and Preliminary Release Assessment*. Biomacromolecules, 2006. **7**(8): p. 2327-2330.

203. Kolambkar, Y.M., et al., *Spatiotemporal delivery of bone morphogenetic protein enhances functional repair of segmental bone defects*. Bone, 2011. **49**(3): p. 485-492.

204. Luu, Y.K., et al., *Development of a nanostructured DNA delivery scaffold via electrospinning of PLGA and PLA-PEG block copolymers*. J Control Release, 2003. **89**(2): p. 341-353.

205. Nie, H. and C.H. Wang, *Fabrication and characterization of PLGA/HAp composite scaffolds for delivery of BMP-2 plasmid DNA*. J Control Release, 2007. **120**(1-2): p. 111-121.

206. Liang, D., et al., *In vitro non-viral gene delivery with nanofibrous scaffolds*. Nucleic Acids Res, 2005. **33**(19): p. 170.

207. Luong-Van, E., et al., *Controlled release of heparin from poly([epsilon]-caprolactone) electrospun fibers*. Biomaterials, 2006. **27**(9): p. 2042-2050.

208. Gandhi, M., et al., *Mechanistic Examination of Protein Release from Polymer Nanofibers*. Molecular Pharmaceutics, 2009. **6**(2): p. 641-647.

209. Verreck, G., et al., *Incorporation of drugs in an amorphous state into electrospun nanofibers composed of a water-insoluble, nonbiodegradable polymer*. J Control Release, 2003. **92**(3): p. 349-360.

210. Srikar, R., et al., *Desorption-Limited Mechanism of Release from Polymer Nanofibers*. Langmuir, 2008. **24**(3): p. 965-974.

211. Li, W.J., R.L. Mauck, and R.S. Tuan, *Electrospun Nanofibrous Scaffolds: Production, Characterization, and Applications for Tissue Engineering and Drug Delivery*. J Biomed Nanotechnol., 2005. **1**(3): p. 259-275.

212. Barnes, C.P., et al., *Nanofiber technology: designing the next generation of tissue engineering scaffolds*. Adv Drug Deliv Rev, 2007. **59**(14): p. 1413-33.

213. Li, W.J., et al., *Engineering controllable anisotropy in electrospun biodegradable nanofibrous scaffolds for musculoskeletal tissue engineering*. J Biomech, 2006. **40**(8): p. 1686-93.

214. Courtney, T., et al., *Design and analysis of tissue engineering scaffolds that mimic soft tissue mechanical anisotropy*. Biomaterials, 2006. **27**(19): p. 3631-8.

215. Ayres, C.E., et al., *Incremental changes in anisotropy induce incremental changes in the material properties of electrospun scaffolds*. Acta Biomater, 2007. **3**(5): p. 651-61.

216. Li, D., et al., *Collecting electrospun nanofibers with patterned electrodes*. Nano Letters, 2005. **5**(5): p. 913-6.

217. Li, D., Y. Wang, and Y. Xia, *Electrospinning Nanofibers as Uniaxially Aligned Arrays and Layer-by-Layer Stacked Films*. Adv Mater, 2004. **16**(4): p. 361-366.

218. Nerurkar, N.L., D.M. Elliott, and R.L. Mauck, *Mechanics of oriented electrospun nanofibrous scaffolds for annulus fibrosus tissue engineering*. J Orthop Res., 2007. **25**(8): p. 1018-1028.

219. Moffat, K.L., et al., *Orthopedic interface tissue engineering for the biological fixation of soft tissue grafts*. Clin Sports Med, 2009. **28**(1): p. 157-76.

220. Fujimoto, K.L., et al., *An elastic, biodegradable cardiac patch induces contractile smooth muscle and improves cardiac remodeling and function in subacute myocardial infarction*. J Am Coll Cardiol., 2007. **49**(23): p. 2292-300.

221. Li, W.J., Y.J. Jiang, and R.S. Tuan, *Chondrocyte phenotype in engineered fibrous matrix is regulated by fiber size*. Tissue Eng Part A, 2006. **12**(7): p. 579-587.

222. Li, W.J., Y.J. Jiang, and R.S. Tuan, *Cell-nanofiber-based cartilage tissue engineering using improved cell seeding, growth factor, and bioreactor technologies*. Tissue Eng Part A, 2008. **14**(5): p. 639-48.

223. Nerurkar, N.L., R.L. Mauck, and D.M. Elliott, *ISSLS prize winner: integrating theoretical and experimental methods for functional tissue engineering of the annulus fibrosus*. Spine, 2008. **33**(25): p. 2691-701.

224. Hadjiargyrou, M. and J.B. Chiu, *Enhanced composite electrospun nanofiber scaffolds for use in drug delivery*. Expert Opin Drug Deliv, 2008. **5**(10): p. 1093-106.

225. Katti, D.S., et al., *Bioresorbable nanofiber-based systems for wound healing and drug delivery: optimization of fabrication parameters*. J Biomed Mater Res B Appl Biomater, 2004. **70**(2): p. 286-96.

226. Kenawy, E.R., et al., *Release of tetracycline hydrochloride from electrospun poly(ethylene-co-vinylacetate), poly(lactic acid), and a blend*. J Control Release, 2002. **17**(81): p. 57-64.

227. Jiang, H., et al., *A facile technique to prepare biodegradable coaxial electrospun nanofibers for controlled release of bioactive agents*. J Control Release, 2005. **108**(2-3): p. 237-243.

228. Jiang, H., et al., *Modulation of protein release from biodegradable core-shell structured fibers prepared by coaxial electrospinning*. J Biomed Mater Res B Appl Biomater, 2006. **79B**(1): p. 50-57.

229. Zhang, Y.Z., et al., *Coaxial Electrospinning of (Fluorescein Isothiocyanate-Conjugated Bovine Serum Albumin)-Encapsulated Poly(e-caprolactone) Nanofibers for Sustained Release*. Biomacromolecules, 2006. **7**(4): p. 1049-1057.

230. Maretschek, S., A. Greiner, and T. Kissel, *Electrospun biodegradable nanofiber nonwovens for controlled release of proteins*. J Control Release, 2008. **127**(2): p. 180-187.

231. Yang, Y., et al., *Release pattern and structural integrity of lysozyme encapsulated in core-sheath structured poly(dl-lactide) ultrafine fibers prepared by emulsion electrospinning*. Eur J Pharm Biopharm, 2008. **69**(1): p. 106-116.

232. Chew, S.Y., et al., *Sustained Release of Proteins from Electrospun Biodegradable Fibers*. Biomacromolecules, 2005. **6**(4): p. 2017-2024.

233. Liao, I.C., S.Y. Chew, and K.W. Leong, *Aligned core-shell nanofibers delivering bioactive proteins*. Nanomedicine, 2006. **1**(4): p. 465-471.

234. Li, C., et al., *Electrospun silk-BMP-2 scaffolds for bone tissue engineering*. Biomaterials, 2006. **27**(16): p. 3115-3124.

235. Huang, Z.M., et al., *Encapsulating drugs in biodegradable ultrafine fibers through co-axial electrospinning*. J Biomed Mater Res A, 2006. **77A**(1): p. 169-179.

236. Cohen, S., et al., *Controlled delivery systems for proteins based on poly(lactic/glycolic acid) microspheres*. Pharm Res, 1991. **8**(6): p. 713-20.

237. Peltz, C.D., et al., *Mechanical properties of the long-head of the biceps tendon are altered in the presence of rotator cuff tears in a rat model*. J Orthop Res, 2009. **27**(3): p. 416-20.

238. Lim, J.M., et al., *Fabrication of One-Dimensional Colloidal Assemblies from Electrospun Nanofibers*. Langmuir, 2006. **22**(8): p. 3445-3449.

239. Melaiye, A., et al., *Silver Imidazole Cyclophane gem-Diol Complexes Encapsulated by Electrospun Tecophilic Nanofibers: Formation of Nanosilver*

Particles and Antimicrobial Activity. J Am Chem Soc, 2005. **127**(7): p. 2285-2291.

240. Bursac, P., et al., *Influence of donor age on the biomechanical and biochemical properties of human meniscal allografts*. Am J Sports Med, 2009. **37**(5): p. 884-9.

241. Tan, A.R., et al., *Electrospinning of photocrosslinked and degradable fibrous scaffolds*. J Biomed Mater Res A, 2008. **15**(87): p. 1034-43.

242. Lee, W., et al., *The reliable targeting of specific drug release profiles by integrating arrays of different albumin-encapsulated microsphere types*. Biomaterials, 2009. **30**(34): p. 6648-54.

243. Barnes, C.P., et al., *Nanofiber technology: Designing the next generation of tissue engineering scaffolds*. Adv Drug Deliv Rev., 2007. **59**(14): p. 1413-1433.

244. Ladewig, K., *Drug delivery in soft tissue engineering*. Expert Opin Drug Deliv, 2011. **8**(9): p. 1175-88.

245. Royce, S.M., M. Askari, and K.G. Marra, *Incorporation of polymer microspheres within fibrin scaffolds for the controlled delivery of FGF-1*. J Biomater Sci Polym Ed, 2004. **15**(10): p. 1327-36.

246. Jaklenec, A., et al., *Sequential release of bioactive IGF-I and TGF-beta 1 from PLGA microsphere-based scaffolds*. Biomaterials, 2008. **29**(10): p. 1518-25.

247. King, T.W. and C.W. Patrick, *Development and in vitro characterization of vascular endothelial growth factor (VEGF)-loaded poly(DL-lactic-co-glycolic acid)/poly(ethylene glycol) microspheres using a solid encapsulation/single emulsion/solvent extraction technique*. J Biomed Mater Res, 2000. **51**(3): p. 383-90.

248. Sinha, V.R. and A. Trehan, *Biodegradable microspheres for protein delivery*. J Control Release, 2003. **90**(3): p. 261-80.

249. Yan, C., et al., *Characterization and morphological analysis of protein-loaded poly(lactide-co-glycolide) microparticles prepared by water-in-oil-in-water emulsion technique*. J Control Release, 1994. **32**(3): p. 231-241.

250. Ungaro, F., et al., *Microsphere-integrated collagen scaffolds for tissue engineering: effect of microsphere formulation and scaffold properties on protein release kinetics*. J Control Release, 2006. **113**(2): p. 128-36.

251. Ashraf, A., et al., *Effect of sustained-release PDGF and TGF-beta on cyclophosphamide-induced impaired wound healing*. Plast Reconstr Surg., 2009. **124**(4): p. 1118-24.

252. Park, H., et al., *Effect of dual growth factor delivery on chondrogenic differentiation of rabbit marrow mesenchymal stem cells encapsulated in injectable hydrogel composites*. J Biomed Mater Res A, 2009. **88**(4): p. 889-97.

253. Manning, M.C., K. Patel, and R.T. Borchardt, *Stability of protein pharmaceuticals*. Pharm Res, 1989. **6**(11): p. 903-18.

254. Gospodarowicz, D., J.A. Abraham, and J. Schilling, *Isolation and characterization of a vascular endothelial cell mitogen produced by pituitary-derived folliculo stellate cells*. Proc Natl Acad Sci U S A., 1989. **86**(19): p. 7311-5.

255. Bauters, C., et al., *Site-specific therapeutic angiogenesis after systemic administration of vascular endothelial growth factor*. J Vasc Surg., 1995. **21**(2): p. 314-24.

256. Lazarous, D.F., et al., *Comparative effects of basic fibroblast growth factor and vascular endothelial growth factor on coronary collateral development and the arterial response to injury*. Circulation, 1996. **94**(5): p. 1074-82.

257. Laschke, M.W., et al., *Angiogenesis in tissue engineering: breathing life into constructed tissue substitutes*. Tissue Eng, 2006. **12**(8): p. 2093-104.

258. Rocha, F.G., et al., *The effect of sustained delivery of vascular endothelial growth factor on angiogenesis in tissue-engineered intestine*. Biomaterials, 2008. **29**(19): p. 2884-90.

259. Kedem, A., et al., *Vascular endothelial growth factor-releasing scaffolds enhance vascularization and engraftment of hepatocytes transplanted on liver lobes*. Tissue Eng Part A, 2005. **11**(5-6): p. 715-22.

260. Silva, E.A. and D.J. Mooney, *Effects of VEGF temporal and spatial presentation on angiogenesis*. Biomaterials, 2010. **31**(6): p. 1235-41.

261. Sundararaghavan, H.G., R.B. Metter, and J.A. Burdick, *Electrospun fibrous scaffolds with multiscale and photopatterned porosity*. Macromol Biosci., 2010. **10**(3): p. 265-70.

262. Kanitkar, M., H.D. Tailor, and W.S. Khan, *The use of growth factors and mesenchymal stem cells in orthopaedics*. Open Orthop J, 2011. **5**(Suppl 2): p. 271-5.

263. Wernike, E., et al., *VEGF incorporated into calcium phosphate ceramics promotes vascularisation and bone formation in vivo*. Eur Cell Mater19, 2010: p. 30-40.

264. Jay, S.M. and W.M. Saltzman, *Controlled delivery of VEGF via modulation of alginate microparticle ionic crosslinking*. J Control Release, 2009. **134**(1): p. 26-34.

265. Sun, Q., et al., *Sustained release of multiple growth factors from injectable polymeric system as a novel therapeutic approach towards angiogenesis*. Pharm Res, 2010. **27**(2).

266. Thakur, R.A., et al., *Electrospun nanofibrous polymeric scaffold with targeted drug release profiles for potential application as wound dressing*. Int J Pharm, 2008. **364**(1): p. 87-93.

267. Qu, F., et al., *Enzymatic Delivery from Functionalized Sacrificial Nanofibers for Tissue Repair and Regeneration*. Orthopaedic Research Society Annual Meeting, 2011(Long Beach, CA, January 13-16).